




# Building Better Full Manganese-Based Cathode Materials for Next-Generation Lithium-Ion Batteries

Jin Song<sup>1</sup> · Hangchao Wang<sup>1</sup> · Yuxuan Zuo<sup>1</sup> · Kun Zhang<sup>1</sup> · Tonghuan Yang<sup>1</sup> · Yali Yang<sup>1</sup> · Chuan Gao<sup>1</sup> · Tao Chen<sup>1</sup> · Guang Feng<sup>1</sup> · Zewen Jiang<sup>2</sup> · Wukun Xiao<sup>1</sup> · Tie Luo<sup>3</sup> · Dingguo Xia<sup>1</sup> 

Received: 6 July 2022 / Revised: 21 October 2022 / Accepted: 2 March 2023 / Published online: 9 June 2023  
© The Author(s) 2023

## Abstract

Lithium-manganese-oxides have been exploited as promising cathode materials for many years due to their environmental friendliness, resource abundance and low biotoxicity. Nevertheless, inevitable problems, such as Jahn-Teller distortion, manganese dissolution and phase transition, still frustrate researchers; thus, progress in full manganese-based cathode materials (FMCs) has been relatively slow and limited in recent decades. Recently, with the fast growth of vehicle electrification and large-scale energy-storage grids, there has been an urgent demand to develop novel FMCs again; actually, new waves of research based on FMCs are being created. Herein, we systematically review the history of FMCs, correctly describe their structures, evaluate the advantages and challenges, and discuss the resolution strategies and latest developments. Additionally, beyond FMCs, a profound discussion of current controversial issues, such as oxygen redox reaction, voltage decay and voltage hysteresis in  $\text{Li}_2\text{MnO}_3$ -based cathode materials, is also presented. This review summarizes the effectively optimized approaches and offers a few new possible enhancement methods from the perspective of the electronic-coordination-crystal structure for building better FMCs for next-generation lithium-ion batteries.

**Keywords** Energy storage · Lithium-ion batteries · Cathode materials · Manganese oxides

## 1 Introduction

The use of energy can be roughly divided into the following three aspects: conversion, storage and application. Energy storage devices are the bridge between the other two aspects and promote the effective and controllable utilization of renewable energy without the constraints of space and time [1–3]. Among the diverse energy storage devices, lithium-ion batteries (LIBs) are the most popular and extensively applied in daily life due to their high energy density, long cycle life, and other outstanding properties [1, 4, 5]. The rapid expansion of portable electronics, electric vehicles,

and smart grid systems calls for more advanced LIB materials, which should not only have excellent performance but also cost less [6–9]. At the cell level, LIBs mainly consist of cathodes, anodes, separators and electrolytes, and cathode materials account for approximately 50% of all the material costs due to the expensive lithium and transition metal (TM) elements and lower practical capacity delivered by cathode materials; therefore, cathode materials play a significant role in increasing the comprehensive performance of practical batteries and obtain much more attention than the other materials [10–12].

Traditional cathode materials, such as  $\text{LiFePO}_4$ ,  $\text{LiMn}_2\text{O}_4$ ,  $\text{LiCoO}_2$ , and  $\text{LiMO}_2$  ( $M = \text{Ni}, \text{Co}$ , etc.), have been pervasive in today's society [11, 13–17]. However, due to their lower energy density and/or reliance on constrained natural resources, they cannot meet the demands for both excellent performance and low-cost LIBs [6, 7, 18]. Although Fe-based olivine  $\text{LiFePO}_4$  and Mn-based spinel  $\text{LiMn}_2\text{O}_4$  have been widely utilized as commercial cathode materials, these compounds suffer from low theoretical/practical specific capacities; thus, they have been replaced in the literature in the pursuit of higher energy density. Co or

✉ Dingguo Xia  
dgxia@pku.edu.cn

<sup>1</sup> Beijing Key Laboratory of Theory and Technology for Advanced Battery Materials, School of Materials Science and Engineering, Peking University, Beijing 100871, China

<sup>2</sup> College of Chemistry and Molecular Science, Wuhan University, Wuhan 430072, Hubei, China

<sup>3</sup> College of Engineering, Peking University, Beijing 100871, China

Ni-based layered cathode materials have theoretical capacities of over 270 mAh g<sup>-1</sup>; nonetheless, only < 70% of the Li ions can be reversibly inserted in/extracted from the canonical LiCoO<sub>2</sub> cathode material [19], and for Ni-rich electrodes, less than 80% Li can cycle reversibly even under laboratory conditions [16, 20]; furthermore, once the electrodes are under deep delithiation, oxygen evolution and structure collapse occur, which could give rise to severe safety issues and hinder their extensive commercial application [21–24]. Moreover, compared with manganese, cobalt and nickel are not economical enough and have higher biotoxicity. According to the latest data from the U.S. Geological Survey (USGS), 1.5 billion t of world land-based Mn reserves have been identified, which is far more than the land-based reserves of Co and Ni, which are approximately 7.6 and 95 million t, respectively. Furthermore, the land-based Co and Ni resources are irregularly distributed. Co reserves are highly concentrated in Congo (Kinshasa, 46.05%), Australia (18.42%) and Indonesia (7.89%), which together account for approximately 72% of the world's Co reserves. Ni reserves are mainly distributed in Australia (22.10%), Indonesia (22.10%), Brazil (16.84%) and Russia (7.89%), which together account for approximately 68% of the world's Ni reserves. However, the world's top power battery manufacturers, which are mainly in East Asia (China, the Republic of Korea, and Japan), have a great demand for upstream raw materials; therefore, a significant amount of money has to be spent on transportation, which will ultimately increase the costs to end customers. China was already the world's largest producer and consumer of LIBs. The development of power batteries in China will have a profound impact on the world's carbon neutrality process. Nevertheless, the reserves of Co (80 000 t) and Ni (2.8 million t) in China are limited,

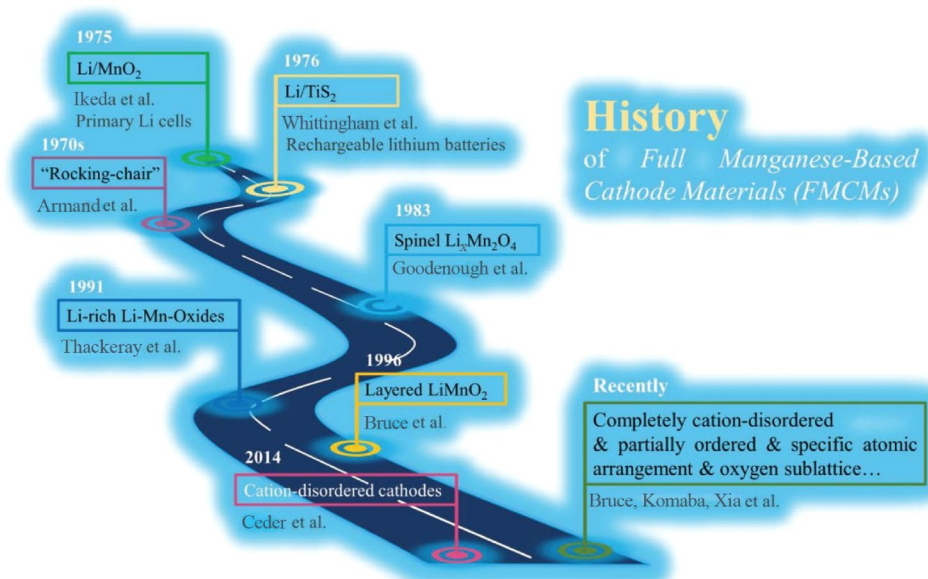
and the quality is not sufficient; therefore, processing is difficult. Fortunately, there are approximately 54 million t of Mn reserves in China, and once full manganese-based cathode materials (FMCMs) are widely exploited in the market, they will rapidly promote the progress of the new energy industry. Therefore, developing better FMCMs for next-generation LIBs seems an encouraging direction [18, 25–27].

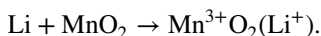
The use of manganese resources as raw materials for potential cathode materials has been studied in recent decades due to their low cost and low biotoxicity compared with nickel and cobalt. In recent years, various breakthroughs have emerged, including a few new structural cathode material emergences and some novel charge compensation mechanism proposals [28–30]. Herein, we methodically combine the history of FMCMs, correctly describe their structures, evaluate the advantages and challenges, and pay much attention to the resolution strategies and latest developments. In particular, this review summarizes the effectively optimized approaches and offers some new possible enhancement methods at different research scales, which will accelerate the research process and practical application of FMCMs. Let us begin with a brief history of the FMCMs for LIBs.

## 2 History of FMCMs for LIBs

Figure 1 describes the historical development of FMCMs. In 1975, manganese dioxide (MnO<sub>2</sub>) was first proposed as a cathode material in Li batteries by Ikeda et al. [31], and the anode material was Li-metal, so the discharge mechanism of MnO<sub>2</sub>/Li cells was as follows:

**Fig. 1** History of full manganese-based cathode materials (FMCMs)





$\text{Mn}^{3+}\text{O}_2(\text{Li}^+)$  signified that Li ions were inserted into the  $\text{MnO}_2$  crystal lattice, and charge neutrality was achieved by the reduction of  $\text{Mn}^{4+}$  to  $\text{Mn}^{3+}$ . However, at that moment, they were called primary Li cells, which were not rechargeable.

The concept of rechargeable Li batteries was first demonstrated by Whittingham et al. [32], in a Li-TiS<sub>2</sub> system, where TiS<sub>2</sub> was used as the cathode and Li metal was used as the anode (with a nonaqueous electrolyte). During the discharging process, Li ions were introduced into the van der Waals gap between the TiS<sub>2</sub> layers and were accompanied by the reduction of Ti<sup>4+</sup> ions to Ti<sup>3+</sup>. When charging the electrode, the reverse process occurred, and the charge balance was maintained by the oxidation of Ti<sup>3+</sup> ions to Ti<sup>4+</sup>. Throughout the discharge/charge (Li insertion/extraction) process, the layered structure was well maintained, which resulted in quite good reversibility. However, although the cathode materials operated flawlessly, this system was not sufficiently viable. The shortcomings of a Li-metal/liquid electrolyte combination-dendritic Li soon emerged [33], which gradually grew during subsequent discharge/recharge cycles and then pierced a separator, leading to serious explosion hazards. Methods involving replacing metallic Li with a second insertion material, formerly known as “rocking-chair” or “shuttle” battery technology, were proposed by Armand in the 1970s [34]. Later, Goodenough et al. proposed a layered Li<sub>x</sub>CoO<sub>2</sub> cathode material that is still extensively applied in batteries today [19, 35]. Inspired by the lithiation of Fe<sub>3</sub>O<sub>4</sub> to LiFe<sub>3</sub>O<sub>4</sub>, they further synthesized a lithium manganese oxide spinel (Li<sub>x</sub>Mn<sub>2</sub>O<sub>4</sub>) as a cathode material in 1983, which exhibited certain electrochemical performance at that time and is still commonly used in electric vehicles [36, 37].

At the early research stage of FMCMs, there was a great deal of interest in developing new Li-Mn oxides; thus, various Li-Mn oxide phases have been synthesized by many groups. Thackeray et al. developed a Li<sub>2-x</sub>MnO<sub>3-x</sub> cathode by acid leaching of Li<sub>2</sub>O from the rock salt phase Li<sub>2</sub>MnO<sub>3</sub> (Li<sub>2</sub>O\* $\text{MnO}_2$ ) in 1991, which provided a reversible capacity of approximately 200 mAh g<sup>-1</sup> [38]. Meanwhile, the synthesis of layered LiMnO<sub>2</sub>, which exhibits a structure analogous to LiCoO<sub>2</sub> with two-dimensional (2D) Li-ion channels, has been a long-standing goal. However, the monoclinic layered LiMnO<sub>2</sub> (m-LiMnO<sub>2</sub>) was not thermodynamically stable; instead, it was an orthorhombic phase o-LiMnO<sub>2</sub> (zigzag layered structure), even though the stability difference between the two structures was quite small [25, 39, 40]. Compared with o-LiMnO<sub>2</sub>, m-LiMnO<sub>2</sub> attracted the attention of more researchers, as mentioned above, as its structure was very similar to LiCoO<sub>2</sub>, and it was more likely

to be a practical electrode material. Layered m-Li<sub>x</sub>MnO<sub>2</sub> has been prepared by several groups; however, these interesting materials, in general, were hydrated, contained protons or were nonstoichiometric [41–45]. In 1996, Bruce et al. first reported the synthesis of anhydrous and stoichiometric m-LiMnO<sub>2</sub>, which was obtained by Li/Na ion exchange from NaMnO<sub>2</sub> and showed a rather high charge specific capacity of 270 mAh g<sup>-1</sup> and fairly good stability over a few cycles [46, 47]. Later, Tabuchi et al. also independently reported the hydrothermal synthesis of layered m-LiMnO<sub>2</sub> [48]. The template method was also an attractive synthesis approach for layered LiMnO<sub>2</sub> at the beginning of this century and could effectively control the size of the prepared nanocrystals [49, 50]. Another thermodynamically stable FMCM was layered monoclinic Li<sub>2</sub>MnO<sub>3</sub> (or Li[Li<sub>1/3</sub>Mn<sub>2/3</sub>]O<sub>2</sub>), whose additional Li ions in the Mn layer forming the Li-Mn-Mn superlattice led to *C2/m* symmetry [51–53]. Due to the excess Li in Mn layers exhibiting a “Li-O-Li” configuration that created orphaned oxygen states (an unhybridized O 2p state or nonbonding O 2p orbital), which facilitated the charge compensation of oxygen in the Li<sub>2</sub>MnO<sub>3</sub> system, a higher energy density was theoretically achievable [54–56]. Nevertheless, Li<sub>2</sub>MnO<sub>3</sub> could only exhibit considerable electrochemical performance by nanosizing its particles or through high-temperature testing. With pure oxygen redox occurring during the activation process because of the unavailability of Mn redox (which is controversial and will be discussed in detail later), much O<sub>2</sub> gas is released, resulting in irreversible structural transformation and poor cycle performance [57–60].

In the next decade or so, there was no significant progress in the development of FMCMs, and most other FMCMs could be regarded as combinations of the above structures, such as Li<sub>2</sub>MnO<sub>3</sub>\*LiMnO<sub>2</sub> and Li<sub>2</sub>MnO<sub>3</sub>\*LiMn<sub>2</sub>O<sub>4</sub> [61–64]. Considering environmental issues and the rapid development of electric vehicles in recent years, an increasing number of researchers are studying FMCMs again, and some intriguing FMCMs have been successfully synthesized, which have exhibited extraordinary electrochemical performance. In 2014, the percolation theory was introduced in LIBs by Ceder et al., which expanded the design space of cathode materials [65]. Later, many completely cation-disordered rock-salt and partial spinel-like cation-ordered FMCMs were creatively developed and showed great potential for use as cathode materials due to their ultrahigh energy density achieved by multielectron redox [18, 27, 66–70]. Furthermore, by giving more attention to the atomic ordering within the TM layers, a series of FMCMs with different intralayer M/vacancies/TM orderings were designed and synthesized, which resulted in the construction of a correlation between intralayer atomic arrangement, structural response and anionic reversibility/stability [71–74]. Interestingly, the Jahn-Teller distortion of Mn<sup>3+</sup> could be well controlled by

structural symmetry and/or interfacial orbital ordering [71, 75, 76]. FMCs with different oxygen sublattices were also proposed and synthesized by a few groups. O2-type FMCs showed no obvious voltage decay, resulting from no layered-to-spinel phase transformation because of the difficulty for TM ions to migrate to octahedral sites in Li layers [77–79]. Mainly based on bulk redox, most FMCs displayed insufficient rate capability, which was limited by the slow Li-ion diffusion process in the electrodes; thus, some groups focused on the surface redox reaction, synthesized some intriguing FMCs and proposed a few unusual charge compensation mechanisms [80–82]. These materials and concepts give researchers much confidence and inspiration regarding the study of FMCs, greatly expanding the designable and exploitable space of excellent cathode materials.

### 3 Advantages of FMCs

FMCs have attracted much attention because of their many significant advantages. Cathode materials have proven to be the bottleneck in the building of better batteries considering their cost and electrochemical performance [7, 11]. The distributions of manufacturing costs and material costs at the cell level are shown in Fig. 2a. The cell manufacturing costs

are dominated by materials, which contribute to approximately 75% of the total cost, and the cathode material contributes to approximately 50% of all the material costs [11], as shown in Fig. 2a (the upper left corner). To achieve attractive cost structures and profit margins, low-cost and high-energy-density cathode material acquisition is essential. Figure 2b summarizes the price change trend of three common elements over the last two years. The price of Co fluctuates significantly, while there is a gradual increase in the Ni price and a relatively stable Mn price. However, the high cost and toxicity of cobalt compounds have prompted the development of alternative cathode materials. Nickel-rich cathode materials have been widely researched and gradually applied in the market due to their relatively high capacity and good stability; however, the single-cell price is still beyond expectations and still faces the problems stemming from oxygen evolution in a deeply delithiated state, as well as synthesis difficulties [23, 84–87]. In addition, it is expected that with the large-scale popularization of electric vehicles and energy storage grids, the price and consumption rate of Ni and Co resources will increase, and as reported by a few groups, once the Li-ion industry grows to 1 TWh of production per year, approximately one million t of cobalt/nickel combinations will be needed, thereby placing vast pressure on metal resources [6, 28]. Comparing the price of

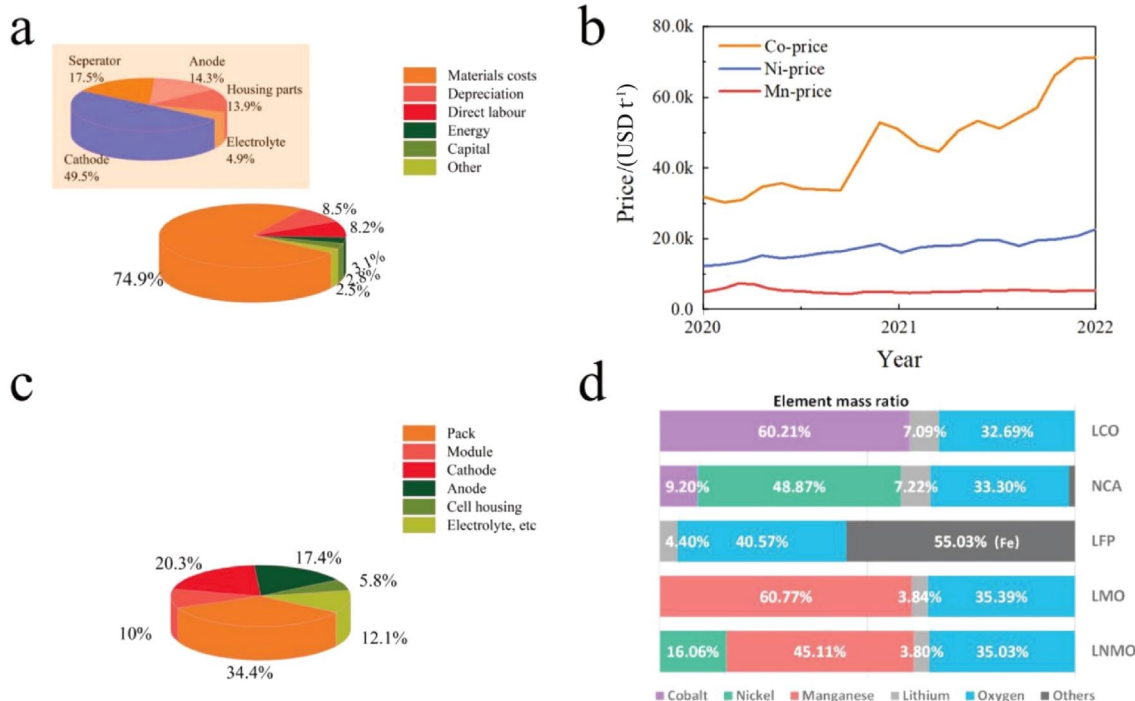


**Fig. 2** **a** The distribution of manufacturing costs at the cell level; the distribution of material costs is displayed in the upper left corner [11]. Data were taken from Ref. [11]. **b** Annual price of a few metal elements (source: <https://tradingeconomics.com/>). **c** A breakdown

of the mass content in a battery system [11]. Data were taken from Ref. [11]. **d** Elemental mass ratios in five common cathode materials. Adapted with permission from Ref. [83]. Copyright 2020 Elsevier

Mn with that of Co and Ni, the Mn price is far lower than the Co price and less than a quarter of the Ni price, as shown in Fig. 2b. On the other hand, the mass ratio of electrode materials in the battery module is near 40%, and the cathode material accounts for over 20% of the mass, as presented in Fig. 2c; the elemental mass ratios in different types of common cathode materials are exhibited in Fig. 2d, and Co and Ni account for a large proportion in layered oxide materials [83]. Therefore, constructing high energy density and low cost FMCMs by replacing Co and Ni with Mn could be a good alternative, which will significantly reduce the cost of batteries and powerfully promote the rapid development of lightweight or long-range electric vehicles.

Moreover, Li-Mn oxides and their derivatives with various components and structures, as shown in Table 1, can be utilized and part of which have been applied as FMCMs. These FMCMs exhibit a relatively high redox potential based on Mn redox, which is compatible with the current electrolyte system. Oxygen redox reactions can also occur in some Li-rich or Li-excess FMCMs, which further increases the practical release capacity [54, 55, 95]. Amazingly, some FMCM electrodes can even deliver an ultrahigh capacity of over 350 mAh g<sup>-1</sup> [27, 28], which is much higher than that of Ni/Co based cathode materials. Mn ions are also a type of polyvalent ions; thus, it is possible to manipulate the Mn redox couples from Mn<sup>2+</sup> to Mn<sup>5+</sup> [27], and even to Mn<sup>7+</sup> [96, 97], and studies have demonstrated that FMCMs are safer when overcharging occurs [25]. Therefore, there is no doubt that FMCMs are potential cathode candidates for next generation LIBs.

## 4 Structures of Common FMCMs

As mentioned above, the structural chemistry of FMCMs is very complex; fortunately, a variety of structures have been successfully synthesized and explored in detail, which also offers a wide selection for cathode material studies. Here, we focus on the structures of FMCMs commonly used in the field of LIBs and describe them accurately.

### 4.1 Spinel LiMn<sub>2</sub>O<sub>4</sub>

The most readily prepared lithiated manganese oxide is LiMn<sub>2</sub>O<sub>4</sub>, which has found some application in commercial LIBs. LiMn<sub>2</sub>O<sub>4</sub> does not have a layered crystal structure; instead, it exhibits a spinel structure [88, 98]. The spinel structure has been refined with space group  $Fd\bar{3}mm$ , whose face-centred cubic oxygen (the Wyckoff position of 32e site) array provides a three-dimensional (3D) array of edge-shared  $\lambda$ -MnO<sub>2</sub> octahedra for the Li-ions, and the stable 3D channels allow the fast diffusion of Li-ions. In detail, the tetrahedral (8a) and octahedral (16d) sites are occupied

by Li- and Mn-ions, respectively, which are indicated by the green LiO<sub>4</sub> tetrahedra and light blue MO<sub>6</sub> octahedra in Fig. 3a, so the atomic distribution of LiMn<sub>2</sub>O<sub>4</sub> can be written as [Li<sub>1</sub>]<sub>(8a)</sub>[Mn<sub>2</sub>]<sub>(16d)</sub>[O<sub>4</sub>]<sub>(32e)</sub>.

### 4.2 Stoichiometric LiMnO<sub>2</sub>

Stoichiometric LiMnO<sub>2</sub> is also a type of FMCM that has two common structures (layered and orthorhombic structures) used as cathode materials [46, 99]. The crystal structure of layered LiMnO<sub>2</sub> is similar to that of LiMO<sub>2</sub> (M = Co, Ni, etc.). LiMO<sub>2</sub> oxides crystallize in a completely ordered  $\alpha$ -NaFeO<sub>2</sub> rock-salt structure with rhombohedral ( $R\bar{3}m$ ) symmetry, in which the Li- and M-ions occupy the alternate (111) planes to give a layer sequence of O-Li-O-M-O along the *c* axis, thus yielding an A<sub>Li</sub>B<sub>M</sub>C<sub>Li</sub>A<sub>M</sub>B<sub>Li</sub>C (the capital letters, A, B, and C represent the oxygen sublattice in the rock-salt structure; the subscripts Li and M denote Li-layers and M-layers, respectively) array, and cations are located in octahedral sites [25, 100], as shown in Fig. 3b. There are three rigid MO<sub>2</sub><sup>(-)</sup> sheets formed by the M-ions and O-ions per unit cell, so the structure is an O3-type structure (O here referring to octahedral structure). The Li ions (octahedral sites) between the sheets are mobile; therefore, Li ions can be reversibly extracted/reinserted from/into the Li planes electrochemically, which forms fast two-dimensional (2D) Li-ion diffusion channels; furthermore, this structural material displays good electronic conductivity provided by the edge-shared MO<sub>6</sub> octahedral arrangement with a direct M-M interaction, depending on the electronic configuration of the M<sup>3+</sup> ions. As a consequence, various O3 structure layered LiMO<sub>2</sub> oxides have become attractive cathode materials, such as LiCoO<sub>2</sub>, ternary oxide, and Ni-rich cathode materials. The layered monoclinic LiMnO<sub>2</sub> (m-LiMnO<sub>2</sub>) is also an O3 structure oxide; however, it does not have a perfect  $\alpha$ -NaFeO<sub>2</sub> structure because of the cooperative Jahn-Teller (J-T) effect caused by all of the high-spin state Mn<sup>3+</sup> ions, leading to a monoclinic unit cell (the space group: *C2/m*), in which the lattice constants and angles are distorted because of the higher rhombohedral symmetry [25, 46], as shown in Fig. 3d. Additionally, it is not thermodynamically stable compared with o-LiMnO<sub>2</sub> [25, 39, 40]. The o-LiMnO<sub>2</sub> (the space group: *Pmnm*) has an ordered rock-salt structure, as shown in Fig. 3c. Interestingly, the LiO<sub>6</sub> and MnO<sub>6</sub> octahedra are arranged in corrugated layers, so o-LiMnO<sub>2</sub> is also called zig-zag layered LiMnO<sub>2</sub>.

### 4.3 Layered Li<sub>2</sub>MnO<sub>3</sub> (or Li[Li<sub>1/3</sub>Mn<sub>2/3</sub>O<sub>2</sub>])

The layered Li<sub>2</sub>MnO<sub>3</sub> (or Li[Li<sub>1/3</sub>Mn<sub>2/3</sub>O<sub>2</sub>]) has an oxygen stacking sequence analogous to that of LiMO<sub>2</sub>, as shown in Fig. 3e, whereas the TM layer is no longer a Mn-only layer. Twenty-five percent of the total amount of Li atoms

**Table 1** Common FCMCs and their related information

FMCs	Component	Structure	Space group	Redox couples	Theoretical capacity/ (mAh g <sup>-1</sup> )	Practical capacity/ (mAh g <sup>-1</sup> )	Middle voltage/V	References
Traditional FCMCs	LiMn <sub>2</sub> O <sub>4</sub>	Spinel	<i>Fd</i> $\bar{3}m$	Mn <sup>3.5+/4+</sup>	148	120 (3.0–4.3 V); 120 (3.5–4.45 V)	4.0	[88, 89]
	LiMnO <sub>2</sub>	Zigzag layered	<i>Pmmn</i>	Mn <sup>3+/4+</sup>	285	190 (2.5–4.2 V); 200 (2.0–4.5 V)	3.0	[90, 91]
		Layered	<i>C2/m</i>	Mn <sup>3+/4+</sup>	285	200 (3.4–4.3 V); 220 (2.0–4.5 V)	3.0 3.2	[46, 92]
	Li <sub>2</sub> MnO <sub>3</sub>	Layered	<i>C2/m</i>	O redox + Mn <sup>4+/3+</sup>	458	220 (2.0–5.0 V); 170	3.2	[60, 93]
Completely cation-disordered oxides	LiMnO <sub>2</sub>			Mn <sup>3+/4+</sup>	285	250	3.0	[69]
	Li <sub>2</sub> MnO <sub>3</sub>	Rock-salt	<i>Fd</i> $\bar{3}m$	O redox + Mn <sup>4+/3+</sup>	458	320 (1.5–4.8 V)	2.9	[70]
	Li <sub>4</sub> Mn <sub>2</sub> O <sub>5</sub>			Mn <sup>3+/5+</sup> + O redox	491	355 (1.2–4.8 V)	2.8	[27]
	Li <sub>2</sub> Mn <sub>2/3</sub> Nb <sub>1/3</sub> O <sub>2</sub> F			Mn <sup>2+/4+</sup> + O redox	401	304 (1.5–5.0 V)	3.1	[18]
Partially ordered oxides	Li <sub>1.68</sub> Mn <sub>1.6</sub> O <sub>3.7</sub> F <sub>0.3</sub>	Spinel-like	<i>Fd</i> $\bar{3}m$	Mn <sup>2+/3+/4+</sup> + O redox	273 (Vacancies not considered)	363 (1.5–4.8 V)	3.1	[28]
NaCl-type cation disordered Li <sub>2</sub> MnO <sub>3</sub> @LiMn <sub>2</sub> O <sub>4</sub>	Li <sub>2</sub> MnO <sub>3</sub> :Li <sub>0.5</sub> MnO <sub>2</sub> = 1:1	NaCl-Li <sub>2</sub> MnO <sub>3</sub> & Spinel-LiMn <sub>2</sub> O <sub>4</sub>	<i>Fd</i> $\bar{3}m$ & <i>Fd</i> $\bar{3}m$	Mn <sup>2+/3+/4+</sup> + O redox	303	388 (1.5–4.8 V)	3.0	[94]
Intralayer Li/Mn disordering in Mn layers	Li <sub>0.700</sub> Li <sub>0.222</sub> Mn <sub>0.756</sub> O <sub>2</sub>	Layered	<i>R</i> $\bar{3}m$	Mn <sup>3+/4+</sup> + O redox	308 (Vacancies not considered)	304 (2.0–4.8 V)	3.2	[71]
LMO consists of 0.48Li@Mn <sub>6</sub> ordering and 0.52Mn@Mn <sub>6</sub> structure units	Li <sub>0.83</sub> Mn <sub>0.84</sub> O <sub>2</sub>	Layered	<i>R</i> $\bar{3}m$	Mn <sup>3+/4+</sup> (octahedral Li <sup>+</sup> & tetrahedral Li <sup>+</sup> ) + O redox	265 (Charge capacity)	412 (1.3–4.9 V); 610 (0.6–4.9 V)	2.8	[72]
Li-O-vacancy LMO	Li <sub>4/7</sub> V <sub>1/7</sub> Mn <sub>6/7</sub> O <sub>2</sub>	Layered	<i>R</i> $\bar{3}m$	Mn <sup>2+/3+/4+</sup> + O redox	184 (Charge capacity)	312 (2.0–4.8 V)	3.0	[73]
Oxygen sublattice	Li <sub>3</sub> [Li <sub>1/4</sub> Mn <sub>3/4</sub> ]O <sub>2</sub>	Layered	<i>P63/mc</i>	Mn <sup>3+/4+</sup> + O redox	None	200 & 275 (2.0–4.8 V)	3.2	[77, 79]
Surface redox reaction	LiF-MnO	Rock-salt	<i>Fm</i> $\bar{3}m$	Mainly Mn <sup>2+/3+</sup> and Mn <sup>3+/4+</sup>	None	240 (1.5–4.8 V)	2.8	[81]

Table 1 (continued)

FMCMs	Component	Structure	Space group	Redox couples	Theoretical capacity/(mAh g <sup>-1</sup> )	Practical capacity/(mAh g <sup>-1</sup> )	Middle voltage/V	References
	Mn <sub>3</sub> O <sub>4</sub> -LiPF <sub>6</sub>	Spinel	<i>I41/amd</i>	F redox + Mn <sup>3+/2+</sup>	None	265 (1.5–4.8 V)	2.6	[82]
Interfacial orbital ordering	LiMnO <sub>2</sub>	Spinel-layered	<i>I41/amd</i> & <i>C2/m</i>	Mn <sup>3+/4+</sup> + O	285	254 (2.0–4.5 V)	3.2	[75]

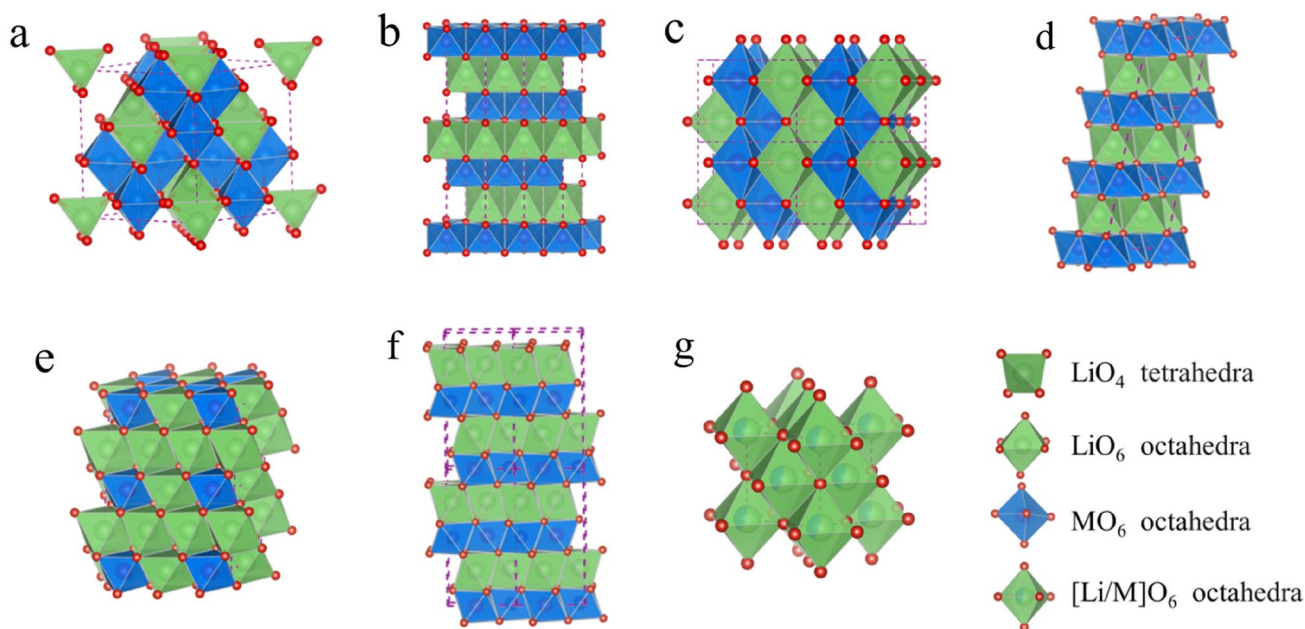


**Fig. 3** Structures of partially important FMCMs: **a** spinel LiMn<sub>2</sub>O<sub>4</sub> (*Fd* $\bar{3}mm$ ); **b** layered LiMO<sub>2</sub> (*R* $\bar{3}m$ ); **c** zigzag layered LiMnO<sub>2</sub> (*Pmmn*); **d** layered LiMnO<sub>2</sub> (*C2/m*); **e** Li<sub>2</sub>MnO<sub>3</sub> (*C2/m*); **f** O2-type layered LiMnO<sub>2</sub> (*P63/mc*); and **g** cation-disordered Li-Mn-oxide (*Fm* $\bar{3}mm$ )

are found in the simulation cell, replacing 33% of the total Mn sites (the Wyckoff position of the 2b site) to form an ordered Li-Mn mixing layer (Li<sub>1/3</sub>Mn<sub>2/3</sub> or LiMn<sub>2</sub>). This ordered arrangement and the difference in the Li/Mn ionic radius reduce its symmetry from *R* $\bar{3}m$  symmetry to monoclinic *C2/m* symmetry [58, 101–103]. Thus, its chemical formula can also be written as Li<sub>1.0(4b)</sub>Li<sub>0.5(2c)</sub>[Li<sub>0.5(2b)</sub>Mn<sub>(4g)</sub>](O<sub>1</sub>)<sub>4i</sub>(O<sub>2</sub>)<sub>8j</sub>.

#### 4.4 O2-Type FMCMs

Another layered FMCM is layered O2-type Li-Mn oxides. Delmas et al. first reported an O2-type LiCoO<sub>2</sub> with a unique ABCBAB oxygen packing in 2001 [104] that is thermodynamically metastable compared to layered O3-type LiCoO<sub>2</sub> with ABCABC oxygen packing. The meaning of “O” in O2-type here is the same as that in the

O3-type layered structure mentioned above (O refers to octahedral structure), and here, “2” means that the minimum number of MO<sub>2</sub><sup>(-)</sup> sheets required to describe its unit cell is “2”. The form of the LiO<sub>6</sub> octahedra and MO<sub>6</sub> octahedra connections in the O2-type structure is distinct from those in the O3-type structure. The LiO<sub>6</sub> octahedra share edges and faces with MO<sub>6</sub> octahedra in the O2-type structure, as shown in Fig. 3f, whereas for the O3-type structure, the LiO<sub>6</sub> octahedra share only edges with the MO<sub>6</sub> octahedra. More importantly, it is difficult for M ions to migrate from octahedral sites in the M layer to octahedral sites in the Li layer through tetrahedral sites. Even if the M-ion can migrate to the tetrahedral position, the large repulsive interaction between the migrated M-ions and the face-shared M-ions will impede further migration; thus, it is almost impossible for the layered-to-spinel phase transition to occur in O2-type FMCMs [78].

## 4.5 New-Type FCMCs

Recently, a new type of FCMC was reported with the introduction of percolation theory to LIBs [65, 105]. This cathode also has a rack-salt structure (the space group:  $Fm\bar{R}3m$ ) and a close-packed oxygen framework similar to that of a layered structure, but the atomic arrangements of Li- and M-ions are different. The Li- and M-ions in the layered structure occupy alternate (111) planes. For this new cathode, Li- and M-ions are mostly randomly distributed in metal layers, i.e., the so-called cation-disordered rock-salt cathode materials, as shown in Fig. 3g.

## 5 Issues and Challenges of FCMCs

### 5.1 Common Issues

Although FCMCs exhibit considerable attraction because of their significant advantages, various barriers still exist and greatly hinder the penetration of FCMCs into the market due to the electronic, coordination structure of Mn ions and electrodes' crystal structure [30, 40]. Most common TM oxide cathodes have six ligands symmetrically arranged around their central TM atoms, leading to octahedral (Oh) coordination [100, 106]. According to ligand field theory, the five 3d orbitals in the octahedral environment split into two degenerate orbitals, generally,  $t_{2g}$  orbitals ( $3d_{xy}$ ,  $3d_{yz}$ , and

$3d_{xz}$ ) and  $e_g$  orbitals ( $3d_{x^2-y^2}$  and  $3d_{z^2}$ ), as shown in Fig. 4a (left). However, due to the high-spin state  $Mn^{3+}$  ion, whose electron distribution is  $t_{2g}^3e_g^1$ , the ligand field in high-spin state  $Mn^{3+}$ -containing Li-Mn oxides distorts the six-equivalent M–O bonds (left) into four shorter equatorial bonds and two longer axial bonds (right), which further splits the energy level of d orbitals, as indicated in Fig. 4a. This phenomenon is called J-T distortion [112, 113], which involves the partial removal of the atoms' d-electron degeneracy in a crystal field and then reduces the lattice symmetry. Cooperative J-T distortion further significantly impacts the symmetry of the electrodes' crystal structure, which accounts for the lack of ideal layered  $R\bar{3}m$   $LiMnO_2$  [76, 113–115]; for spinel  $LiMn_2O_4$ , the unit cell volume change is too drastic for the electrodes to maintain structural integrity during continuous cycles, which is one important reason for the rapid capacity degradation in the spinel  $LiMn_2O_4$  electrode through the 3.0 V region [30, 36].

Another common problem is Mn-ion dissolution, which is a challenging issue in most Mn-based cathode materials. It directly compromises the crystal structural integrity, greatly degrading the capacity and cycle performance of batteries; moreover, the dissolved Mn ions will migrate through the liquid electrolyte and deposit on the surface of the anode material, causing serious damage to the solid electrolyte interface (SEI) film formed between the electrolyte and the anode materials, further decreasing the batteries' electrochemical performance [116, 117]. Many studies have been

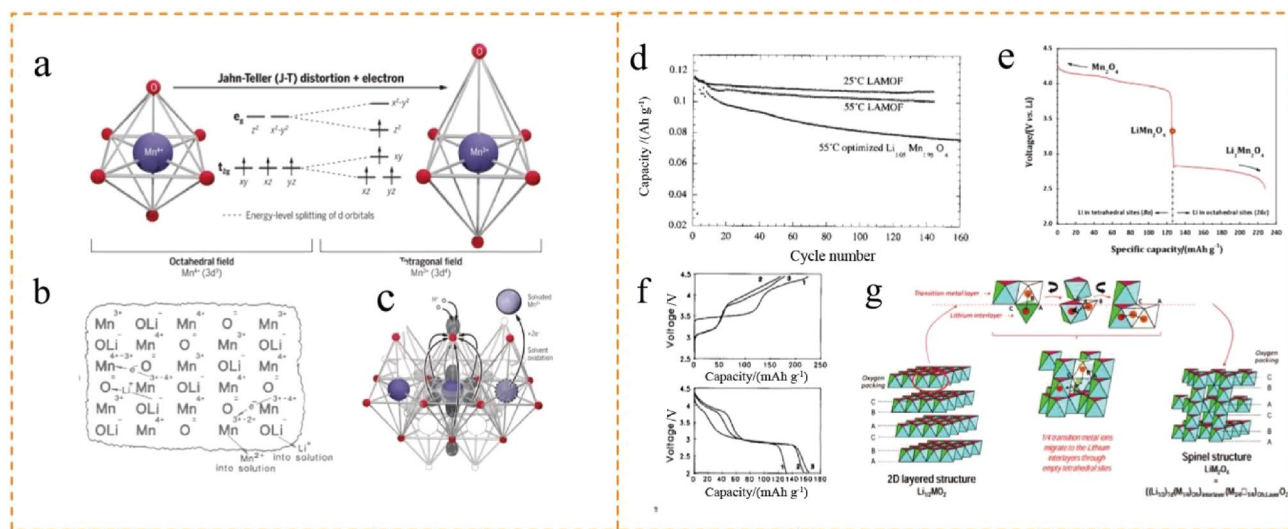


**Fig. 4** Common issues and challenges of FCMCs. **a** Jahn-Teller distortion of the high spin state  $Mn^{3+}$ . Adapted with permission from Ref. [106]. Copyright 2020 American Association for the Advancement of Science. **b** Adapted with permission from Ref. [98]. Copyright 1981 Elsevier. **c** Two main mechanisms of Mn-ion dissolution. Adapted with permission from Ref. [106]. Copyright 2020 American Association for the Advancement of Science. **d** Capacity retention of optimized and nonsubstituted spinel/Li cells at different temperatures.

Adapted with permission from Ref. [107]. Copyright 1999 Elsevier. **e** Voltage profile of  $LiMn_2O_4$  during discharging to the 3.0 V range. Adapted with permission from Ref. [108]. Copyright 2013 American Chemical Society. **f** Galvanostatic cycling curves of Li/LiMnO<sub>2</sub> cells. Adapted with permission from Ref. [109]. Copyright 1993 Elsevier. **g** Scheme of Mn migration and layered-to-spinel transition in layered  $LiMnO_2$ . Adapted with permission from Ref. [110]. Copyright 2015 American Chemical Society



conducted in this area, but there is no consensus on the mechanism of Mn-ion dissolution. According to previous studies, the following two main Mn-ion dissolution mechanisms were proposed: (i) a disproportionation reaction of  $\text{Mn}^{3+}$  ( $2\text{Mn}^{3+} \rightarrow \text{Mn}^{4+} + \text{Mn}^{2+}$ ) occurred, and then  $\text{Mn}^{2+}$  dissolved in the electrolyte, as shown in Fig. 4b [89, 98, 118]; or (ii) corrosion of cathode materials occurred due to acidic substances in the electrolyte, causing Mn-ion dissolution, as shown in Fig. 4c [119–121]. Both mechanisms are correlated with J-T distortion, and J-T distortion may facilitate the disproportionation reaction of  $\text{Mn}^{3+}$  and/or induce higher reactivity with an acid (such as HF that is generated in the electrolyte due to the hydrolysis of the  $\text{LiPF}_6$  salt) [122–124], thus increasing Mn-ion dissolution in LIBs [106, 125]. However, a few groups found that as the electrode became overcharged, the dissolved  $\text{Mn}^{2+}$  ion concentration also increased rapidly. The maximum dissolution occurs at the end of charging, where the Mn-ion oxidation state is  $4+$ , indicating that there is some other significant mechanism in addition to the ion disproportionation reaction. The intrinsic instability in the delithiated state results in the loss of  $\text{MnO}_x$  to form a stabler single phase structure that cannot be ignored [126, 127]. Furthermore, the interface reaction between highly active delithiated  $\text{MnO}_x$  and the electrolyte deserves sufficient attention. These challenging issues occur in almost all FCMs and significantly impact the structural evolution and electrochemical performance of FCMs and need to be deeply studied and resolved.

## 5.2 Problems of Spinel $\text{LiMn}_2\text{O}_4$

Spinel  $\text{LiMn}_2\text{O}_4$  can cycle well in the 4.0 V range at room temperature. In the completely delithiated state,  $\text{Mn}_2\text{O}_4$  is also a spinel structure, and thanks to the strong edge-shared octahedral  $\text{Mn}_2\text{O}_4$  array, Li ions can reversibly insert into/extract from the tetrahedral sites without destroying its spinel 3D framework [123, 128]. However, when cycled at an elevated temperature, the performance degrades rapidly, as shown in Fig. 4d, which is usually attributed to the dissolution of Mn ions into the electrolyte, electrolyte decomposition at high voltages, and/or irreversible phase transition caused by J-T distortion in the lithiated state [26, 88, 107, 129, 130]. The reasons for the performance degradation mentioned above are not independent but more likely a synergistic effect of all the following: J-T distortions facilitate the disproportionation of  $\text{Mn}^{3+}$ , inducing higher reactivity with acids, and  $\text{Mn}^{4+}$  can attack the electrolyte and cause electrolyte decomposition. When discharged to a lower voltage (3.0 V) range, extra Li ions can be inserted into the empty 16c octahedral sites, which provide another 145 mAh  $\text{g}^{-1}$  capacity. Nevertheless, the Li ions in 8a tetrahedral sites share a common face with Li ions in 16c octahedral sites; thus, strong electrostatic repulsion

causes Li ions in 8a tetrahedral sites to displace into the adjacent empty 16c octahedral sites (8a-to-16c), resulting in an ordered rock salt structure with a new ion distribution of  $[\text{Li}_2]_{(16c)}[\text{Mn}_2]_{(16d)}[\text{O}_4]_{(32e)}$  [108, 128]. The collective Li-ion migration from the 8a to 16c sites results in a first-order phase transition and a low voltage plateau when the electrode is lithiated over the  $\text{LiMn}_2\text{O}_4$  composition [108], which increases the difficulty of battery system management in actual applications, as shown in Fig. 4e; furthermore,  $\text{LiMn}_2\text{O}_4$  electrodes cycle poorly in the 3.0 V range as a result of the destruction of the integrity of the spinel framework. Meanwhile, the Li-ion diffusion pathway is blocked by the J-T distortion and the mismatch between the tetragonal and cubic lattices, leading to sluggish kinetics and capacity deterioration during cycling [25].

## 5.3 Problems of $\text{LiMnO}_2$

$\text{LiMnO}_2$  suffers greatly from the J-T effect because all Mn ions here are trivalent valences of the high-spin state. In both polymorphs of  $\text{LiMnO}_2$  mentioned above, m- and o- $\text{LiMnO}_2$ , the sublattice of oxygen anions is distorted at room temperature from ideal cubic-close-packing as a result of the cooperative J-T effect [99]. Considering the synthesis conditions, they can be further divided into the following two categories: low temperature (LT) m/o- $\text{LiMnO}_2$  materials and high temperature (HT) m/o- $\text{LiMnO}_2$  materials. LT o- $\text{LiMnO}_2$  shows relatively better cycling stability achieved by cycling on either the 4.0 or 2.8 V plateau [131]; nevertheless, roughly half of its theoretical capacity can be released, which defeats the purpose of obtaining high energy density. Cycling over both plateaus, the LT o- $\text{LiMnO}_2$  electrodes can provide a relatively high capacity of 190 mAh  $\text{g}^{-1}$ , while the capacity retention with extended cycling appeared to be poor [132]. The HT o- $\text{LiMnO}_2$  materials generally exhibited better stability than the LT phases over a wide voltage range [25, 90, 131, 133–136]. Unfortunately, all the stoichiometric  $\text{LiMnO}_2$  FCMs experienced a severe layered-to-spinel phase transition under the cycling process, as shown in Fig. 4f [109]. Moreover, it has been found that charging o- $\text{LiMnO}_2$  electrodes to a higher voltage (a deeper delithiated state) increases the speed of this transformation, which limits the reversible capacity that can be utilized practically [25]. m- $\text{LiMnO}_2$  is of high commercial and scientific interest because its structure is analogous to that of the successfully commercialized  $\text{LiCoO}_2$  cathode material, and the cost of manganese is far less than that of cobalt. Stoichiometrically pure m- $\text{LiMnO}_2$  was first prepared by a “soft” chemistry method—Li/Na ion-exchange, and later, Tabuchi et al. reported another “soft” chemistry method—hydrothermal synthesis of layered m- $\text{LiMnO}_2$ . m- $\text{LiMnO}_2$  is not a thermodynamically stable structure;

thus, HT stoichiometric  $m\text{-LiMnO}_2$  is almost nonexistent.  $m\text{-LiMnO}_2$  prepared by “soft” chemistry methods, here referred to as LT  $m\text{-LiMnO}_2$ , delivered a considerable capacity ( $> 200 \text{ mAh g}^{-1}$ ); however, they did not cycle sufficiently, and subsequent discharges showed declining capacity and continuous layered-to-spinel phase transition [46]. Ceder et al. [110, 111, 137] proposed that the transformation of delithiated  $\text{Li}_x\text{MnO}_2$  layered materials into spinel occurred in two processes, as shown in Fig. 4g. Specifically, in the first stage, a significant portion of the Mn ions rapidly migrate into tetrahedral positions surrounded by Li vacancies when the material is partially delithiated, forming a metastable intermediate. The activation barriers for this are calculated to be low, partly because the Mn migration into a tetrahedral site is assisted by the charge disproportionation of  $\text{Mn}^{3+}$  ( $2\text{Mn}^{3+}_{\text{oct}} \rightarrow \text{Mn}^{2+}_{\text{tet}} + \text{Mn}^{4+}_{\text{oct}}$ ). In the second stage, the tetrahedral Mn ions and the remaining octahedral Li ions perform a coordinated rearrangement to form the final spinel phase, which is slower because of its complexity and higher activation barriers. Layered-to-spinel transformation directly influences the voltage profile, and a two-plateau voltage profile appears, which is obviously different from that in other layered  $\text{LiMO}_2$  ( $M = \text{Ni, Co, etc.}$ ) cathode materials and increases the difficulty of battery state monitoring.

## 5.4 Problems of $\text{Li}_2\text{MnO}_3$ and $\text{Li}_2\text{MnO}_3$ -Based Materials

Layered  $\text{Li}_2\text{MnO}_3$  is another important FCMC with a theoretical capacity of  $458 \text{ mAh g}^{-1}$ . Generally, well-crystallized  $\text{Li}_2\text{MnO}_3$  does not exhibit any electrochemical activity under normal conditions; however, when cycled at higher temperatures, it will deliver considerable reversible capacity. Furthermore,  $\text{Li}_2\text{MnO}_3$  with oxygen vacancies, stacking faults or nanostructures also shows obvious electrochemical activity [57–60]. Understanding the origin of the anomalous first charge capacity of  $\text{Li}_2\text{MnO}_3$  and other  $\text{Li}_2\text{MnO}_3$ -based materials presents a challenge and is still controversial. It has been demonstrated that it is difficult to oxidize  $\text{Mn}^{4+}$  ions in  $\text{Li}_2\text{MnO}_3$  to  $\text{Mn}^{5+}$  [138]; however, some research groups believe that  $\text{Mn}^{4+/7+}$  redox occurs at high potential accompanied by Mn-ion migration to tetrahedral sites [96, 97], which cannot be ruled out because  $\text{Mn}^{7+}$  ions might be in a metastable state or serve as a reaction intermediate for the oxidation of the  $\text{O}^{2-}$  ions forming molecular  $\text{O}_2$  trapped in the particles that is difficult to characterize.

Ceder et al. [54] proposed that the O 2p orbitals along the Li-O-Li configuration form unhybridized O 2p states, whose energy is higher than that of bonding O states, and thus can be more easily oxidized, as shown in Fig. 5a and b. The labile electron from unhybridized O 2p states along the Li-O-Li configurations is the source of the extra capacity

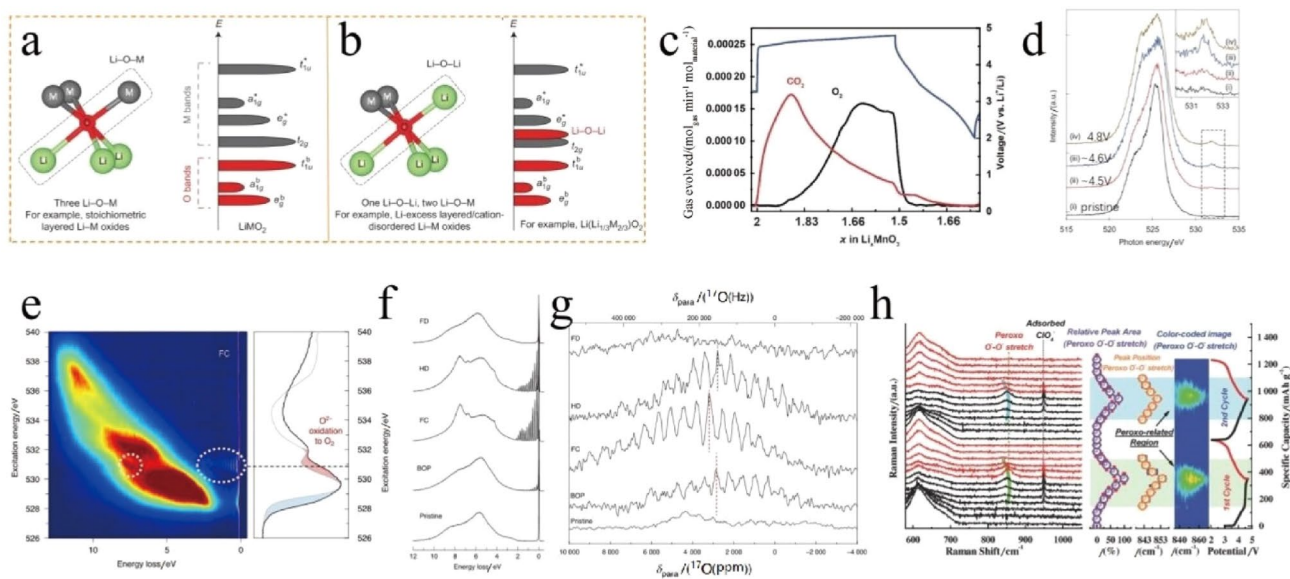


**Fig. 5** **a** Hybridization of O 2p orbitals with the M d/s/p orbital. **b** Li-O-Li configuration and unhybridized O 2p orbital. Adapted with permission from Ref. [54]. Copyright 2016 Nature. **c** Voltage profile and gas evolution of pure  $\text{Li}_2\text{MnO}_3$ . Adapted with permission from Ref. [139]. Copyright 2020 American Chemical Society. **d** RIXS spectra on the O K-edge of  $\text{Li}_{1.2}\text{Ni}_{0.13}\text{Co}_{0.13}\text{Mn}_{0.54}\text{O}_2$  (excitation energy = 531.8 eV). Adapted with permission from Ref. [140].

Copyright 2016 Nature. **e** HR-RIXS map and O K-edge partial fluorescence yield sXAS data for  $\text{Li}_{1.2}\text{Ni}_{0.13}\text{Co}_{0.13}\text{Mn}_{0.54}\text{O}_2$  at full charge. **f** HR-RIXS spectra (excitation energy = 531 eV) and **g** solid-state  $^{17}\text{O}$  MAS-NMR spectra at different charge states. Adapted with permission from Ref. [141]. Copyright 2020 Nature. **h** In situ Raman spectra of  $\text{Li}_{1.2}\text{Ni}_{0.2}\text{Mn}_{0.6}\text{O}_2$ . Adapted with permission from Ref. [142]. Copyright 2018 Wiley-VCH

beyond the theoretical TM redox capacity in Li-excess materials, which is now widely accepted. However, new debates have arisen over the specific forms of the oxidized O species. Bruce et al. [139] proposed that singlet  $O_2$  could be produced at high voltage and interact with the electrolyte to generate  $CO_2$ . Once the oxide ions were uncoordinated, the O-loss would dominate the oxygen evolution [143]. For  $Li_2MnO_3$ , they quantitatively demonstrated that Li extraction was only charge compensated by oxygen loss (O-loss) at the shells of the particles during the first charge process rather than the oxidation of the  $O^{2-}$  ions that were retained within the crystal framework (O-redox) according to the operando mass spectroscopy (Fig. 5c) and  $^6Li$  NMR spectra results. This result was confirmed by Zhou et al. [144–146], who also emphasized that the combination of surface carbonate species decomposition and oxygen release, both in the near-surface region, accounted for the first charge plateau of  $Li_2MnO_3$ . However, interestingly, some groups found that partial reversible oxygen redox was observed in  $Li_2MnO_3$  [68, 147, 148]. Li-rich cathode materials exhibited significant differences in the reversibility of O redox with pure  $Li_2MnO_3$ . Bruce et al. [140] demonstrated that in addition to oxygen loss, the removal of  $Li^+$  was charge compensated through the generation of localized electron holes on oxygen rather than the formation of true  $O_2^{2-}$  dimer species by combining various advanced characteristic technologies, such as resonant inelastic X-ray scattering spectroscopy (RIXS, Fig. 5d), soft X-ray absorption spectroscopy (sXAS), Raman spectroscopy and X-ray absorption near edge structure spectroscopy. They further characterized molecular  $O_2$  by RIXS and  $^{17}O$  magic angle spinning nuclear magnetic resonance (MAS-NMR) spectroscopy [141], as shown in Fig. 5e–g, which formed within the Li-rich cathode particles upon the oxidation of  $O^{2-}$  at a potential of 4.6 V (vs.  $Li^+/Li$ ) during the charge process and could be reduced back to  $O^{2-}$  during discharge but at the lower voltage of 3.75 V. In contrast, Zhou et al. [142] believed that for a typical Li-rich  $Li_{1.2}Ni_{0.2}Mn_{0.6}O_2$  cathode material,  $O^-O^-$  peroxy oxygen dimers and the reversible  $O^{2-}/O^-$  redox process were demonstrated by applying in situ technologies such as Raman spectroscopy and X-ray diffraction (XRD), as presented in Fig. 5h. Interestingly, Xia et al. [149] discovered that the oxygen redox reaction can be responded to in the form of the telescopic O-Ru-O configuration by local symmetry manipulation rather than O-O dimerization. Altogether, there are still a few mysteries and controversies surrounding the charge mechanism in  $Li_2MnO_3$  and  $Li_2MnO_3$ -based cathode materials [150], and more work needs to be done, especially on the specific forms and evolution of the oxidized O species during the cycle process. On the other hand, in both pure  $Li_2MnO_3$  and Li-rich cathode materials, O-loss appears, and the amount of pure oxygen redox leads to the evolution of much  $O_2$  gas or  $CO_2$  gas [30, 139, 151], which

was characterized by differential electrochemical mass spectrometry (DEMS), as shown in Figs. 5e and 6a, resulting in an irreversible structure transition, formation of a surface dense phase and poor electrochemical activity [60, 103, 139].

Furthermore,  $Li_2MnO_3$  has a large bandgap and sluggish O redox, leading to poor rate performance and making it less attractive to the industry [153–156]. Therefore, researchers have paid more attention to  $Li_2MnO_3$ -based materials, mainly Li-rich cathodes ( $Li_2MnO_3^*LiMO_2$ ,  $M=Ni, Co, Mn$  et al.), which exhibit better electrochemical performance due to the introduction of Ni, Co and other active elements with layered  $LiMO_2$  structures. Li-rich cathodes can release higher capacity by combining cationic TM redox with anionic O redox rather than pure O redox in  $Li_2MnO_3$  and have quite good cycle stability [95, 157, 158]. However, Li-rich cathodes exhibited obvious voltage decay during subsequent cycles [152, 158–162], as shown in Fig. 6b. Voltage decay is a unique problem in Li-rich cathodes compared with other cathode materials. Its major detrimental effect is the difficulty of building an effective battery management system; additionally, the practical output energy density decreases as the voltage fades, thus greatly hindering commercial applications of Li-rich cathodes [159, 163].

Another challenging issue in  $Li_2MnO_3$ -based materials is the less-studied voltage hysteresis. Voltage hysteresis causes huge energy loss and presumably dissipated in the form of heat, consequently resulting in additional energy costs for the end user, which also complicates the thermal management and state monitoring of batteries [160, 164–168]. Generally, voltage hysteresis can be roughly regarded as the charge and discharge voltage deviating from the equilibrium potential under the same Li content, which has the following two origins: dynamic and thermodynamic [169, 170]. Voltage hysteresis originating from dynamic origins, the so-called overpotential, can be decreased either by reducing the impedance resulting from charge transport or by reducing the current density and can be so small that it almost vanishes when the current is decreased to a sufficiently small value [169]. The thermodynamic origin hysteresis is usually path dependent, originating from the asymmetric reaction pathways during the charge/discharge process, and consequently, has different intermediate phases with different Gibbs free energies that show different charge/discharge voltage values, which is a thermodynamic hysteretic characteristic [171, 172]. Early researchers found that the first cycle voltage curve of an  $Li_2MnO_3$ -based cathode material is significantly different from the following cycle curves [95, 165], as shown in Fig. 6c and d. The 4.5 V plateau and lower initial Coulombic efficiency, as shown in Fig. 6c, was explained by the activation of the  $Li_2MnO_3$  component, accompanied by O-redox, O-loss and ion rearrangement. However, more details about the ion rearrangement are still needed [173–175], and there

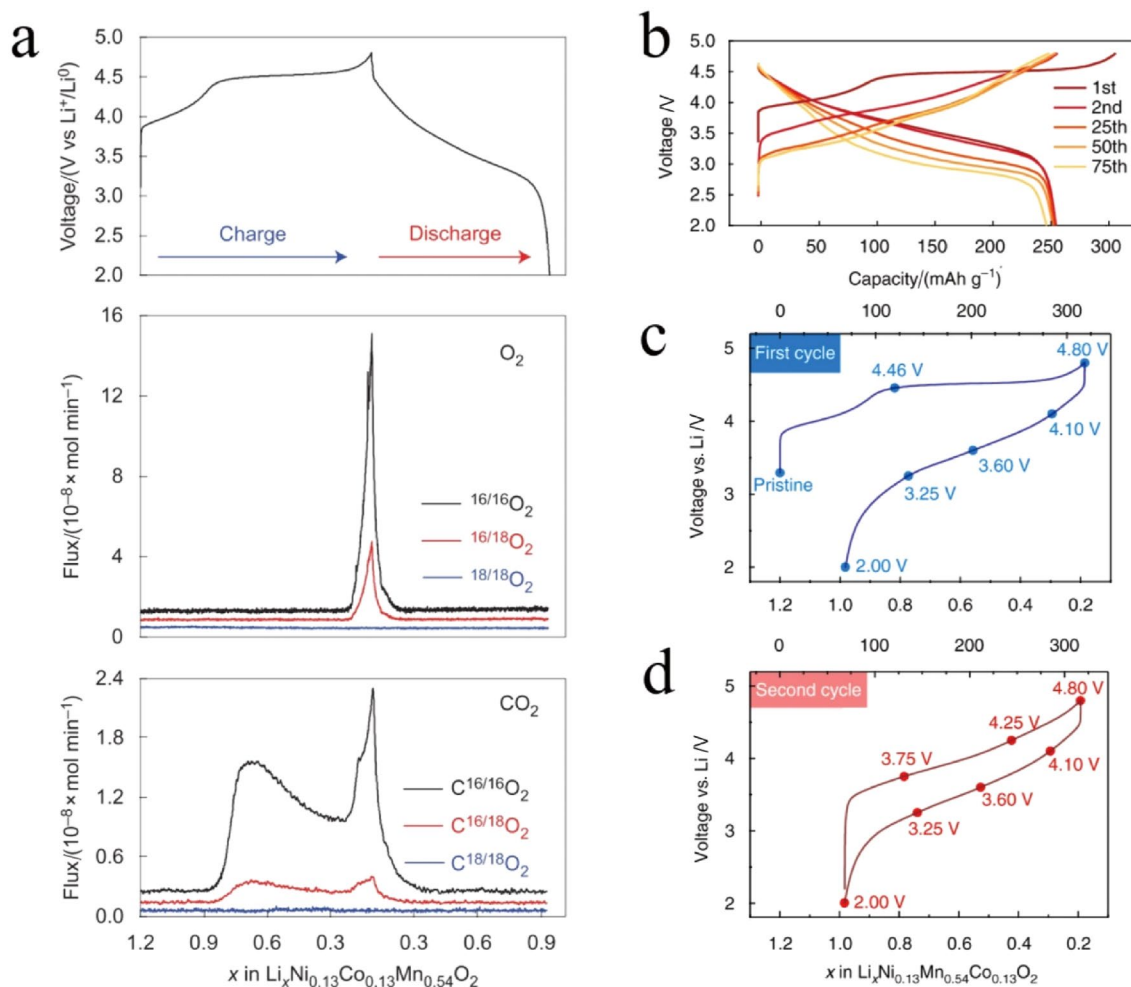


**Fig. 6** Issues and challenges in Li<sub>2</sub>MnO<sub>3</sub>-based materials: **a** O<sub>2</sub> evolution; adapted with permission from Ref. [140], copyright 2016 Nature; **b** voltage decay; adapted with permission from Ref. [152],

copyright 2018 Nature; **c** voltage curve of the first cycle and **d** second cycle for the Li-rich cathode material; adapted with permission from Ref. [95], copyright 2017 Nature

is still no direct characterization to quantify the relationship between the structural response and performance curves. Furthermore, it was puzzling that galvanostatic intermittent titration technique (GITT) results showed that the charge/discharge voltage in Li-rich cathodes with the activation of the Li<sub>2</sub>MnO<sub>3</sub> component did not return to the same equilibrium potential after sufficient relaxation time, and the voltage gap was approximately 200 mV, which was in contrast with that in common layered LiMO<sub>2</sub> (M = Co, Ni, etc.) cathodes or Li-rich cathodes without Li<sub>2</sub>MnO<sub>3</sub> component activation [160, 165, 170]. Moreover, researchers also observed the following interesting phenomenon: generally, when heating an electrode system, the slow Li-ion diffusion and migration process in a solid matrix could be accelerated. However, Ohzuku et al. found that the hysteresis loop observed in a Li-rich cathode material at 55 °C was larger than that at room temperature [176]. These results suggest that voltage hysteresis in Li<sub>2</sub>MnO<sub>3</sub>-based Li-rich cathode materials is

nonnegligible, significantly different from other traditional layered cathodes and more complicated. The origin of voltage hysteresis in Li<sub>2</sub>MnO<sub>3</sub>-based Li-rich cathodes and the corresponding solution urgently needs to be developed.

## 6 Strategies and Progress

### 6.1 For Spinel LiMn<sub>2</sub>O<sub>4</sub>-Based Cathodes

As mentioned above, when the spinel LiMn<sub>2</sub>O<sub>4</sub> electrode experiences a low voltage discharging process, it will show a two-voltage plateau, fast capacity degradation and poor rate capability. Therefore, spinel LiMn<sub>2</sub>O<sub>4</sub> electrodes are currently mainly cycled in the 4.0 V range when used as commercial cathode materials. However, they still suffer from significant capacity deterioration at elevated temperatures, which is strongly related to Mn dissolution caused

by Mn-ion J-T distortion and/or disproportionation reactions. Therefore, methods that can restrain Mn dissolution are provided to enhance the electrode performance [107]. According to its formula, half of the Mn ions are high-spin state  $Mn^{3+}$  ions; thus, strategies used to increase the average valence of Mn ions could work effectively, such as the use of a monovalent cation (mainly  $Li^+$ ) or divalent cation doping ( $Mg^{2+}$ ,  $Zn^{2+}$ , etc.) [177–180]. Certainly, trivalent cation doping is also common and effective and can be divided into the following two parts: inactive trivalent cation doping and active trivalent cation doping.  $Al^{3+}$  was early and widely used as an inactive doping ion [181, 182]. The calculated Al–O bonding was much stronger than Mn–O bonding [26]; thus,  $Al^{3+}$  substitution might suppress the expansion or contraction of the spinel during Li insertion/extraction. Ga, La, etc. [183, 184] were also used to improve the electrode performance; however, because those ions did not have electrochemical activity, the practical capacity was reduced. Active ions, such as Cr, Co, and Ni, were also used as doping ions [185]. The cycle stability of Cr-doped materials is improved by stronger Cr–O bonds [186], suppressed local distortion ( $MO_6$  octahedra), and decreased volume shrinkage. Co ions and Ni ions partially replaced Mn ions in  $LiMn_2O_4$  [185, 187–189]; thus, the proportion of  $Mn^{4+}$  ions increased and the J-T distortion caused by high-spin  $Mn^{3+}$  ions was also suppressed, leading to better capacity retention than that achieved with undoped spinels, and more Co or Ni ion doping will build high-voltage spinel cathodes [190–198], which will not be discussed in this paper. Tetravalent or higher valence cation doping was also investigated; however, the incorporation of high-valent ions might accelerate Mn dissolution in the doped spinel material due to the increase in the  $Mn^{3+}/Mn^{4+}$  ratio [199, 200]. Certainly, studies have also developed multiple ion doping methods, such as combining different TM ions or anion–cation cooping [183, 201–204], because these ions could cooperate with others to enhance the electrochemical performance to some extent. In recent years, some progress has been made in the research of blending modified cathode materials, which has proven to be a promising approach to improve the electrochemical performance in battery production processes. For  $LiMn_2O_4$ , researchers found that blending  $LiMn_2O_4$  with other cathode materials, such as  $LiCoO_2$ ,  $LiFePO_4$  and Ni-based cathodes [205–209], can inhibit the dissolution of Mn ions and improve the thermal stability of these materials, greatly promoting the wider application of  $LiMn_2O_4$  cathode materials.

Because Mn dissolution usually occurs at the surface of the electrode, surface modifications [210–213], such as coating and surface doping, are another controllable and effective approach to stabilize the cathode/electrolyte interface (CEI) and/or create an artificial protective layer that prevents the dissolution of Mn in the  $LiMn_2O_4$  spinel. Inactive oxides, fluorides, or phosphates are common

coating materials that work as HF scavengers to effectively suppress HF damage and hinder the spinel particles from directly contacting the electrolyte, thus inhibiting Mn dissolution and maintaining structural integrity during cycling [214–221]. Surface ion doping, such as with Ni, Al and Mg [210, 222, 223], greatly enhanced the electrode stability. Furthermore, many functional electrolyte additives, such as tris(trimethylsilyl) borate, vinylene carbonate, and succinic anhydride [224–226], were developed to eliminate HF and  $H_2O$ , thus modifying the solid (the anode and cathode)-electrolyte-interface layer and further promoting the wide application of  $LiMn_2O_4$ -based materials.

## 6.2 For $LiMnO_2$ -Based Cathodes

None of the  $LiMnO_2$  materials mentioned in Sect. 4.2 displayed sufficient electrochemical performance. To the best of our knowledge, methods applied to enhance the performance of the o- $LiMnO_2$  structure are limited [91, 134, 227–232], and m- $LiMnO_2$  has received much more attention [25]. LT layered m- $LiMnO_2$  exhibited rapid capacity fading and severe layered-to-spinel transformation during subsequent cycles [46, 47]. Later, Bruce et al. further reported that partial replacement of Mn with Co or Ni in the  $NaMnO_2$  precursor can significantly enhance the cycling stability and rate capability of the  $LiMnO_2$ -based material through ion exchange [233–239]. Interestingly, the ion-exchange samples with approximately 10% Co or Ni substitution exhibited  $R\bar{3}m$  lattice symmetry rather than  $C2/m$  lattice symmetry, and the layered-to-spinel transformation was also slowed. It should be noted that the soft chemistry method is not an industrial solution, as the cost is too high. HT m- $LiMnO_2$  is more attractive, but pure m- $LiMnO_2$  is almost impossible to use at high temperatures; thus many groups were in search of high Mn-based m- $LiMnO_2$  with small amounts of other doped metal ions [240–242]. Researchers found that a stable layered m- $LiMnO_2$  structure could be synthesized at high temperatures ( $> 900$  °C) by substituting 5%–10% of the Mn with  $Al^{3+}$ ,  $Cr^{3+}$  or  $Ga^{3+}$  ions [25, 243–246]. The HT Al/Ga-substituted  $LiMnO_2$  showed that the substituted elements served only to slow the transformation from a layered to spinel structure but did not prevent it from occurring. However, Cr substitution was particularly effective in inhibiting the layered to spinel phase transition, but the cycling sample underwent the first stage of this transformation, which was discussed in Sect. 5.3, and showed that a portion of the Mn ions were displaced in a disorderedly way from the initial octahedral sites to the tetrahedral sites located between the TM and Li layers [243]. Moreover, Cr ions are highly biotoxic. Sufficient Ni and/or Co doping makes a remarkable difference; however, such materials are no longer inexpensive compared with FMCMs, although they have been extensively used in electric vehicles [247–249]. Overall, there

has been some progress in the stabilization of  $\text{LiMnO}_2$  electrodes, but more studies are needed.

### 6.3 $\text{Li}_2\text{MnO}_3$ -Based Cathodes

Pure  $\text{Li}_2\text{MnO}_3$  undergoes severe  $\text{O}_2$  release, side reactions and phase transitions and does not show the expected performance; thus, the modification of  $\text{Li}_2\text{MnO}_3$  is relatively low and does not show a significant effect.  $\text{Li}_2\text{MnO}_3$ -based Li-rich cathode materials (or  $\text{Li}_2\text{MnO}_3 \cdot \text{LiMO}_2$ ;  $\text{M} = \text{Mn}, \text{Co}, \text{Ni}, \text{etc.}$ ) have received increasing attention since they were first put forwards due to their higher energy density based on cationic and anionic redox, although their structures were more complicated. Some researchers proposed that  $\text{Li}_2\text{MnO}_3$ -based Li-rich cathode materials are composed of  $C2/m$   $\text{Li}_2\text{MnO}_3$  and  $R\bar{3}m$   $\text{LiMO}_2$  nanocomposite phases [157, 250–252], but many believed they are composed of a  $C2/m$  or  $R\bar{3}m$  solid solution [253–255]. Furthermore,  $\text{O}_2$  release resulting from  $\text{Li}_2\text{MnO}_3$  component activation also appeared in Li-rich cathode materials. Modifications, such as doping, coating and surface treatment [256–261], were adopted by many groups to reduce the oxygen activity or impede  $\text{O}_2$  gas generation to advance the electrochemical performance of Li-rich cathode materials, and some good results were obtained.

Voltage decay is an important and challenging issue hindering the application of Li-rich cathode materials, as mentioned above; therefore, many studies have investigated the origin and mechanism of voltage decay, and various attempts have been made to address this problem. Actually, Li-rich cathode materials can cycle well at low charge cut-off voltages of  $< 4.5$  V without voltage decay or hysteresis, where the  $\text{Li}_2\text{MnO}_3$  component is not activated; however, this is at the cost of losing much capacity. Almost all problems occurring in Li-rich cathode materials originate from the activation of  $\text{Li}_2\text{MnO}_3$  accompanied by oxygen redox evolution and TM-ion rearrangement. Tarascon et al. [163] proposed that TM migration between TM layers and Li layers (TM ions trapped in tetrahedral sites) was an intrinsic feature of the electrochemical process and showed a strong correlation between TM migration and voltage decay. Chen et al. [155, 262] proposed that the oxygen vacancies and the Li vacancies generated during the extraction of Li ions were responsible for Mn ion migration into the Li layer, which accounted for the voltage decay of  $\text{Li}_2\text{MnO}_3$ . A considerable number of researchers tended to associate this voltage decay in Li-rich cathodes with structural effects, more specifically, with the formation of spinel-like domains and/or cubic rock salt phases [263–268]. With the help of neutron powder diffraction (NPD), Mohanty et al. [269] proposed that the structural layered-to-spinel evolution in Li-rich cathode materials occurred through a tetrahedral cation intermediate. Specifically, at first, Li-ions in Li-layers diffused from octahedral

to tetrahedral sites ( $\text{Li}_{\text{LiOct}} \rightarrow \text{Li}_{\text{LiTet}}$ ), followed by the diffusion of the Li-ions in TM-layers from the octahedral sites to the tetrahedral sites of the Li-layer ( $\text{Li}_{\text{TMOct}} \rightarrow \text{Li}_{\text{LiTet}}$ ); then, TM-ions migrated from the TM-layer octahedral sites to the “permanent” Li-layer octahedral sites via Li-layer tetrahedral sites ( $\text{Mn}_{\text{TMOct}} \rightarrow \text{Mn}_{\text{LiTet}} \rightarrow \text{Mn}_{\text{LiOct}}$ ), resulting in the formation of a spinel-like phase and voltage decay. Wang et al. [263] observed that two different layered structures, i.e.,  $R\bar{3}m$   $\text{LiMO}_2$  and  $C2/m$   $\text{Li}_2\text{MO}_3$  phases, in Li-rich cathode materials progressively transform to spinel structures, which correspond to the continuous voltage fading. Some researchers believed that the spinel structure further converted to a NiO-type rock-salt phase [270] because of the structural instability caused by the high charge voltage ( $> 4.6$  V). By employing scanning transmission electron microscopy (STEM), they found that a spinel-like phase was formed in the intermediate area between the layered structure and the disordered rock-salt phase. The formation of a spinel-like phase and disordered rock-salt phase accounted for the voltage decay and capacity degradation of Li-rich cathode materials during continuous cycles. Hu et al. found that nanosized microstructural defects, especially the large number of grain boundaries produced by prelithiation, greatly accelerated O-loss and voltage decay [271]. They also believed that the lower-voltage  $\text{Mn}^{3+}/\text{Mn}^{4+}$  and  $\text{Co}^{2+}/\text{Co}^{3+}$  redox couples could be activated by the layered-to-spinel phase transition and oxygen release, thus leading to continuous voltage fading [152]. Therefore, strategies involving manipulating the oxygen activity (such as reducing O redox activity or inhibiting  $\text{O}_2$  release), especially oxygen ions exposed to the surface, and avoiding TM migration can be exploited to improve the voltage stability. Surface modification methods, such as coating, surface doping, etc., are effective in alleviating voltage decay. Many inert oxides, fluorides or metal phosphates against electrolytes [272–275], such as  $\text{Al}_2\text{O}_3$ ,  $\text{CeO}_2$ ,  $\text{TiO}_2$ ,  $\text{AlPO}_4$  and  $\text{AlF}_3$ , were utilized as coating materials to maintain the oxygen vacancies generated through anion redox or to maintain structural integrity. Carbon-based material coatings can not only prohibit  $\text{O}_2$  release but also increase the electrode conductivity, therefore improving the electrode cycle stability and rate capability [260, 276]. Meng et al. [277] directly constructed a surface with oxygen vacancies to achieve delicate control of oxygen activity, and a significant difference in electrode performance was achieved. Surface-ion (Nb, Ru, etc.) doped Li-rich cathode materials showed quite good performance thanks to the stabilized surface structure, which exhibited moderate oxygen redox activity during the cycle process [258, 278]. Many groups constructed stabler spinels or no Li-excess shells, which significantly avoid severe oxygen loss [279–282]. Zhu et al. [282] reported a Li-gradient structure of TM oxides obtained by a selective molten molybdate-assisted Li–O leaching process that displayed virtually zero

oxygen loss and exhibited extraordinary performance. Bulk doping was also adopted by researchers to tune the bulk electronic structures to alter the electronic state. For example, Li et al. [261] doped polyanions ( $\text{BO}_3$ )<sup>3-</sup> and ( $\text{BO}_4$ )<sup>5-</sup> into Li-rich cathodes to decrease the energy level of O 2p to reduce the anion activity. Some active TM ions were also used to participate in charge compensation to reduce the degree of oxygen redox, and a few groups maintained the ratio of the capacity contributed by O, Mn, Ni, etc., to the redox reaction to avoid lower-voltage redox couples from occurring by using more active ion centres as buffer zones [283–285] or through artificial surface preconstruction [286], which greatly stabilized the voltage during the cycling process as well. Moreover, large-scale atoms, such as Zr, Sn, and La, were also applied to mitigate TM migration [287–289], inhibiting the transition from layered to spinel structures, stabilizing the layered structures, and thus avoiding severe voltage decay. Furthermore, in regard to the structure correlated with voltage decay, there is no doubt that voltage decay is associated with its O3-type crystal structure, in which the migration of TM ions to octahedral sites in Li layers and layered-to-spinel phase conversion can easily occur [77, 290]. Therefore, new structures that can avoid layered-to-spinel transitions have been explored by some research groups. It has proven almost impossible for O2-type  $\text{Li}_x\text{MO}_2$  to experience a layered-to-spinel transition because the oxygen lattice

rearrangement requires breaking all the Mn–O bonds. Based on this, a few groups successfully synthesized a few O2-type Li-rich cathode materials via ion-exchange methods, which exhibited stable voltage curves without voltage fading [77, 104, 290, 291]. In summary, voltage decay in Li-rich cathodes has been well studied and resolved.

The voltage hysteresis research is currently stuck in the phenomenon description and qualitative explanation phase, and only a few relevant studies have examined it or attempted to solve it. There are a few mechanisms proposed to account for the voltage hysteresis in Li-rich cathode materials, such as sluggish O redox behaviour, reversible TM ion migration, and a combination of these factors. Some researchers have proposed that the sluggish solid-state redox reactions of oxide ions are responsible for voltage hysteresis [95, 295], which also occurs in Li-O<sub>2</sub> batteries and causes a huge overpotential [292, 296, 297]; however, it brings some problems. (i) GITT cannot eliminate the voltage gap (overpotential) in Li-rich cathodes [170], which is different from that in Li-O<sub>2</sub> batteries [292, 297], as shown in Fig. 7a and b. The O species formed at high voltage in a Li-rich cathode is coordinated with high-valence TM ions rather than TM atoms in Li-O<sub>2</sub> batteries. (ii) the O redox is not slow (Fig. 7c) [28]. (iii) Voltage hysteresis at the voltage region of oxygen redox is quite small (4.6–3.5 V), which is apparent only in the full voltage range (Fig. 7c and e) [165]. (iv)

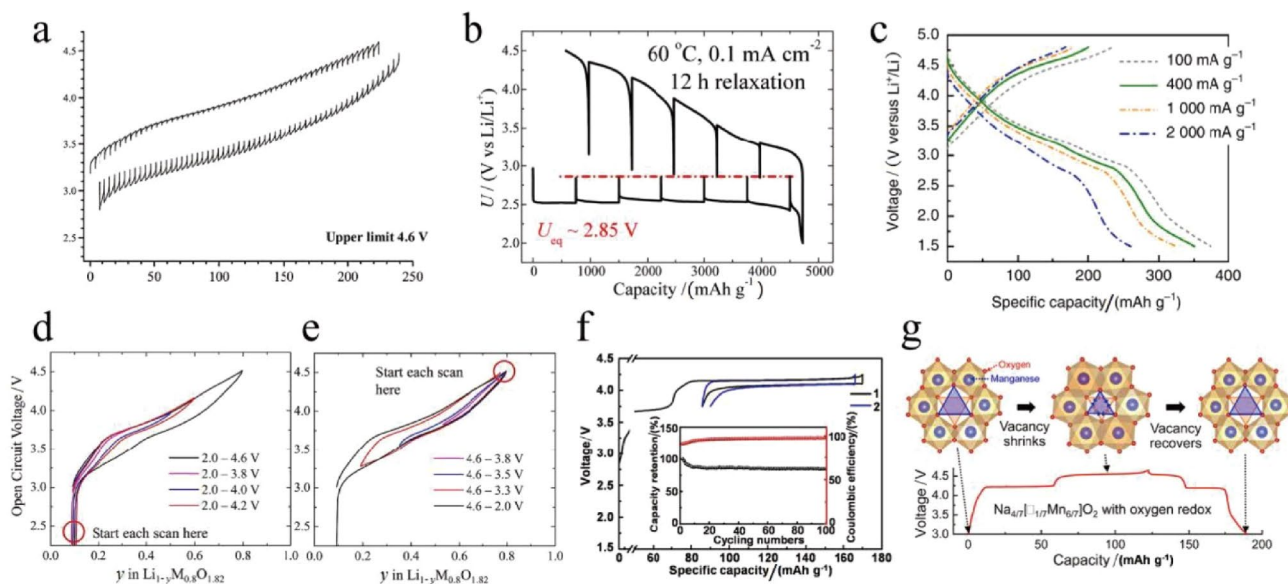


**Fig. 7** **a** The second GITT curves of Li-rich cathode materials. Adapted with permission from Ref. [170]. Copyright 2014 Elsevier. **b** GITT curves of the Li-O<sub>2</sub> battery. Adapted with permission from Ref. [292]. Copyright 2015 Royal Society of Chemistry. **c** Galvanostatic voltage profiles of  $\text{Li}_{1.68}\text{Mn}_{1.6}\text{O}_{3.7}\text{F}_{0.3}$ . Adapted with permission from Ref. [28]. Copyright 2020 Nature. Scanning open-circuit voltage (OCV) curves measured by GITT **d** beginning at 2 V with different upper voltage cut-offs and **e** beginning at 4.6 V with differ-

ent lower voltage cut-offs. Adapted with permission from Ref. [165]. Copyright 2013 American Chemical Society. **f** Voltage curves of  $\text{Na}_{0.5}\text{Ni}_{0.25}\text{Mn}_{0.75}\text{O}_2$ . Inset: cycling performance. Copyright 2018 Elsevier. **g** The charge/discharge curves of the  $\text{Na}_{47/17}\text{Mn}_{67/7}\text{O}_2$  cathode and schematic of the configuration change upon O evolution. Adapted with permission from Ref. [294]. Copyright 2019 American Chemical Society

Oxygen-redox-involved cathode materials can also exhibit small voltage hysteresis (Fig. 7f and g) [293, 294, 298, 299].

A few voltage window experiments were conducted and showed that anionic oxidation at high potential seemed to correspond to a reduction at substantially lower potential [95, 165, 300, 302], as shown in Fig. 8a. Croy et al. [165, 168] believed that the reversible migration of TM ions between the octahedral sites in the TM layer and the metastable tetrahedral sites in the Li layer could affect neighbouring Li ions, so a small percentage of Li ions could experience a hysteresis of approximately 1 V in the site energy, and irreversible TM migration caused continuous voltage decay, as shown in Fig. 8b. Some groups proposed that the partially reversible migration of TM ions decreased the potential of the bulk oxygen redox couple by > 1 V, resulting in a reordering of the redox potentials of anions and cations during cycling [95, 300], which can well explain the first cycle voltage profile; however, they do not further explain the hysteresis in subsequent cycles (Fig. 8c). Doublet et al. [301]

unified the picture of anionic redox in Li/Na-ion batteries and proposed that O exhibited different reversibility at different redox states, as shown in Fig. 8d, which significantly impacted the voltage profile. Once the metallic band located between the  $\sigma^*$  and  $\pi^*$  bands (the horizontal blue line (1)-(2) region) resulting from O–O pairing (as the O–O distance shrank, the narrow O(2p) lone band split into  $\sigma$ ,  $\pi$ ,  $\pi^*$  and  $\sigma^*$  discrete bands) formed,  $(O_2)^{2-}$  peroxides could form. Due to the inversion of the  $\sigma^*/M(d)$  band, a cationic reduction was expected to occur in the first-step discharge process, resulting in voltage hysteresis. Tarascon et al. [164] revealed that cationic redox was fully path-reversible, while anionic redox adopted different metastable paths with nonidentical enthalpy potentials on the charge and discharge processes and was responsible for the quasistatic voltage hysteresis; additionally, the quasistatic voltage hysteresis was associated with heat dissipation due to the production of nonequilibrium entropy, which provided a good understanding from the thermodynamics' view (Fig. 8e). Recently, focusing

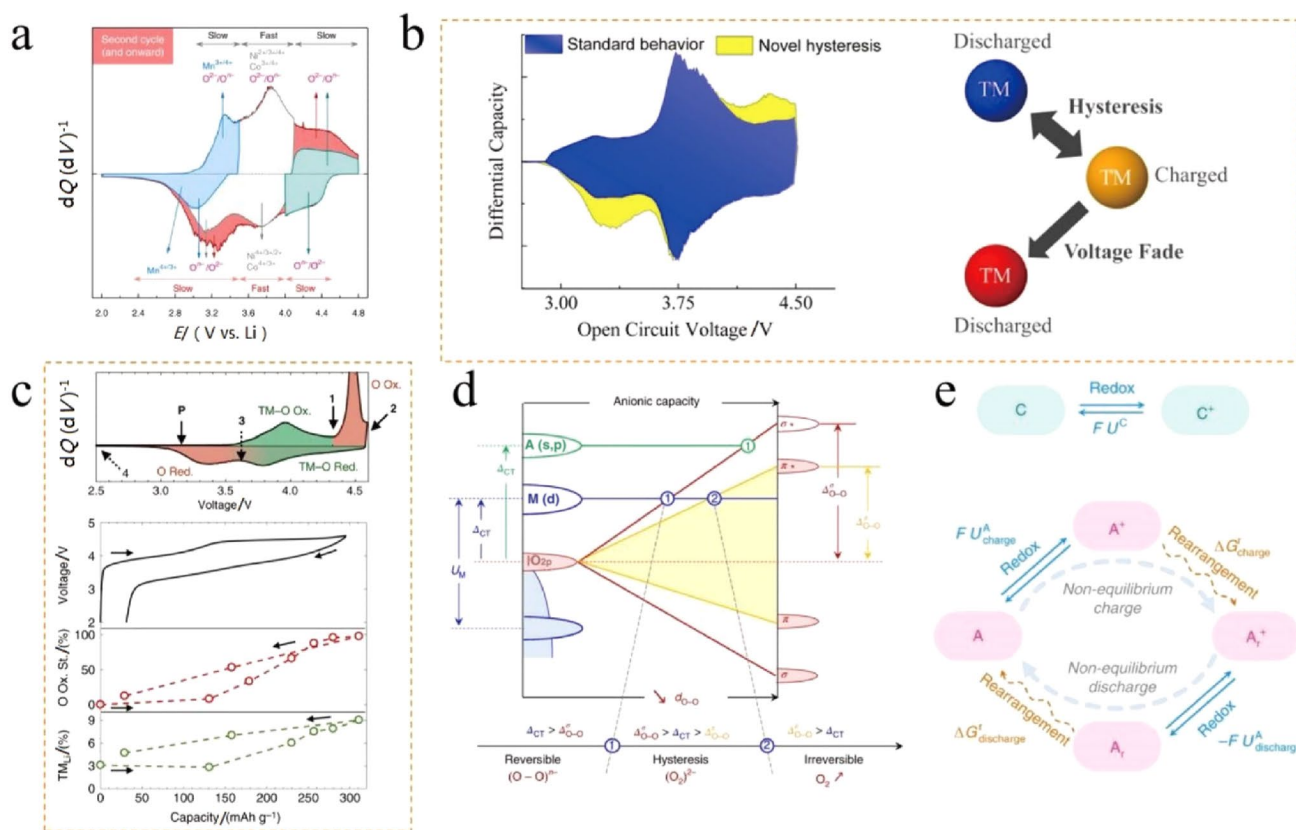


**Fig. 8** **a** Summary of the charge-compensation mechanism and electrochemical kinetics of activated Li-rich cathode materials. Adapted with permission from Ref. [95]. Copyright 2017 Nature. **b** Schematic correlation of hysteresis and voltage fade. Adapted with permission from Ref. [165]. Copyright 2013 American Chemical Society. Adapted with permission from Ref. [159]. Copyright 2013 Elsevier. **c** The first cycle  $dQ dV^{-1}$  and voltage curves of Mn-based Li-rich

cathode materials and the corresponding O redox and TM migration evolution. Adapted with permission from Ref. [300]. Copyright 2017 Nature. **d** The oxidation process dynamics in charge-transfer alkali-rich TMOs. Adapted with permission from Ref. [301]. Copyright 2019 Nature. **e** Proposed mechanism for hysteretic bulk anionic redox in activated  $Li_2Ru_{0.75}Sn_{0.25}O_3$ . Adapted with permission from Ref. [164]. Copyright 2019 Nature



on cation-disordered rock-salt cathode materials, they successfully captured dynamic ligand-to-metal charge transfer (LMCT) processes and believed that the LMCT process could account for anionic redox activation, cationic-anionic redox inversion, and voltage hysteresis [303, 304].

Bruce et al. [305] first demonstrated that the first-cycle voltage hysteresis in O-redox cathodes was controlled by the superstructure, specifically the local ordering of Li- and TM-ions in the TM-layers, as shown in Fig. 9. They creatively synthesized two sodium lithium manganese oxides (NLMO) with different superstructures in TM layers that exhibited obviously distinguished voltage profiles (Fig. 9a and b). After sufficient experimental characterization and

theoretical calculation (Fig. 9c–g), they found that the superstructure significantly influenced the behaviour of O redox as follows: [305] molecular  $O_2$  formed inside the honeycomb-ordered  $Na_{0.75}[Li_{0.25}Mn_{0.75}]O_2$  solid upon charging, whereas in ribbon-ordered  $Na_{0.6}[Li_{0.2}Mn_{0.8}]O_2$ , Mn-ion disordering was inhibited, and as a result,  $O_2$  formation was mitigated, leading to stable electron holes on  $O^{2-}$  and less voltage hysteresis, which was confirmed by higher resolution RIXS spectroscopy.

Recently, they further showed that this phenomenon also took place in a Li-rich  $Li_{1.2}Ni_{0.13}Co_{0.13}Mn_{0.54}O_2$  cathode material [141]. It was molecular  $O_2$  rather than  $O_2^{2-}$  as the species of oxidized  $O^{2-}$  that formed in the deeply delithiated

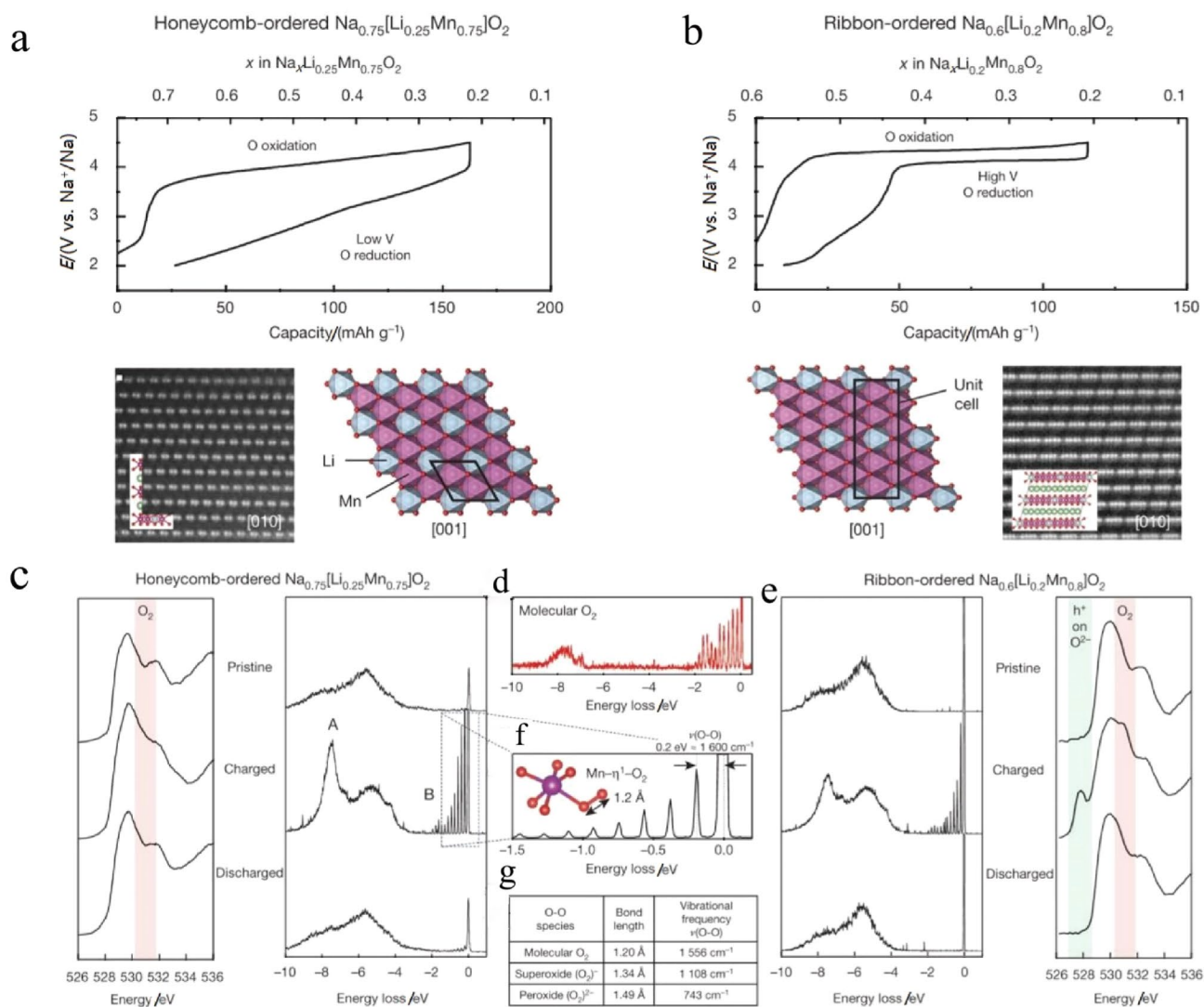


**Fig. 9** Charge/discharge behaviour and structure of **a** honeycomb-ordered  $Na_{0.75}[Li_{0.25}Mn_{0.75}]O_2$  and **b** ribbon-ordered  $Na_{0.6}[Li_{0.2}Mn_{0.8}]O_2$ . **c** O K-edge XAS and HR-RIXS spectra at 531 eV for **c** honeycomb and **e** ribbon-ordered cathode materials at different states of charge. **d** Molecular  $O_2$  HR-RIXS spectrum at 530.3 eV (reproduced with

permission). **f** Feature B is resolved into a progression of energy loss peaks with HR-RIXS. **g** Literature values for the bond lengths and frequencies of O–O species for comparison. Adapted with permission from Ref. [305]. Copyright 2019 Nature

state due to the intralayer TM-ion disordering associated with the honeycomb-ordered structure loss, which thus provided vacancy clusters to accommodate molecular  $O_2$ , as shown in Fig. 10a. By combining RIXS and  $^{17}O$  MAS-NMR spectroscopy (Fig. 10b), they proposed that these  $O_2$  molecules were reduced back to  $O^{2-}$  upon discharging to a lower voltage of 3.75 V, which was very similar to the process observed in NLMO cathodes. To provide a reasonable

explanation for these intriguing experimental results, DFT calculations were performed. They calculated a total of 60 unique configurations out of all 500 nonsymmetry-equivalent configurations, as shown in Fig. 10c, and found that the ground-state configuration contained two  $O_2$  molecules and a four-vacancy cluster and was the lowest in energy compared with other computed configurations. Using this stable configuration, they calculated an average voltage of 3.75 V

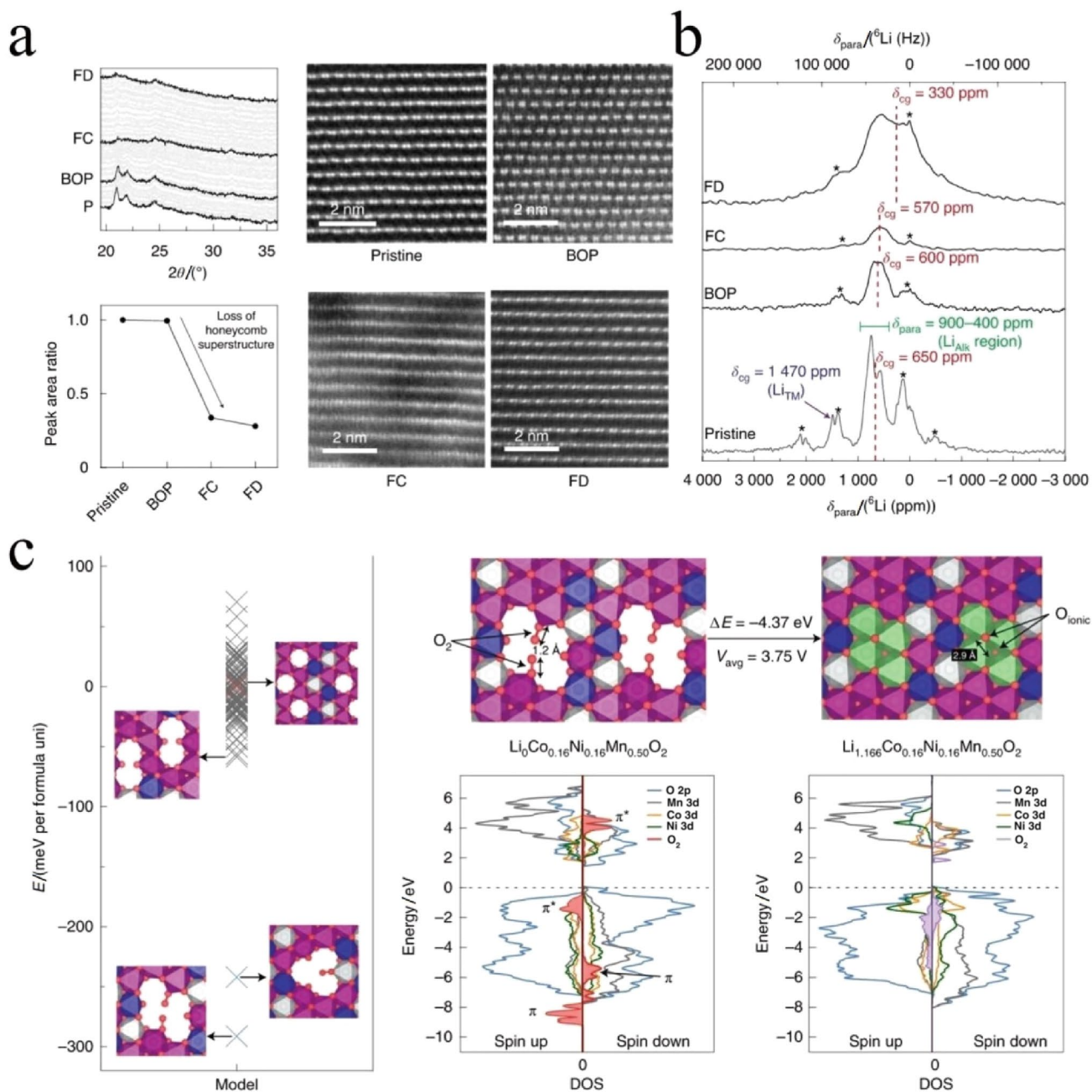


**Fig. 10** **a** Indicating the irreversible loss of honeycomb ordering during the first charge and discharge process by operando X-ray diffraction and STEM. **b**  $^6Li$  NMR data for  $Li_{1.2}Ni_{0.13}Co_{0.13}Mn_{0.54}O_2$  during the first charge and discharge process. **c** Structural models for TM

disorder and the discharge process considering molecular  $O_2$  and the migration of TM ions to form vacancy clusters. Adapted with permission from Ref. [141]. Copyright 2020 Nature

versus  $\text{Li}^+/\text{Li}$ , which was consistent with the experimental discharge voltage. Finally, a single unified model was proposed involving  $\text{O}^{2-}$  oxidation to form  $\text{O}_2$ , of which a very small fraction evolved from the surface and most was trapped in the bulk. They also attempted to use this model to explain the voltage hysteresis in Li-rich cathode materials, as shown in Fig. 11 [306]. During the initial charge process,  $\text{Li}^+$  in pristine structure A is extracted from the TM layer to form structure B, and later, driven in part by the energy stabilization obtained from  $\text{O}_2$  formation, this evolution is followed by structural relaxation and honeycomb ordering loss across the plateau through in-plane TM migration to produce structure C. During the discharge process, the disordered atomic arrangement remains, but  $\text{Li}^+$  ions return to the TM layers and occupy the vacancy clusters to form D. After the first cycle, the  $\text{O}_{2p}$  states change substantially with the change in the O coordination structure. The O-ions that have four coordinating Li ions and two coordinating TM

ions ( $\text{O-TM}_4\text{Li}_2$ ) are lower in energy than those that have six coordinating Li ions ( $\text{O-Li}_6$ ). This is why the first discharge voltages are distinct from and far lower than the first charge voltages. During the second and subsequent cycle processes, TM-layer disorder remains throughout, so the charge/discharge curves are more similar, but the path-dependent voltage hysteresis still exists, which could be explained by the strain release from  $\text{O}_2$  formation and reduction.

The above models provided various qualitative explanations of voltage hysteresis in Li-rich cathode materials, but quantitatively correlating hysteresis behaviour with oxygen redox or TM migration is still an unclear and challenging problem. Furthermore, when we examine the ion rearrangement during the activation of the  $\text{Li}_2\text{MnO}_3$  component, many problems arise, and too much detail is missing. The following questions need to be addressed. (i) Why is the oxygen redox reaction occurring in pure  $\text{Li}_2\text{MnO}_3$  different from that occurring in Li-rich cathode materials, and what are

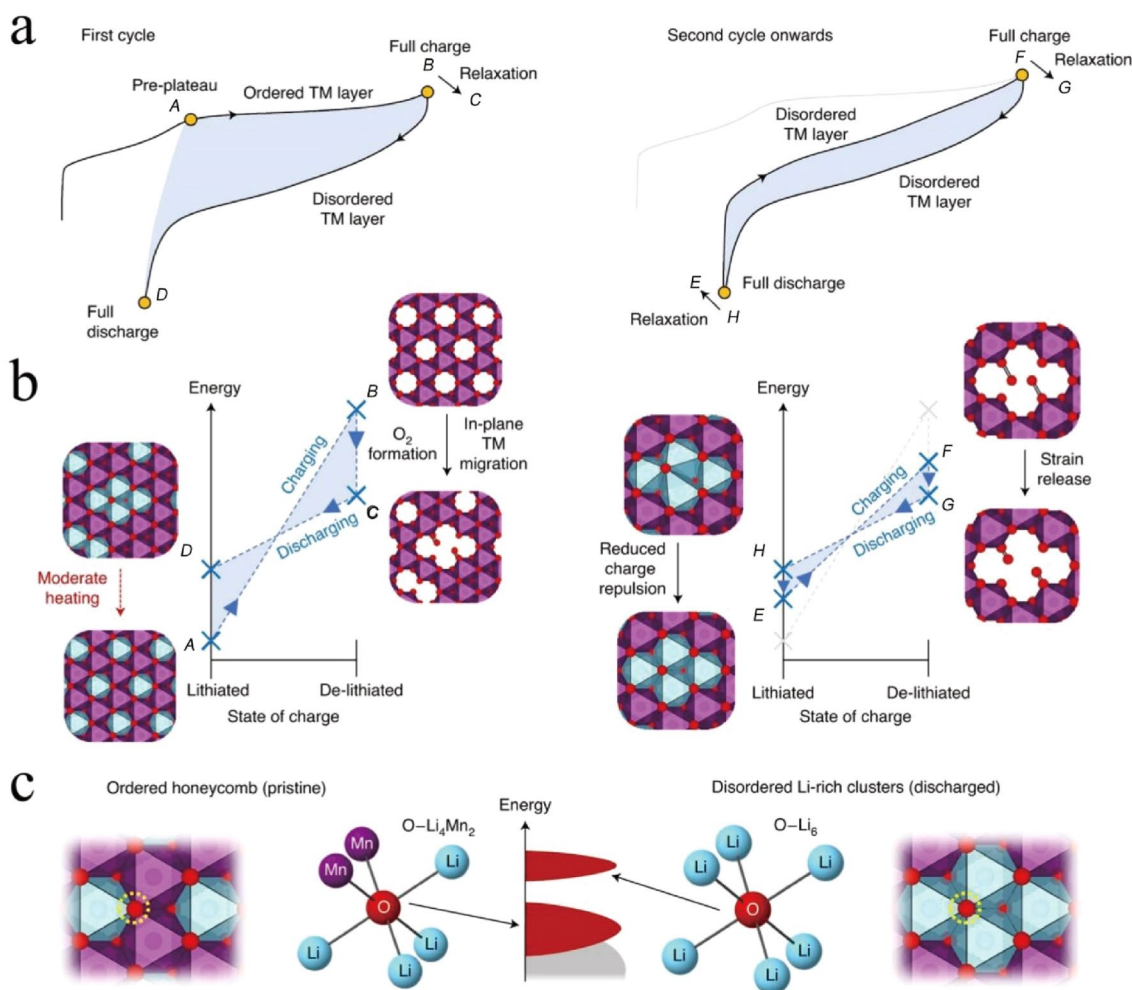


**Fig. 11** a First- and second-cycle curves of Li-rich cathode materials. b Schematics of voltage hysteresis in Li-rich cathodes. c O local coordination environment and corresponding band structure in pris-

tine honeycomb-ordered Li-rich cathodes ( $\text{O-Li}_4\text{Mn}_2$ , left) and after the first cycle ( $\text{O-Li}_6$ , right). Adapted with permission from Ref. [306]. Copyright 2021 Nature

the roles of other active TM ions, such as Ni and Co? Furthermore, why do some  $\text{Li}_2\text{MnO}_3$  materials exhibit certain electrochemical performance or anion redox reversibility? (ii) To what extent and how are the atoms rearranged during the activation process? (iii) What sites do the atoms occupy at different states of charge or discharge, and are these sites thermodynamically stable? How can this be accurately characterized? (iv) How do atoms migrate during the subsequent cycle process? (v) How do the composition and phase structure of the electrode from particle to particle and surface to bulk change during the charge/discharge process? (vi) In the subsequent charge/discharge cycles, why does the activated structure not display complete reversibility, and why can GITT not completely eliminate the voltage gap? More work needs to be conducted to explain this thorny but crucial issue.

## 7 Novel Materials and New Methods

Researchers have made many efforts and achieved significant progress in the study of traditional FCMs in recent decades. Encouragingly, a few novel FCMs and new

modification methods have recently been developed by some groups, and great breakthroughs have been made.

### 7.1 Cation-Disordered Rock Salt and Partially Ordered Oxide Cathodes

Cation-disordered rock-salt oxide cathodes were synthesized and further studied by Ceder's group after they first introduced percolation theory into the LIB field [65, 105, 307, 308]. They found that the layered structure characteristic of  $\text{Li}_{1.211}\text{Mo}_{0.467}\text{Cr}_{0.3}\text{O}_2$  (LMCO) started to be lost after one cycle and essentially disappeared after 10 cycles [65], as shown in Fig. 12a. The STEM images of the cycled sample displayed an obviously cation-disordered atomic arrangement. Cation disorder has been considered detrimental to  $\text{Li}^+$  transport for decades because there are no 1D, 2D or 3D Li-ion channels in such a structure. However, this LMCO electrode still released a remarkably high reversible capacity ( $> 265 \text{ mAh g}^{-1}$ ), even after disordering, as shown in Fig. 12b, which is counterintuitive. They proposed that Li diffusion proceeds in a cation-disordered rock-salt structure that could be realized by octahedral-tetrahedral-octahedral jumps (o-t-o diffusion). Li in the intermediate tetrahedral

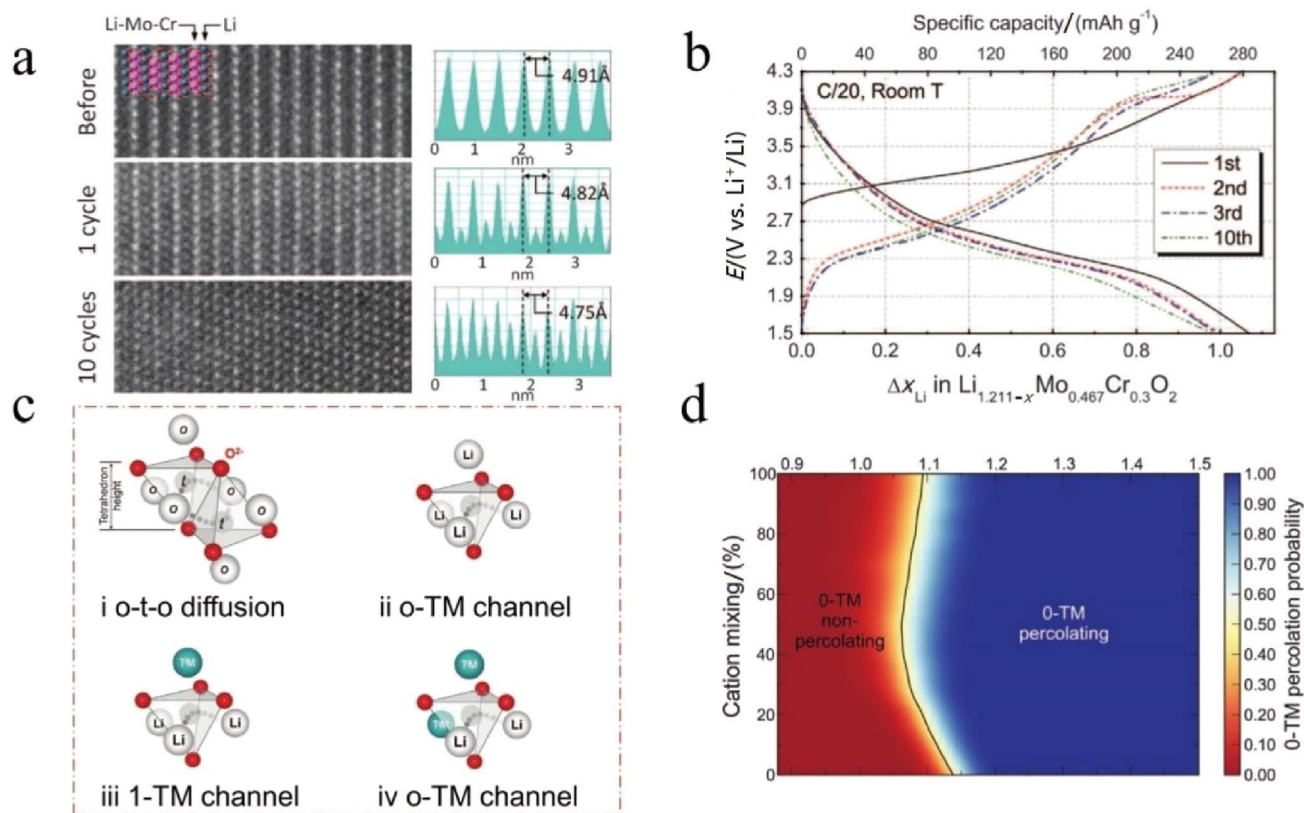


**Fig. 12** **a** STEM images for the  $\text{Li}_{1.211}\text{Mo}_{0.467}\text{Cr}_{0.3}\text{O}_2$  (LMCO) cathode at different cycles. **b** Voltage profile of LMCO. **c** Possible environments for an o-t-o Li hop in rock-salt-like Li-TM oxides. **d** Com-

puted probability of finding a percolating network of 0-TM channels. Adapted with permission from Ref. [65]. Copyright 2014 American Association for the Advancement of Science

site was the activated state in Li diffusion. Considering the number of TM ions that the activated state could share faces with, they illustrated three possible types of diffusion channels in Li-TM oxides, which were 0-TM, 1-TM channels and 2-TM channels, as shown in Fig. 12c. The energy in the activated state reflecting the Li-ion migration barrier was essentially dominated by electrostatic repulsion between the activated  $\text{Li}^+$  ion and its face-sharing species; thus, it depended on the face-sharing species' valence, the available space for  $\text{Li}^+$  ions and the face-sharing species' relaxation. Both 0-TM and 1-TM channels could support the o-t-o mechanism, but strong electrostatic repulsion to the activated Li ions would occur in the presence of more than two face-sharing TM ions. Fortunately, the 0-TM channels exhibited a relatively low barrier compared with that in 1-TM channels, indicating that Li-ion migration could easily occur in disordered LMCO electrodes. They further demonstrated the feasibility of cation-disordered rock-salt cathodes, as follows: as  $x$  in  $\text{Li}_x\text{TM}_{2-x}\text{O}_2$  exceeds  $\sim 1.09$  (the percolation threshold), the 0-TM channel network could be opened, as shown in Fig. 12d. Increasing the concentration of Li in the electrode structure added more 0-TM channels to a percolating 0-TM network, enhancing the network's connectivity. Thus, Li ions could hop through 0-TM channels in cation-disordered rock-salt materials, achieving Li-ion reversible de/intercalation. This type of material widens researchers' pot regarding cathode materials, which apparently contains FMCs, where great process has occurred in recent years. Cation-disordered rock-salt  $\text{Li}_2\text{MnO}_3$  ( $\text{Li}_1[\text{Li}_{1/3}\text{Mn}_{2/3}]\text{O}_2$ ) or  $\text{Li}_2\text{MnO}_3$ -based FMCs satisfy the critical condition ( $\text{Li} > 1.09$ ) and were synthesized by many groups and exhibited considerable electrochemical activity [66, 67, 70, 94]. Interestingly, stoichiometric  $\text{LiMnO}_2$  with a cation-disordered rock-salt structure was also developed by Yabuuchi et al. [69], and good electrochemical activity, which did not reach the percolation threshold according to percolation theory, was demonstrated. They believed that excess Li was not a necessary condition to extract Li ions from the cation-disordered structure; instead, excellent electrochemical performance could be achieved by shortening the migration length of particles.

Moreover, a multielectron redox reaction based on unusual Mn redox couples and O ions was then exploited by some researchers to achieve ultrahigh capacity FMCs. Pralong's group first reported a cation-disordered "Li<sub>4</sub>Mn<sub>2</sub>O<sub>5</sub>" cathode material [27] that was prepared by using a direct mechanochemical method. This ordinary material delivered an extraordinary discharge capacity of up to 355 mAh g<sup>-1</sup> through  $\text{Mn}^{3+}/\text{Mn}^{4+}/\text{Mn}^{5+}$  and a small amount of oxygen redox, as confirmed by magnetic measurements. Subsequent in-depth DFT calculation results showed that the delithiation process occurred via a three-step reaction pathway involving the complex interplay of cation and anion redox

reactions [309]. During the first charge stage, the delithiation process occurred mainly via Mn oxidation,  $\text{Mn}^{3+} \rightarrow \text{Mn}^{4+}$  ( $\text{Li}_x\text{Mn}_2\text{O}_5$ ,  $4 > x > 2$ ); later, anions participate in charge compensation,  $\text{O}^{2-} \rightarrow \text{O}^{1-}$  ( $2 > x > 1$ ); and finally, further metal oxidation,  $\text{Mn}^{4+} \rightarrow \text{Mn}^{5+}$  ( $1 > x > 0$ ), occurs. Tetrahedrally coordinated  $\text{Mn}^{4+}$  oxidized to  $\text{Mn}^{5+}$  was energetically favoured compared to octahedrally coordinated  $\text{Mn}^{4+}$ . Thus, they suggested that Mn ion migration to tetrahedral sites was required in the final delithiation process towards  $\text{Mn}_2\text{O}_5$ , which enabled  $\text{Mn}^{4+}$  oxidation to  $\text{Mn}^{5+}$ . Based on  $\text{Mn}^{2+}/\text{Mn}^{4+}$  and little oxygen redox, Ceder's group also achieved an energy density of nearly 1 000 Wh kg<sup>-1</sup> [18]. Through a combined strategy of high-valent cation ( $\text{Nb}^{5+}$ ,  $\text{Ti}^{4+}$ ) substitution and partial  $\text{O}^{2-}$  replacement by  $\text{F}^-$ , they successfully synthesized  $\text{Mn}^{2+}$ -containing Li-rich cathode materials. Such materials increase the diversity and designability of cathode materials. However, the rate capability and cycle stability were not satisfactory in completely cation-disordered rock-salt cathode materials [308]. Ceder et al. [28] further adopted a new strategy by combining substantial Li excess and a partial spinel-like cation order; thus, they obtained a specific energy of  $> 1\ 100$  Wh kg<sup>-1</sup> and a discharge rate up to 20 A g<sup>-1</sup>, which changed the stereotype of slow Li diffusion in disordered materials and provided a model for realizing both dense and ultrafast energy storage in Li-ion cathode materials.

## 7.2 Manipulating Atomic Ordering and Structural Symmetry

An increasing number of researchers are paying attention to the arrangement and distribution of atoms in cathode materials rather than just the crystal structure. Xia et al. [71] synthesized an  $R\bar{3}m$  Li-Mn-O Li-rich cathode via intralayer Li/Mn disordering in the Mn layer, which showed high capacity, excellent rate performance and good cycle stability, as shown in Fig. 13a–c. Due to the specific atomic arrangement and high structure symmetry,  $\text{Mn}^{3+}$  ions in the as-prepared material were in a low-spin state; thus, J-T distortion was mitigated. The oxygen reactivity and Li-ion diffusion were also modulated, exhibiting moderate oxygen redox activity and fast 2D Li-ion channels. They further found that the oxygen redox reaction occurring in intralayer Li/Ru disordered  $\text{Li}_2\text{RuO}_3$  via the structural response of the telescopic O-Ru-O configuration rather than O-O dimerization [149]. Cho et al. [310] explored the correlation between sustainable O-redox chemistry/TM migration and excess Li localization in Li-rich layered oxides. The calculation results showed that the O p-band centre induced by the Li-O-Li configurations near the Fermi level in the excess-Li localization Li-rich cathode material (L-LMR, Fig. 13d) shifted upward compared with the delocalized excess-Li Li-rich cathode material (D-LMR, Fig. 13g), as shown in Fig. 13e

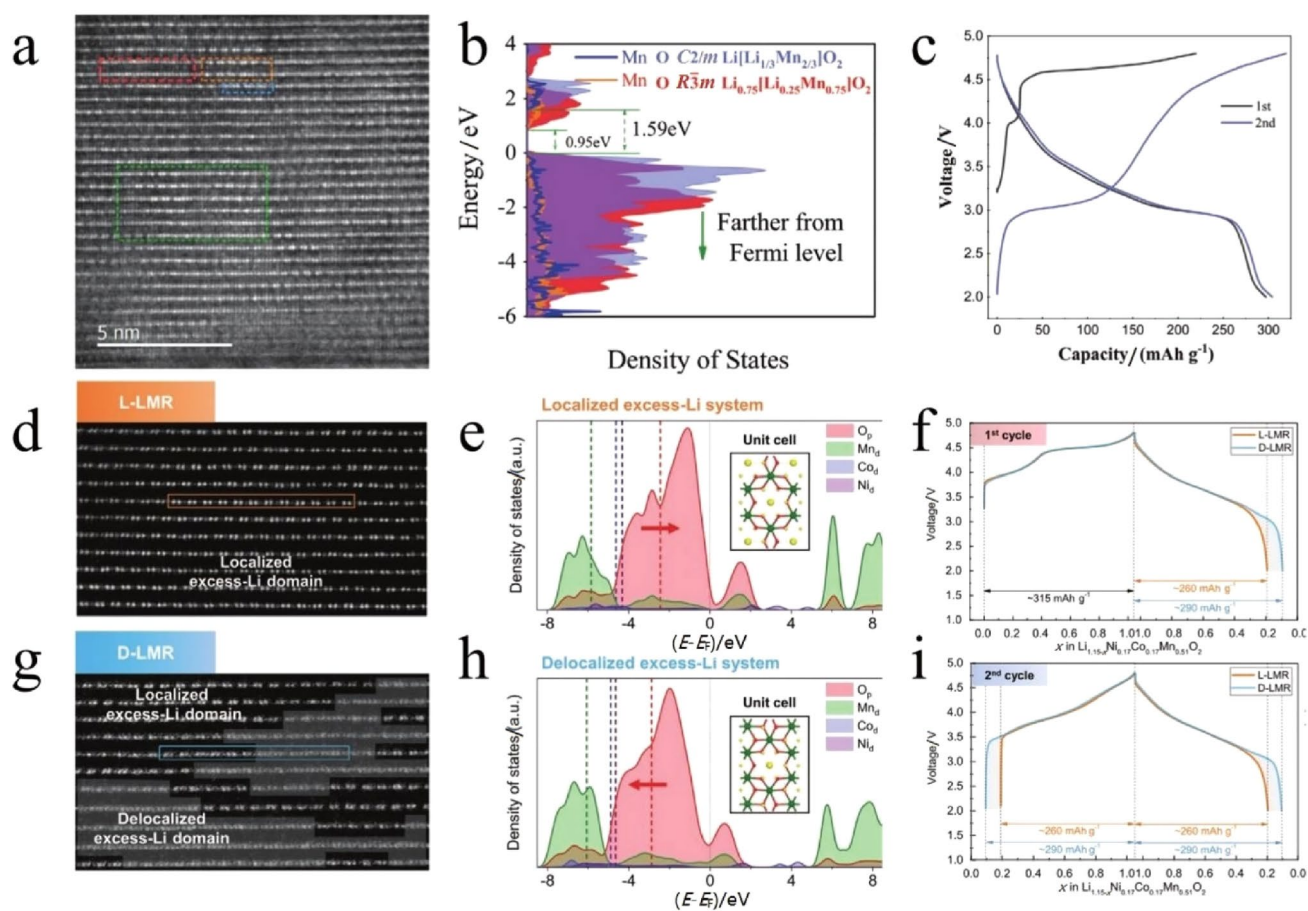


**Fig. 13** **a** HAADF-STEM images of  $R\bar{3}m$   $\text{Li}_{0.700}\text{Li}_{0.222}\text{Mn}_{0.756}\text{O}_2$  projected along the  $[1010](R\bar{3}m)$  direction. **b** Calculated Mn and O DOS of  $C2/m$   $\text{Li}[\text{Li}_{1/3}\text{Mn}_{2/3}]\text{O}_2$  and  $R\bar{3}m$   $\text{Li}_{0.700}\text{Li}_{0.222}\text{Mn}_{0.756}\text{O}_2$ . **c** Electrochemical profiles of the  $R\bar{3}m$   $\text{Li}_{0.700}\text{Li}_{0.222}\text{Mn}_{0.756}\text{O}_2$  electrode. Adapted with permission from Ref. [71]. Copyright 2020 Wiley-

VCH. HAADF-STEM analyses in the  $[100]$  monoclinic direction of **d** L-LMR and **g** D-LMR. The p-DOS of O 2p orbitals and TM 3d orbitals of **e** a localized excess-Li system and **h** a delocalized excess-Li system. **f** First cycle and **i** 2nd cycle voltage profiles of L-LMR and D-LMR. Adapted with permission from Ref. [310]. Copyright 2020 Wiley-VCH

and **h**, respectively. Thus, D-LMR exhibits more moderate and reversible O redox activity, as well as stabler structural integrity than L-LMR, leading to outstanding performance, as shown in Fig. 13f and i. These intralayer disordering and/or delocalized excess-Li systems are available designs for practically feasible Li-rich cathode materials with suppressed TM migration and sustainable O-redox chemistry.

For spinel  $\text{LiMn}_2\text{O}_4$ -based FCMs, Amine et al. [29] demonstrated that stoichiometric  $\text{LiMn}_2\text{O}_4$  underwent a severe irreversible phase transformation with unexpected phase generation, such as  $\text{Mn}_3\text{O}_4$ ,  $\text{Li}_4\text{Mn}_5\text{O}_{12}$ , and overlithiated  $\text{Li}_2\text{Mn}_2\text{O}_4$ , and particle surface cracks formed during the charge/discharge process, leading to poor surface stability and fast Mn dissolution. In turn, Mn dissolution combined with J-T distortion further accelerated the irreversible phase transition, leading to increased capacity degradation. Therefore, a Li-rich  $\text{LiMn}_2\text{O}_4$  with Li/Mn disorder and surface reconstruction was developed to effectively inhibit the

dissolution of Mn ions and the irreversible phase transition. Even after 25 cycles, almost no unexpected phases were detected in the XRD pattern. Pan et al. [311] further proposed that cationic disordering could intrinsically suppress the cooperative J-T distortion (CJTD) of  $\text{Mn}^{3+}\text{-O}_6$  octahedra, prevent the elongation of  $\text{Mn}^{3+}\text{-O}_6$  octahedrons along one direction and inhibit  $\text{Mn}^{3+}$  disproportionation in the spinel bulk. With such a strategy, they achieved double capacity with good cycle stability in micro-sized  $\text{LMn}_2\text{O}_4$ -based materials.

We believe that atomic ordering can significantly impact electrode properties and electrochemical performance. Manipulating the electrode crystal structure via a completely disordered or partially disordered atomic arrangement can significantly impact the stability and reversibility of the cathode materials' electrochemical performance. Going a step further, a more uniform distribution of Li and/or TM ions in the TM layers, such as intralayer ion disordering in

TM layers or the concept of a superlattice (periodic Li/TM arrangement in the TM layer), can also effectively impact the material performance. The use of intralayer ion disordering to control the performance of cathode materials has been reported in both Li- and Na-ion batteries [71, 312, 313], while the use of a superlattice to control the performance of cathode materials has mainly been reported in sodium-ion batteries. Partial superlattices consist of different transition metal ions (TM/TM') [314–318], and some are composed of Li-, M-, and TM-ions with different ratios [74, 305]. Interestingly, vacancies/TM ions can also form superlattices or disordering arrangements in the TM layer, making a significant difference in cathode performance [319–321]. In the latest literature, FMCs with various Li/V/TM orders were designed and synthesized, which provided extra available Li storage sites and highly stable, reversible anionic redox, greatly promoting the development of FMCs [72, 73, 322].

Structure symmetry is another important factor that can affect cathode properties. Almost all traditional layered  $\text{LiMO}_2$  oxide cathodes with  $R\bar{3}m$  symmetry show better performance than  $C2/m$   $\text{LiMnO}_2$ . Li-rich cathode materials, regarded as  $(C2/m \text{Li}_2\text{MnO}_3)^*(R\bar{3}m \text{LiMO}_2)$ , also show higher stability and reversibility than pure  $C2/m \text{Li}_2\text{MnO}_3$  or  $(C2/m \text{Li}_2\text{MnO}_3^* C2/m \text{LiMnO}_2)$ . Certainly, we cannot rule out the contribution of active TM ions (TM = Ni, Co, etc.). Chen et al. [76, 113–115] predicted that low-spin state  $\text{Mn}^{3+}$  could exist; once  $\text{LiMnO}_2$  had a structure with  $R\bar{3}m$  symmetry, then there might be no obvious J-T effect. Low-spin  $\text{Mn}^{3+}$  ions were indeed characterized in the intralayer Li/Mn disordering  $R\bar{3}m$  Li-Mn-O oxide material [71] and benefited greatly to the electrochemical performance of these FMCs. Recently, Xia et al. [75] designed a  $\text{LiMnO}_2$  cathode with interwoven spinel and layered domains. The Mn  $d_{2z}$  orbitals were oriented perpendicular to each other at the interface between these two domains, which gave rise to interfacial orbital ordering and then suppressed the otherwise cooperative J-T distortion and Mn dissolution, leading to superior cycle performance. Works that manipulate the electronic structure of Mn ions, especially the spin state, deserve more attention.

### 7.3 Manipulating Oxygen Sublattice

The Mn migration and layered-to-spinel phase transition occurring in layered  $\text{LiMnO}_2$  or Li-rich  $\text{Li}_2\text{MnO}_3$ -based cathodes are undoubtedly associated with the O3-type structure, which has the same close-packed oxygen sublattice as the spinel structure [25]. Thus, a layered-to-spinel transition can be easily realized in Mn-based O3-type layered oxide materials. Once Mn ions migrate to the intermediary Li-layer tetrahedral site, it is possible for them to move to neighbouring octahedral Li sites to complete the layered to spinel-like transition [290], as the vacant octahedral sites

formed during delithiation in the Li layers share only edges with  $\text{MnO}_6$  octahedra. Therefore, it is possible to avoid the transformation by preparing FMCs with different oxygen sublattices, such as tunnel-type or O2-type FMCs. O2-type FMCs were proposed and synthesized by a few groups early in the FMC literature [77–79] and showed no obvious voltage decay, resulting from no layered-to-spinel phase transition. For O2-type Li-TM-oxides, it is expected to be unfavourable for TM ions to migrate from the intermediate sites to adjacent Li sites due to the large electrostatic repulsion between face-shared cations. Thus, the layered-to-spinel transition is highly unlikely to occur at room temperature in O2-type cathode materials. A few groups have successfully synthesized a series of O2-type Li-rich cathode materials with excellent performance without obvious voltage decay. However, controlling the oxygen sublattice in layered oxide cathodes is achieved by the ion-exchange method, which is not an industrial process. The use of an in situ electrochemical method to directly synthesize FMCs with different oxygen sublattices or other new methods are worth studying.

### 7.4 Interface or Surface Redox

Relatively slow bulk-diffusion-controlled reactions generally occur in intercalation-based positive electrodes, leading to limited rate capabilities. Therefore, a few groups focused on the interface or surface redox reaction [80–82, 323], simultaneously achieving high capacity and high rate capability. Kang et al. [81] demonstrated that Li-free metal monoxides (MO) that did not have Li-ion diffusion channels in their crystal structure could be converted into high-capacity and fast-rate cathode materials by initially decorating the MO surface with nanosized LiF, as indicated in Fig. 14a. This material exhibited a smooth voltage profile, higher capacity and excellent rate performance, as shown in Fig. 14b and c, which was ascribed to a surface conversion reaction based mainly on Mn redox, unlike the classic Li intercalation reaction. Xia et al. [82] showed that electrolytic-anion-redox adsorption pseudocapacitance could be realized via the reversible adsorption/desorption of  $\text{PF}_6^-$  on the surface of TM oxides (e.g.,  $\text{Mn}_3\text{O}_4$ ), with charge transfer between  $\text{Mn}_3\text{O}_4$  and  $\text{PF}_6^-$  through Mn–F bonds, where F ions act as redox centres, providing greater design freedom for high-capacity and power energy storage devices, as shown in Fig. 14d–f. Furthermore, these materials can also avoid continuous variation of the voltage profile and poor stability due to the progressive phase change and the collapse of the material structure caused by the Li-insertion/extraction mechanism in bulk.

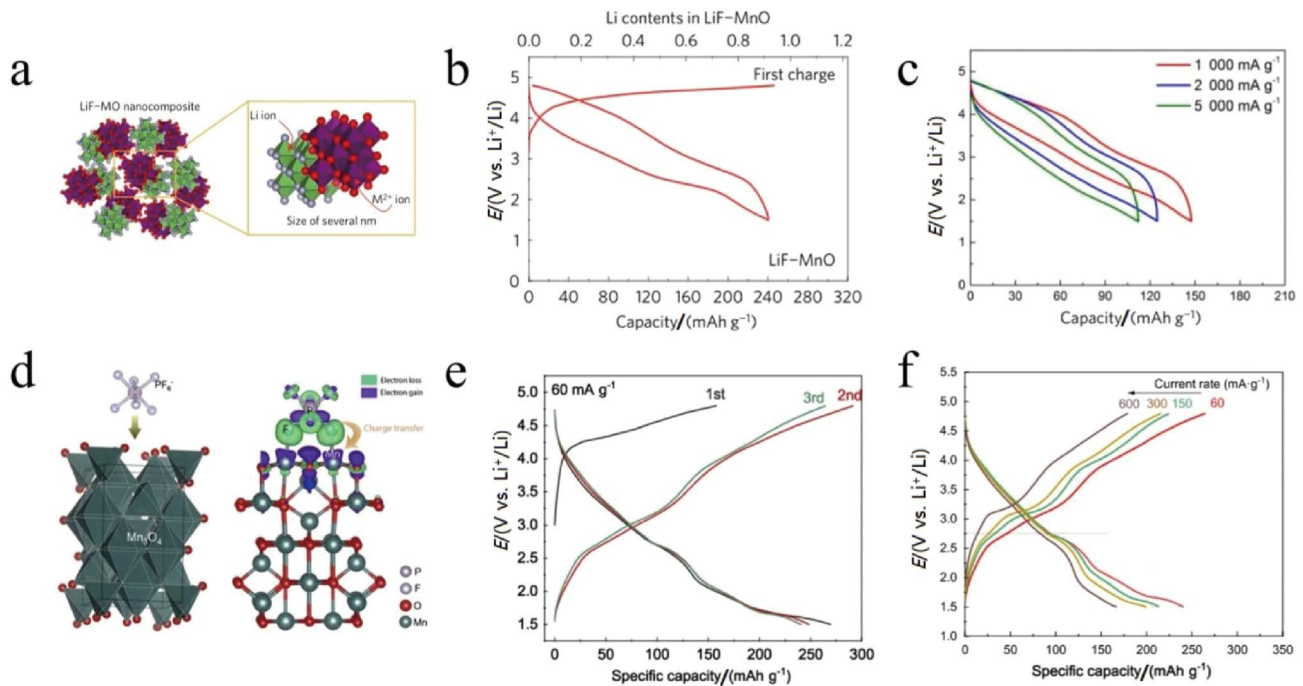


**Fig. 14** **a** Schematic of the metal monoxide (MO)+LiF cathode material. **b** Electrochemical profiles and **c** rate performance of the LiF-MnO nanocomposite electrode. Adapted with permission from Ref. [81]. Copyright 2017 Nature. **d** Schematic of the adsorption

process between  $\text{PF}_6^-$  and  $\text{Mn}_3\text{O}_4$  and their charge-transfer process. **e** Electrochemical profiles and **f** rate performance of the  $\text{Mn}_3\text{O}_4$  electrode. Adapted with permission from Ref. [82]. Copyright 2020 Elsevier

## 7.5 Entropy Stabilization Strategy

The entropy stabilization strategy could be a promising approach to enhancing the electrochemical performance of FMCs. The entropy stabilization strategy has been widely introduced in the field of conventional alloys for a long time, and it has achieved great progress in energy conversion and storage [324–326]. In our earlier research, from ordered  $\text{Li}_2\text{MnO}_3$  to an intralayer cation-disordered Li-Mn-O cathode to common Li-rich Mn-based cathode materials [60, 71, 261, 327], the cycle stability improved with an increase in intralayered configuration entropy. Some high-entropy electrode materials have been reported recently but have mainly focused on sodium cathode materials, LIB oxide anodes and cation-disordered cathode materials [328–333]. In fact, these new classes of oxide systems, also known as high entropy oxides (HEOs) [330], were formulated and reported with the first demonstrations of transition-metal-based HEOs a few years ago. Breitung et al. [329] presented some new results on the electrochemical properties of several TM-HEOs, such as the storage capacity and cycling stability of HEO structures. It was shown that the stabilization effect of entropy significantly enhanced the cycle stability and offered important benefits for the storage capacity retention of HEOs. Furthermore, it was observed that the electrochemical behaviour of the HEOs was dependent on each of the

metal cations present, opening the door to tailoring the electrochemical characteristics by simply altering the elemental composition. Hu et al. [328] reported a new concept of high-entropy chemistry for Na-ion cathodes. The layered O3-type  $\text{NaNi}_{0.12}\text{Cu}_{0.12}\text{Mg}_{0.12}\text{Fe}_{0.15}\text{Co}_{0.15}\text{Mn}_{0.1}\text{Ti}_{0.1}\text{Sn}_{0.1}\text{Sb}_{0.04}\text{O}_2$  cathode exhibited good cycle stability and outstanding rate capability, which were attributed to the multicomponent transition metals' accommodation of the local interaction changes during  $\text{Na}^+$  (de)intercalation. They further found that multicomponent TMO<sub>2</sub> slabs with enlarged interlayer spacing helped strengthen the entire skeleton structure of layered oxides, leading to highly improved electrochemical performance and thermal stability [334]. In the field of LIB cathode materials, only a few high-entropy cation-disordered cathode materials with considerable performance have been reported [296, 335]. Multielement introduction could bring synergistic effects, benefiting cycling stability and thermal safety; thus, it deserves more attention.

## 7.6 Equipped with a Solid-State Electrolyte

Toxic, volatile and flammable organic electrolytes are extensively exploited in commercial LIBs, and thus, there are a number of potential safety issues, including electrolyte leakage, fire, and explosion [336]. Solid-state electrolytes are promising and are now attracting increasing attention



because of their high safety, wide operating temperature range and convenient recovery [337]. Furthermore, solid-state electrolytes allow the use of Li metal as the anode. This in turn increases the cell voltage and thereby increases the energy density of the battery. Current solid-state electrolyte systems can be broadly classified into the following three categories: (1) inorganic electrolytes (oxide-based solid electrolytes, sulfide-based solid electrolytes, etc.), (2) solid polymer electrolytes (SPEs), and (3) composite electrolytes. FMCs, especially high-voltage and high-capacity FMCs, equipped with solid-state electrolytes will make a significant difference; in addition to the benefits of high safety and high energy density, the common issue is that Mn dissolution can be theoretically addressed by solid electrolytes, which will become one of the most important development directions in the future.

After nearly a century of exploration and development, certain achievements have been made in the development of solid electrolytes, but a few shortcomings and challenges have been encountered on the way to commercialization that need to be solved. As battery performance greatly depends on the diffusion properties of Li ions within the electrolyte and the interface compatibility, solid electrolytes need to have high ionic conductivity, negligible electronic conductivity and good infiltration; furthermore, given practical applications, solid-state electrolytes should have good mechanical properties. Almost all inorganic oxide electrolytes face the problems of poor electrode–electrolyte interface contact, and the interface stability is also poor during cycling, leading to a rapid increase in interface impedance and a fast decrease in capacity [338]. Therefore, oxide solid electrolytes often require the addition of some polymer components and mixing with trace ionic liquids/high-performance lithium salts and electrolytes or the use of auxiliary in situ polymerization to manufacture quasisolid batteries to retain some safety advantages and improve the electrolyte–electrode interface contact. Sulfide-based electrolytes have higher ionic conductivity than oxide electrolytes (up to  $10^{-3}$  S  $\text{cm}^{-1}$  at room temperature), which makes them an ideal electrolyte material for solid-state batteries. However, its stability (electrochemical stability and interfacial stability) issue still needs to be solved. Additionally, the main issue with its large-scale application is that, due to the fragility of sulfide to air conditions, any treatment must take place in an inert gas atmosphere. Moreover, the electrode and electrolyte synthesis processes in inorganic electrolytes differ from the standard LIB technique. The variety of possible binders and solvents is narrower, and reducing thickness is also difficult [339]. Solid polymer electrolytes, especially in situ polymerized solid polymer electrolytes, are another promising solid electrolyte type that has the advantages of good safety, ease of processing into films, excellent interface contact, etc. At the same time, it can help to prevent the problem of Li dendrites, which has recently received much

attention. However, many challenges remain, of which the development of polymer electrolytes with high ionic conductivity and wide electrochemical stability windows is particularly important. Compared to pure solid polymer electrolytes and inorganic electrolytes, composite electrolytes have the following advantages [340, 341]: (1) they can combine high mechanical strength and high ionic conductivity, and active inorganic fillers can also provide free-moving Li ions; (2) they can form ordered or disordered inorganic material–polymer interface structures, which provide transport channels for Li-ion migration, resulting in high ion migration numbers; and (3) the presence of inorganic materials can also adsorb trace water and other trace impurities, making the composite electrolyte stabler in the electrochemical environment and widening the electrochemical window of the electrolyte. However, there is a phase boundary between the inorganic material and the organic polymer electrolyte, which leads to phase separation during long charge and discharge cycles, resulting in a sharp drop in discharge capacity. The inorganic fillers are not easily dispersed in the polymer electrolyte, and the nanoscale inorganic particles tend to agglomerate, leading to a decrease in the cycling stability of the battery. Furthermore, the preparation process and conditions of composite electrolytes are more complicated, and the cost is also higher.

The development of FMCs equipped with solid-state electrolytes is a system engineering project involving further exploration of the solid electrolyte mechanism, development of new high-performance solid electrolytes, construction and tuning of the electrode/electrolyte interface, and application of advanced characterization techniques. More work needs to be conducted.

## 8 Conclusions and Perspectives

FMCs display great potential and competitive advantages for next-generation LIBs due to their resource abundance, lower toxicity, controllability of the crystal structure and various Mn-redox couples. However, several challenging issues still exist in the development of FMCs, which are undoubtedly attributed to the electronic structure and coordination structure of Mn ions, as well as the crystal structure of the electrodes. Based on the progress described above and our own experimental analysis, we present several conclusions and perspectives aiming to provide some considerable attractive strategies and research directions for building better FMCs, as shown in Fig. 15, and more details are presented below.

(1) Mn ions in most Li-Mn-oxide cathodes have six oxygen ligands, forming a symmetrical  $\text{MnO}_6$  octahedron. However, once there are enough high-spin state  $\text{Mn}^{3+}$  ions, cooperative J-T distortion will occur and significantly impact

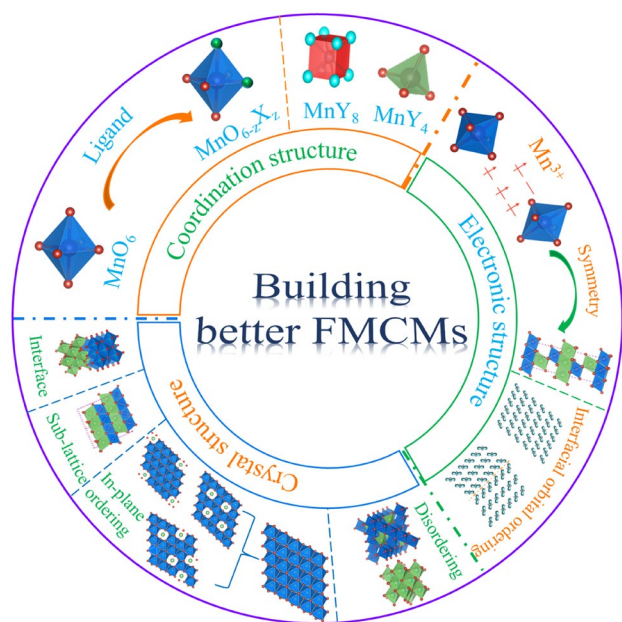


**Fig. 15** Possible strategies for building better FCMCs considering the electronic and coordination structure of Mn ions, as well as the crystal structure of the electrodes

the solid electrolyte interface and electrode structure stability, greatly reducing the material cycle stability.

(i) Inhibition of  $\text{Mn}^{3+}$  as an intermediate of Mn-redox species is a potential direct method; however, it may not be a practical suggestion, as achieving higher capacity is difficult; thus, some groups have introduced other redox centres to reduce the extent of  $\text{Mn}^{4+/3+}$  redox, such as  $\text{Ni}^{2+/4+}$  in Ni-rich cathode materials or oxygen redox in Li-rich cathode materials, although they raise other vexing problems.

(ii) Inhibition of high-spin state  $\text{Mn}^{3+}$  as an intermediate of Mn-redox products, which could be realized by structure symmetry control and has been proven by a few groups.

(iii) Relieving the cooperative J-T distortion by breaking the periodic arrangement of  $\text{Mn}^{3+}$  ions in the (layered/spinel) Li-Mn oxides, for example, constructing disordering or partially disordering materials, containing intralayer vacancies/Li/TM disordering in TM-layer; superstructure materials other than the honeycomb structure; high entropy oxide materials, containing multiple elements mixing in TM-layer, or elements completely disordering in the crystal; or manipulating interfacial orbital ordering.

(iv) Breaking the  $\text{MnO}_6$  coordination structure by ligand substitution, such as F- or S-substituted O ions, or directly building the  $\text{MnY}_8$  or  $\text{MnY}_4$  (Y here represents some anions) coordination structure.

(2) FCMCs with specific structures adopt the corresponding countermeasures.

(i) As for spinel  $\text{LiMn}_2\text{O}_4$ , doping, coating and electrolyte additives are usually effective; the key or future development direction for spinel  $\text{LiMn}_2\text{O}_4$  may be to increase its reversible capacity by a multielectron  $\text{Mn}^{2+/3+/4+}$  redox reaction, meanwhile the rich-Li strategy and/or Li/Mn ordering should be carefully considered.

(ii) For O3-type layered Li-Mn oxides, in addition to traditional modifications, oxygen sublattice engineering could be an attractive approach. O2-type Li-Mn-oxides have demonstrated superior electrochemical performance and avoid the continuous layered-to-spinel phase transition, but the synthetic methods need more exploration.

(iii) For Li-rich Li-Mn-oxides, searching Li-rich FCMCs with different superlattices (considering the arrangement of Li/M/TM/vacancy) could be a promising direction to avoid severe oxygen release and TM-ion migration; furthermore, the origin of voltage hysteresis also needs deeper understanding. More advanced characterization instruments, especially in situ observational characterization, and effective optimized approaches are urgently needed.

(3) Combining the advantages of capacitors and batteries, pseudocapacitance could make a superior difference in FCMCs. Intercalation pseudocapacitance behaviour is not easy to realize in FCMCs, but surface/interface redox pseudocapacitance is accessible and provides a novel possible strategy to enhance the energy density and rate performance of cathode materials.

In conclusion, there are as many opportunities as challenges in the future enhancement of FCMCs, and much work needs to be conducted. In the immediate future, we expect to see rapid development and commercialization of FCMCs with other layered oxide cathodes.

**Acknowledgements** This work was financially supported by the National Natural Science Foundation of China (No. 52130202).

**Conflicts of Interest** Dingguo Xia is an editorial board member for Electrochemical Energy Reviews and was not involved in the editorial review or the decision to publish this article. All authors declare that there are no competing interests.

**Open Access** This article is licensed under a Creative Commons Attribution 4.0 International License, which permits use, sharing, adaptation, distribution and reproduction in any medium or format, as long as you give appropriate credit to the original author(s) and the source, provide a link to the Creative Commons licence, and indicate if changes were made. The images or other third party material in this article are included in the article's Creative Commons licence, unless indicated otherwise in a credit line to the material. If material is not included in the article's Creative Commons licence and your intended use is not permitted by statutory regulation or exceeds the permitted use, you will need to obtain permission directly from the copyright holder. To view a copy of this licence, visit <http://creativecommons.org/licenses/by/4.0/>.

## References

- Tarascon, J.M., Armand, M.: Issues and challenges facing rechargeable lithium batteries. *Nature* **414**, 359–367 (2001). <https://doi.org/10.1038/35104644>
- Liu, C.F., Neale, Z.G., Cao, G.Z.: Understanding electrochemical potentials of cathode materials in rechargeable batteries. *Mater. Today* **19**, 109–123 (2016). <https://doi.org/10.1016/j.mattod.2015.10.009>
- Li, M., Lu, J., Chen, Z.W., et al.: 30 years of lithium-ion batteries. *Adv. Mater.* **30**, 1800561 (2018). <https://doi.org/10.1002/adma.201800561>
- Karden, E., Ploumen, S., Fricke, B., et al.: Energy storage devices for future hybrid electric vehicles. *J. Power Sources* **168**, 2–11 (2007). <https://doi.org/10.1016/j.jpowsour.2006.10.090>
- Scrosati, B., Garche, J.: Lithium batteries: status, prospects and future. *J. Power Sources* **195**, 2419–2430 (2010). <https://doi.org/10.1016/j.jpowsour.2009.11.048>
- Olivetti, E.A., Ceder, G., Gaustad, G.G., et al.: Lithium-ion battery supply chain considerations: analysis of potential bottlenecks in critical metals. *Joule* **1**, 229–243 (2017). <https://doi.org/10.1016/j.joule.2017.08.019>
- Schmich, R., Wagner, R., Hörpel, G., et al.: Performance and cost of materials for lithium-based rechargeable automotive batteries. *Nat. Energy* **3**, 267–278 (2018). <https://doi.org/10.1038/s41560-018-0107-2>
- Nitta, N., Wu, F.X., Lee, J.T., et al.: Li-ion battery materials: present and future. *Mater. Today* **18**, 252–264 (2015). <https://doi.org/10.1016/j.mattod.2014.10.040>
- Turcheniuk, K., Bondarev, D., Singhal, V., et al.: Ten years left to redesign lithium-ion batteries. *Nature* **559**, 467–470 (2018). <https://doi.org/10.1038/d41586-018-05752-3>
- Whittingham, M.S.: Lithium batteries and cathode materials. *Chem. Rev.* **104**, 4271–4302 (2004). <https://doi.org/10.1021/cr020731c>
- Kwade, A., Haselrieder, W., Leithoff, R., et al.: Current status and challenges for automotive battery production technologies. *Nat. Energy* **3**, 290–300 (2018). <https://doi.org/10.1038/s41560-018-0130-3>
- Lee, W., Muhammad, S., Sergey, C., et al.: Advances in the cathode materials for lithium rechargeable batteries. *Angew. Chem. Int. Ed.* **59**, 2578–2605 (2020). <https://doi.org/10.1002/anie.201902359>
- Liu, Q., Su, X., Lei, D., et al.: Approaching the capacity limit of lithium cobalt oxide in lithium ion batteries via lanthanum and aluminium doping. *Nat. Energy* **3**, 936–943 (2018). <https://doi.org/10.1038/s41560-018-0180-6>
- Kang, B., Ceder, G.: Battery materials for ultrafast charging and discharging. *Nature* **458**, 190–193 (2009). <https://doi.org/10.1038/nature07853>
- Lu, Z.H., MacNeil, D.D., Dahn, J.R.: Layered  $\text{Li}[\text{Ni}_x\text{Co}_{1-2x}\text{Mn}_x]\text{O}_2$  cathode materials for lithium-ion batteries. *Electrochem. Solid-State Lett.* **4**, A200 (2001). <https://doi.org/10.1002/chin.200207015>
- Aishova, A., Park, G.T., Yoon, C.S., et al.: Cobalt-free high-capacity Ni-rich layered  $\text{Li}[\text{Ni}_{0.9}\text{Mn}_{0.1}]\text{O}_2$  cathode. *Adv. Energy Mater.* **10**, 1903179 (2020). <https://doi.org/10.1002/aenm.201903179>
- Thackeray, M.M., Johnson, P.J., de Picciotto, L.A., et al.: Electrochemical extraction of lithium from  $\text{LiMn}_2\text{O}_4$ . *Mater. Res. Bull.* **19**, 179–187 (1984). [https://doi.org/10.1016/0025-5408\(84\)90088-6](https://doi.org/10.1016/0025-5408(84)90088-6)
- Lee, J., Kitchaev, D.A., Kwon, D.H., et al.: Reversible  $\text{Mn}^{2+}/\text{Mn}^{4+}$  double redox in lithium-excess cathode materials. *Nature* **556**, 185–190 (2018). <https://doi.org/10.1038/s41586-018-0015-4>
- Wang, L.L., Chen, B.B., Ma, J., et al.: Reviving lithium cobalt oxide-based lithium secondary batteries-toward a higher energy density. *Chem. Soc. Rev.* **47**, 6505–6602 (2018). <https://doi.org/10.1039/c8cs00322j>
- Myung, S.T., Maglia, F., Park, K.J., et al.: Nickel-rich layered cathode materials for automotive lithium-ion batteries: achievements and perspectives. *ACS Energy Lett.* **2**, 196–223 (2017). <https://doi.org/10.1021/acscenergylett.6b00594>
- Wang, H.S., Rus, E., Sakuraba, T., et al.:  $\text{CO}_2$  and  $\text{O}_2$  evolution at high voltage cathode materials of Li-ion batteries: a differential electrochemical mass spectrometry study. *Anal. Chem.* **86**, 6197–6201 (2014). <https://doi.org/10.1021/ac403317d>
- Dahn, J., Fuller, E., Obrovac, M., et al.: Thermal stability of  $\text{Li}_x\text{CoO}_2$ ,  $\text{Li}_x\text{NiO}_2$  and  $\lambda\text{-MnO}_2$  and consequences for the safety of Li-ion cells. *Solid State Ion.* **69**, 265–270 (1994). [https://doi.org/10.1016/0167-2738\(94\)90415-4](https://doi.org/10.1016/0167-2738(94)90415-4)
- Noh, H.J., Youn, S., Yoon, C.S., et al.: Comparison of the structural and electrochemical properties of layered  $\text{Li}[\text{Ni}_x\text{Co}_y\text{Mn}_z]\text{O}_2$  ( $x = 1/3, 0.5, 0.6, 0.7, 0.8$  and  $0.85$ ) cathode material for lithium-ion batteries. *J. Power Sources* **233**, 121–130 (2013). <https://doi.org/10.1016/j.jpowsour.2013.01.063>
- Bak, S.M., Hu, E.Y., Zhou, Y.N., et al.: Structural changes and thermal stability of charged  $\text{LiNi}_x\text{Mn}_y\text{Co}_z\text{O}_2$  cathode materials studied by combined in situ time-resolved XRD and mass spectroscopy. *ACS Appl. Mater. Interfaces* **6**, 22594–22601 (2014). <https://doi.org/10.1021/am506712c>
- Ammundsen, B., Paulsen, J.: Novel lithium-ion cathode materials based on layered manganese oxides. *Adv. Mater.* **13**, 943–956 (2001). [https://doi.org/10.1002/1521-4095\(200107\)13:12/13943::aid-adma943%3e3.0.co;2-j](https://doi.org/10.1002/1521-4095(200107)13:12/13943::aid-adma943%3e3.0.co;2-j)
- Xu, G.J., Liu, Z.H., Zhang, C.J., et al.: Strategies for improving the cyclability and thermo-stability of  $\text{LiMn}_2\text{O}_4$ -based batteries at elevated temperatures. *J. Mater. Chem. A* **3**, 4092–4123 (2015). <https://doi.org/10.1039/c4ta06264g>
- Freire, M., Kosova, N.V., Jordy, C., et al.: A new active Li-Mn-O compound for high energy density Li-ion batteries. *Nat. Mater.* **15**, 173–177 (2016). <https://doi.org/10.1038/nmat4479>
- Ji, H.W., Wu, J.P., Cai, Z.J., et al.: Ultrahigh power and energy density in partially ordered lithium-ion cathode materials. *Nat. Energy* **5**, 213–221 (2020). <https://doi.org/10.1038/s41560-020-0573-1>
- Liu, T.C., Dai, A., Lu, J., et al.: Correlation between manganese dissolution and dynamic phase stability in spinel-based lithium-ion battery. *Nat. Commun.* **10**, 4721 (2019). <https://doi.org/10.1038/s41467-019-12626-3>
- Thackeray, M.M.: Manganese oxides for lithium batteries. *Prog. Solid State Chem.* **25**, 1–71 (1997). [https://doi.org/10.1016/s0079-6786\(97\)81003-5](https://doi.org/10.1016/s0079-6786(97)81003-5)
- Ikeda, H., Narukawa, S.: Behaviour of various cathode materials for non-aqueous lithium cells. *J. Power Sources* **9**, 329–334 (1983). [https://doi.org/10.1016/0378-7753\(83\)87035-9](https://doi.org/10.1016/0378-7753(83)87035-9)
- Whittingham, M.S.: Electrical energy storage and intercalation chemistry. *Science* **192**, 1126–1127 (1976). <https://doi.org/10.1126/science.192.4244.1126>
- Besenhard, J.O., Eichinger, G.: High energy density lithium cells. *J. Electroanal. Chem. Interfacial Electrochem.* **68**, 1–18 (1976). [https://doi.org/10.1016/s0022-0728\(76\)80298-7](https://doi.org/10.1016/s0022-0728(76)80298-7)
- Armand, M.B.: *Materials for Advanced Batteries*. Springer, US, Boston, MA (1980)
- Mizushima, K., Jones, P.C., Wiseman, P., et al.:  $\text{Li}_x\text{CoO}_2$  ( $0 < x < 1$ ): a new cathode material for batteries of high energy density. *Mater. Res. Bull.* **15**, 783–789 (1980)
- Thackeray, M.M., David, W.I.F., Bruce, P.G., et al.: Lithium insertion into manganese spinels. *Mater. Res. Bull.* **18**, 461–472 (1983). [https://doi.org/10.1016/0025-5408\(83\)90138-1](https://doi.org/10.1016/0025-5408(83)90138-1)

37. Thackeray, M.M., Amine, K.:  $\text{LiMn}_2\text{O}_4$  spinel and substituted cathodes. *Nat. Energy* **6**, 566 (2021). <https://doi.org/10.1038/s41560-021-00815-8>
38. Rossouw, M.H., Thackeray, M.M.: Lithium manganese oxides from  $\text{Li}_2\text{MnO}_3$  for rechargeable lithium battery applications. *Mater. Res. Bull.* **26**, 463–473 (1991). [https://doi.org/10.1016/0025-5408\(91\)90186-p](https://doi.org/10.1016/0025-5408(91)90186-p)
39. Mackrodt, W.C., Williamson, E.A.: First-principles Hartree-Fock description of the electronic structure of monoclinic  $C2/m \text{Li}_x\text{MnO}_2$  ( $1 \geq x \geq 0$ ). *Philos. Mag. Part B.* **77**, 1077–1092 (1998)
40. Goodenough, J.B.: On the influence of 3d4 ions on the magnetic and crystallographic properties of magnetic oxides. *J. Phys. Radium* **20**, 155–159 (1959). <https://doi.org/10.1051/jphysrad:01959002002-301500>
41. Leroux, F.: The 2D Rancieite-type manganic acid and its alkali-exchanged derivatives. Part I: chemical characterization and thermal behavior. *Solid State Ion.* **80**, 299–306 (1995). [https://doi.org/10.1016/0167-2738\(95\)00151-u](https://doi.org/10.1016/0167-2738(95)00151-u)
42. Thackeray, M.M.: Structural considerations of layered and spinel lithiated oxides for lithium ion batteries. *J. Electrochem. Soc.* **142**, 2558–2563 (1995). <https://doi.org/10.1149/1.2050053>
43. Rossouw, M.H., Liles, D.C., Thackeray, M.M.: Synthesis and structural characterization of a novel layered lithium manganese oxide,  $\text{Li}_{0.36}\text{Mn}_{0.91}\text{O}_2$ , and its lithiated derivative,  $\text{Li}_{1.09}\text{Mn}_{0.91}\text{O}_2$ . *J. Solid State Chem.* **104**, 464–466 (1993). <https://doi.org/10.1006/jssc.1993.1182>
44. Fuchs, B., Kemmlersack, S.: Synthesis of  $\text{LiMnO}_2$  and  $\text{LiFeO}_2$  in molten Li halides. *Solid State Ion.* **68**, 279–285 (1994). [https://doi.org/10.1016/0167-2738\(94\)90186-4](https://doi.org/10.1016/0167-2738(94)90186-4)
45. Capitaine, F.: A new variety of  $\text{LiMnO}_2$  with a layered structure. *Solid State Ion.* **89**, 197–202 (1996). [https://doi.org/10.1016/0167-2738\(96\)00369-4](https://doi.org/10.1016/0167-2738(96)00369-4)
46. Armstrong, A.R., Bruce, P.G.: Synthesis of layered  $\text{LiMnO}_2$  as an electrode for rechargeable lithium batteries. *Nature* **381**, 499–500 (1996). <https://doi.org/10.1038/381499a0>
47. Vitins, G., West, K.: Lithium intercalation into layered  $\text{LiMnO}_2$ . *J. Electrochem. Soc.* **144**, 2587–2592 (1997). <https://doi.org/10.1149/1.1837869>
48. Tabuchi, M., Ado, K., Kobayashi, H., et al.: Synthesis of  $\text{LiMnO}_2$  with  $\alpha\text{-NaMnO}_2$ -type structure by a mixed-alkaline hydrothermal reaction. *J. Electrochem. Soc.* **145**, L49–L52 (1998). <https://doi.org/10.1149/1.1838411>
49. Zhou, Y.K., Huang, J., Li, H.L.: Synthesis of highly ordered  $\text{LiMnO}_2$  nanowire arrays (by AAO template) and their structural properties. *Appl. Phys. A* **76**, 53–57 (2003). <https://doi.org/10.1007/s003390201299>
50. Feng, Q., Higashimoto, Y., Kajiyoshi, K., et al.: Synthesis of lithium manganese oxides from layered manganese oxides by hydrothermal soft chemical process. *J. Mater. Sci.* **20**, 269–271 (2001)
51. Lei, C.H., Wen, J.G., Sardela, M., et al.: Structural study of  $\text{Li}_2\text{MnO}_3$  by electron microscopy. *J. Mater. Sci.* **44**, 5579–5587 (2009). <https://doi.org/10.1007/s10853-009-3784-1>
52. Robertson, A.D., Bruce, P.G.: The origin of electrochemical activity in  $\text{Li}_2\text{MnO}_3$ . *Chem. Commun.* **23**, 2790–2791 (2002). <https://doi.org/10.1039/b207945c>
53. Phillips, P.J., Iddir, H., Abraham, D.P., et al.: Direct observation of the structural and electronic changes of  $\text{Li}_2\text{MnO}_3$  during electron irradiation. *Appl. Phys. Lett.* **105**, 113905 (2014). <https://doi.org/10.1063/1.4896264>
54. Seo, D.H., Lee, J., Urban, A., et al.: The structural and chemical origin of the oxygen redox activity in layered and cation-disordered Li-excess cathode materials. *Nat. Chem.* **8**, 692–697 (2016). <https://doi.org/10.1038/nchem.2524>
55. Li, B., Xia, D.G.: Anionic redox in rechargeable lithium batteries. *Adv. Mater.* **29**, 1701054 (2017). <https://doi.org/10.1002/adma.201701054>
56. Luo, K., Roberts, M.R., Guerrini, N., et al.: Anion redox chemistry in the cobalt free 3d transition metal oxide intercalation electrode  $\text{Li}[\text{Li}_{0.2}\text{Ni}_{0.2}\text{Mn}_{0.6}]\text{O}_2$ . *J. Am. Chem. Soc.* **138**, 11211–11218 (2016). <https://doi.org/10.1021/jacs.6b05111>
57. Amalraj, S.F., Sharon, D., Talianker, M., et al.: Study of the nanosized  $\text{Li}_2\text{MnO}_3$ : electrochemical behavior, structure, magnetic properties, and vibrational modes. *Electrochim. Acta* **97**, 259–270 (2013). <https://doi.org/10.1016/j.electacta.2013.03.029>
58. Yu, D.Y.W., Yanagida, K., Kato, Y., et al.: Electrochemical activities in  $\text{Li}_2\text{MnO}_3$ . *J. Electrochem. Soc.* **156**, A417–A424 (2009). <https://doi.org/10.1149/1.3110803>
59. Yan, P.F., Xiao, L., Zheng, J.M., et al.: Probing the degradation mechanism of  $\text{Li}_2\text{MnO}_3$  cathode for Li-ion batteries. *Chem. Mater.* **27**, 975–982 (2015). <https://doi.org/10.1021/cm504257m>
60. Rana, J., Stan, M., Kloepsch, R., et al.: Structural changes in  $\text{Li}_2\text{MnO}_3$  cathode material for Li-ion batteries. *Adv. Energy Mater.* **4**, 1300998 (2014). <https://doi.org/10.1002/aenm.20130998>
61. Zhang, Q.G., Peng, T.Y., Zhan, D., et al.: Synthesis and electrochemical property of  $x\text{Li}_2\text{MnO}_3\cdot(1-x)\text{LiMnO}_2$  composite cathode materials derived from partially reduced  $\text{Li}_2\text{MnO}_3$ . *J. Power Sources* **250**, 40–49 (2014). <https://doi.org/10.1016/j.jpowsour.2013.10.139>
62. Saroha, R., Gupta, A., Panwar, A.K.: Electrochemical performances of Li-rich layered-layered  $\text{Li}_2\text{MnO}_3\text{-LiMnO}_2$  solid solutions as cathode material for lithium-ion batteries. *J. Alloys Compd.* **696**, 580–589 (2017). <https://doi.org/10.1016/j.jallcom.2016.11.199>
63. Li, Y.M., Makita, Y., Lin, Z.Z., et al.: Synthesis and characterization of lithium manganese oxides with core-shell  $\text{Li}_4\text{Mn}_5\text{O}_{12}@\text{Li}_2\text{MnO}_3$  structure as lithium battery electrode materials. *Solid State Ion.* **196**, 34–40 (2011). <https://doi.org/10.1016/j.ssi.2011.06.005>
64. Johnson, C.S., Li, N., Vaughey, J.T., et al.: Lithium–manganese oxide electrodes with layered–spinel composite structures  $x\text{Li}_2\text{MnO}_3\cdot(1-x)\text{Li}_{1+y}\text{Mn}_{2-y}\text{O}_4$  ( $0 < x < 1$ ,  $0 \leq y \leq 0.33$ ) for lithium batteries. *Electrochem. Commun.* **7**, 528–536 (2005). <https://doi.org/10.1016/j.elecom.2005.02.027>
65. Lee, J., Urban, A., Li, X., et al.: Unlocking the potential of cation-disordered oxides for rechargeable lithium batteries. *Science* **343**, 519–522 (2014). <https://doi.org/10.1126/science.1246432>
66. Diaz-Lopez, M., Chater, P.A., Joly, Y., et al.: Reversible densification in nano- $\text{Li}_2\text{MnO}_3$  cation disordered rock-salt Li-ion battery cathodes. *J. Mater. Chem. A* **8**, 10998–11010 (2020). <https://doi.org/10.1039/d0ta03372c>
67. Freire, M., Lebedev, O.I., Maigang, A., et al.: Nanostructured  $\text{Li}_2\text{MnO}_3$ : a disordered rock salt type structure for high energy density Li ion batteries. *J. Mater. Chem. A* **5**, 21898–21902 (2017). <https://doi.org/10.1039/c7ta07476j>
68. Oishi, M., Yamanaka, K., Watanabe, I., et al.: Direct observation of reversible oxygen anion redox reaction in Li-rich manganese oxide,  $\text{Li}_2\text{MnO}_3$ , studied by soft X-ray absorption spectroscopy. *J. Mater. Chem. A* **4**, 9293–9302 (2016). <https://doi.org/10.1039/c6ta00174b>
69. Sato, T., Sato, K., Zhao, W.W., et al.: Metastable and nanosize cation-disordered rocksalt-type oxides: revisit of stoichiometric  $\text{LiMnO}_2$  and  $\text{NaMnO}_2$ . *J. Mater. Chem. A* **6**, 13943–13951 (2018). <https://doi.org/10.1039/c8ta03667e>
70. Kataoka, R., Kojima, T., Takeichi, N.: Electrochemical property of Li-Mn cation disordered Li-rich  $\text{Li}_2\text{MnO}_3$  with NaCl type

- structure. *J. Electrochem. Soc.* **165**, A291–A296 (2018). <https://doi.org/10.1149/2.1041802jes>
71. Song, J., Li, B., Chen, Y.Y., et al.: A high-performance Li-Mn-O Li-rich cathode material with rhombohedral symmetry via intra-layer Li/Mn disordering. *Adv. Mater.* **32**, 2000190 (2020). <https://doi.org/10.1002/adma.202000190>
  72. Huang, W.Y., Yang, L.Y., Chen, Z.F., et al.: Elastic lattice enabling reversible tetrahedral Li storage sites in a high-capacity manganese oxide cathode. *Adv. Mater.* **34**, 2202745 (2022). <https://doi.org/10.1002/adma.202202745>
  73. Cao, X., Li, H.F., Qiao, Y., et al.: Reversible anionic redox chemistry in layered  $\text{Li}_{4/7}[\square_{1/7}\text{Mn}_{6/7}]\text{O}_2$  enabled by stable Li–O-vacancy configuration. *Joule* **6**, 1290–1303 (2022). <https://doi.org/10.1016/j.joule.2022.05.006>
  74. Wang, Q., Liao, Y.X., Jin, X., et al.: Dual honeycomb-superlattice enables double-high activity and reversibility of anion redox for sodium-ion battery layered cathodes. *Angew. Chem. Int. Ed.* **61**, e202206625 (2022). <https://doi.org/10.1002/anie.202206625>
  75. Zhu, X.H., Meng, F.Q., Zhang, Q.H., et al.:  $\text{LiMnO}_2$  cathode stabilized by interfacial orbital ordering for sustainable lithium-ion batteries. *Nat. Sustain.* **4**, 392–401 (2020). <https://doi.org/10.1038/s41893-020-00660-9>
  76. Huang, Z.F., Du, F., Wang, C.Z., et al.: Low-spin  $\text{Mn}^{3+}$  ion in rhombohedral  $\text{LiMnO}_2$  predicted by first-principles calculations. *Phys. Rev. B* **75**, 054411 (2007). <https://doi.org/10.1103/physrevb.75.054411>
  77. Yabuuchi, N., Hara, R., Kajiyama, M., et al.: New O2/P2-type Li-excess layered manganese oxides as promising multi-functional electrode materials for rechargeable Li/Na batteries. *Adv. Energy Mater.* **4**, 1301453 (2014). <https://doi.org/10.1002/aenm.201301453>
  78. Paulsen, J.M., Thomas, C.L., Dahn, J.R.: Layered Li-Mn-oxide with the O<sub>2</sub> structure: a cathode material for Li-ion cells which does not convert to spinel. *J. Electrochem. Soc.* **146**, 3560–3565 (1999). <https://doi.org/10.1149/1.1392514>
  79. Shang, H.F., Zuo, Y.X., Shen, F.R., et al.: O2-type  $\text{Li}_{0.78}[\text{Li}_{0.24}\text{Mn}_{0.76}]\text{O}_2$  nanowires for high-performance lithium-ion battery cathode. *Nano Lett.* **20**, 5779–5785 (2020). <https://doi.org/10.1021/acs.nanolett.0c01640>
  80. Zhang, L.T., Chen, G.H., Berg, E.J., et al.: Triggering the in situ electrochemical formation of high capacity cathode material from MnO. *Adv. Energy Mater.* **7**, 1602200 (2017). <https://doi.org/10.1002/aenm.201602200>
  81. Jung, S.K., Kim, H., Cho, M.G., et al.: Lithium-free transition metal monoxides for positive electrodes in lithium-ion batteries. *Nat. Energy* **2**, 16208 (2017). <https://doi.org/10.1038/nenergy.2016.208>
  82. Li, B., Wang, Y.F., Jiang, N., et al.: Electrolytic-anion-redox adsorption pseudocapacitance in nanosized lithium-free transition metal oxides as cathode materials for Li-ion batteries. *Nano Energy* **72**, 104727 (2020). <https://doi.org/10.1016/j.nanoen.2020.104727>
  83. Li, W.K., Cho, Y.G., Yao, W.L., et al.: Enabling high areal capacity for Co-free high voltage spinel materials in next-generation Li-ion batteries. *J. Power Sources* **473**, 228579 (2020). <https://doi.org/10.1016/j.jpowsour.2020.228579>
  84. Zeng, X.Q., Zhan, C., Lu, J., et al.: Stabilization of a high-capacity and high-power nickel-based cathode for Li-ion batteries. *Chem* **4**, 690–704 (2018). <https://doi.org/10.1016/j.chempr.2017.12.027>
  85. Yan, P.F., Zheng, J.M., Liu, J., et al.: Tailoring grain boundary structures and chemistry of Ni-rich layered cathodes for enhanced cycle stability of lithium-ion batteries. *Nat. Energy* **3**, 600–605 (2018). <https://doi.org/10.1038/s41560-018-0191-3>
  86. Muralidharan, N., Essehli, R., Hermann, R.P., et al.: Lithium iron aluminum nickelate,  $\text{LiNi}_x\text{Fe}_y\text{Al}_z\text{O}_2$ : new sustainable cathodes for next-generation cobalt-free Li-ion batteries. *Adv. Mater.* **32**, 2002960 (2020). <https://doi.org/10.1002/adma.202002960>
  87. Kim, J., Lee, H., Cha, H., et al.: Nickel-rich cathodes: prospect and reality of Ni-rich cathode for commercialization. *Adv. Energy Mater.* **8**, 1870023 (2018). <https://doi.org/10.1002/aenm.201870023>
  88. Park, O.K., Cho, Y., Lee, S.H., et al.: Who will drive electric vehicles, olivine or spinel? *Energy Environ. Sci.* **4**, 1621 (2011). <https://doi.org/10.1039/c0ee00559b>
  89. Gummow, R.J., de Kock, A., Thackeray, M.M.: Improved capacity retention in rechargeable 4 V lithium/lithium-manganese oxide (spinel) cells. *Solid State Ion.* **69**, 59–67 (1994). [https://doi.org/10.1016/0167-2738\(94\)90450-2](https://doi.org/10.1016/0167-2738(94)90450-2)
  90. Reimers, J.N., Fuller, E.W., Rossen, E., et al.: Synthesis and electrochemical studies of  $\text{LiMnO}_2$  prepared at low temperatures. *J. Electrochem. Soc.* **140**, 3396–3401 (1993). <https://doi.org/10.1149/1.2221101>
  91. Myung, S.T., Komaba, S., Kumagai, N.: Hydrothermal synthesis of orthorhombic  $\text{LiCo}_x\text{Mn}_{1-x}\text{O}_2$  and their structural changes during cycling. *J. Electrochem. Soc.* **149**, A1349 (2002). <https://doi.org/10.1149/1.1504453>
  92. Li, X.H., Su, Z., Wang, Y.B.: Electrochemical properties of monoclinic and orthorhombic  $\text{LiMnO}_2$  synthesized by a one-step hydrothermal method. *J. Alloys Compd.* **735**, 2182–2189 (2018). <https://doi.org/10.1016/j.jallcom.2017.11.384>
  93. Croy, J.R., Park, J.S., Dogan, F., et al.: First-cycle evolution of local structure in electrochemically activated  $\text{Li}_2\text{MnO}_3$ . *Chem. Mater.* **26**, 7091–7098 (2014). <https://doi.org/10.1021/cm5039792>
  94. Kataoka, R., Taguchi, N., Kojima, T., et al.: Improving the oxygen redox stability of NaCl-type cation disordered  $\text{Li}_2\text{MnO}_3$  in a composite structure of  $\text{Li}_2\text{MnO}_3$  and spinel-type  $\text{LiMn}_2\text{O}_4$ . *J. Mater. Chem. A* **7**, 5381–5390 (2019). <https://doi.org/10.1039/c8ta11807h>
  95. Assat, G., Foix, D., Delacourt, C., et al.: Fundamental interplay between anionic/cationic redox governing the kinetics and thermodynamics of lithium-rich cathodes. *Nat. Commun.* **8**, 2219 (2017). <https://doi.org/10.1038/s41467-017-02291-9>
  96. Radin, M.D., Vinckeviciute, J., Seshadri, R., et al.: Manganese oxidation as the origin of the anomalous capacity of Mn-containing Li-excess cathode materials. *Nat. Energy* **4**, 639–646 (2019). <https://doi.org/10.1038/s41560-019-0439-6>
  97. Zhang, Z.H., Zhao, S., Wang, B.Y., et al.: Local redox reaction of high valence manganese in  $\text{Li}_2\text{MnO}_3$ -based lithium battery cathodes. *Cell Rep. Phys. Sci.* **1**, 100061 (2020). <https://doi.org/10.1016/j.xcrp.2020.100061>
  98. Hunter, J.C.: Preparation of a new crystal form of manganese dioxide:  $\lambda$ - $\text{MnO}_2$ . *J. Solid State Chem.* **39**, 142–147 (1981). [https://doi.org/10.1016/0022-4596\(81\)90323-6](https://doi.org/10.1016/0022-4596(81)90323-6)
  99. Jang, Y.I., Moorehead, W.D., Chiang, Y.M.: Synthesis of the monoclinic and orthorhombic phases of  $\text{LiMnO}_2$  in oxidizing atmosphere. *Solid State Ion.* **149**, 201–207 (2002). [https://doi.org/10.1016/s0167-2738\(02\)00176-5](https://doi.org/10.1016/s0167-2738(02)00176-5)
  100. Nazri, G., Pistoia, G.: *Lithium Batteries: Science and Technology*. Springer Science & Business Media, New York (2003)
  101. Strobel, P., Lambert-Andron, B.: Crystallographic and magnetic structure of  $\text{Li}_2\text{MnO}_3$ . *J. Solid State Chem.* **75**, 90–98 (1988). [https://doi.org/10.1016/0022-4596\(88\)90305-2](https://doi.org/10.1016/0022-4596(88)90305-2)
  102. Boulineau, A., Croguennec, L., Delmas, C., et al.: Structure of  $\text{Li}_2\text{MnO}_3$  with different degrees of defects. *Solid State Ion.* **180**, 1652–1659 (2010). <https://doi.org/10.1016/j.ssi.2009.10.020>
  103. Wang, R., He, X.Q., He, L.H., et al.: Atomic structure of  $\text{Li}_2\text{MnO}_3$  after partial delithiation and re-lithiation. *Adv. Energy*

- Mater. **3**, 1358–1367 (2013). <https://doi.org/10.1002/aenm.201200842>
104. Carlier, D., Saadoun, I., Croguennec, L., et al.: On the metastable O<sub>2</sub>-type LiCoO<sub>2</sub>. *Solid State Ion.* **144**, 263–276 (2001)
  105. Clément, R.J., Lun, Z., Ceder, G.: Cation-disordered rocksalt transition metal oxides and oxyfluorides for high energy lithium-ion cathodes. *Energy Environ. Sci.* **13**, 345–373 (2020). <https://doi.org/10.1039/c9ee02803j>
  106. Asl, H.Y., Manthiram, A.: Reining in dissolved transition-metal ions. *Science* **369**, 140–141 (2020). <https://doi.org/10.1126/science.abc5454>
  107. Amatucci, G., du Pasquier, A., Blyr, A., et al.: The elevated temperature performance of the LiMn<sub>2</sub>O<sub>4</sub>/C system: failure and solutions. *Electrochim. Acta* **45**, 255–271 (1999). [https://doi.org/10.1016/s0013-4686\(99\)00209-1](https://doi.org/10.1016/s0013-4686(99)00209-1)
  108. Goodenough, J.B., Park, K.S.: The Li-ion rechargeable battery: a perspective. *J. Am. Chem. Soc.* **135**, 1167–1176 (2013). <https://doi.org/10.1021/ja3091438>
  109. Gummow, R.J., Liles, D.C., Thackeray, M.M.: Lithium extraction from orthorhombic lithium manganese oxide and the phase transformation to spinel. *Mater. Res. Bull.* **28**, 1249–1256 (1993). [https://doi.org/10.1016/0025-5408\(93\)90172-a](https://doi.org/10.1016/0025-5408(93)90172-a)
  110. Croguennec, L., Palacin, M.R.: Recent achievements on inorganic electrode materials for lithium-ion batteries. *J. Am. Chem. Soc.* **137**, 3140–3156 (2015). <https://doi.org/10.1021/ja507828x>
  111. Guilnard, M., Croguennec, L., Denux, D., et al.: Thermal stability of lithium nickel oxide derivatives. Part I: Li<sub>x</sub>Ni<sub>1.02</sub>O<sub>2</sub> and Li<sub>x</sub>Ni<sub>0.89</sub>Al<sub>0.16</sub>O<sub>2</sub> (x = 0.50 and 0.30). *Chem. Mater.* **15**, 4476–4483 (2003). <https://doi.org/10.1021/cm030059f>
  112. Marianetti, C.A., Morgan, D., Ceder, G.: First-principles investigation of the cooperative Jahn-Teller effect for octahedrally coordinated transition-metal ions. *Phys. Rev. B* **63**, 224304 (2001). <https://doi.org/10.1103/physrevb.63.224304>
  113. Amriou, T., Khelifa, B., Aourag, H., et al.: Ab initio investigation of the Jahn-Teller distortion effect on the stabilizing lithium intercalated compounds. *Mater. Chem. Phys.* **92**, 499–504 (2005). <https://doi.org/10.1016/j.matchemphys.2005.01.061>
  114. Prasad, R., Benedek, R., Kropf, A.J., et al.: Divalent-dopant criterion for the suppression of Jahn-Teller distortion in Mn oxides: first-principles calculations and X-ray absorption spectroscopy measurements for Co in LiMnO<sub>2</sub>. *Phys. Rev. B* **68**, 012101 (2003). <https://doi.org/10.1103/physrevb.68.012101>
  115. Mishra, S.K., Ceder, G.: Structural stability of lithium manganese oxides. *Phys. Rev. B* **59**, 6120–6130 (1999). <https://doi.org/10.1103/physrevb.59.6120>
  116. Nowak, S., Winter, M.: The role of cations on the performance of lithium ion batteries: a quantitative analytical approach. *Acc. Chem. Res.* **51**, 265–272 (2018). <https://doi.org/10.1021/acs.accounts.7b00523>
  117. Gilbert, J.A., Shkrob, I.A., Abraham, D.P.: Transition metal dissolution, ion migration, electrocatalytic reduction and capacity loss in lithium-ion full cells. *J. Electrochem. Soc.* **164**, A389–A399 (2017). <https://doi.org/10.1149/2.1111702jes>
  118. Amine, K., Liu, J., Kang, S., et al.: Improved lithium manganese oxide spinel/graphite Li-ion cells for high-power applications. *J. Power Sources* **129**, 14–19 (2004). <https://doi.org/10.1016/j.jpowsour.2003.11.007>
  119. Inoue, T., Sano, M.: An investigation of capacity fading of manganese spinels stored at elevated temperature. *J. Electrochem. Soc.* **145**, 3704–3707 (1998). <https://doi.org/10.1149/1.1838862>
  120. Han, D.W., Ryu, W.H., Kim, W.K., et al.: Effects of Li and Cl codoping on the electrochemical performance and structural stability of LiMn<sub>2</sub>O<sub>4</sub> cathode materials for hybrid electric vehicle applications. *J. Phys. Chem. C* **117**, 4913–4919 (2013). <https://doi.org/10.1021/jp310011m>
  121. Premanand, R., Durairajan, A., Haran, B.L., et al.: Studies on capacity fade of spinel-based Li-ion batteries. *J. Electrochem. Soc.* **149**, A54 (2002). <https://doi.org/10.1149/1.1426399>
  122. Kanamura, K., Tamura, H., Takehara, Z.I.: XPS analysis of a lithium surface immersed in propylene carbonate solution containing various salts. *J. Electroanal. Chem.* **333**, 127–142 (1992). [https://doi.org/10.1016/0022-0728\(92\)80386-i](https://doi.org/10.1016/0022-0728(92)80386-i)
  123. Choa, J., Thackeray, M.M.: Structural changes of LiMn<sub>2</sub>O<sub>4</sub> spinel electrodes during electrochemical cycling. *J. Electrochem. Soc.* **146**, 3577–3581 (1999). <https://doi.org/10.1149/1.1392517>
  124. Kawamura, T., Okada, S., Yamaki, J.I.: Decomposition reaction of LiPF<sub>6</sub>-based electrolytes for lithium ion cells. *J. Power Sources* **156**, 547–554 (2006). <https://doi.org/10.1016/j.jpowsour.2005.05.084>
  125. Benedek, R.: Role of disproportionation in the dissolution of Mn from lithium manganese spinel. *J. Phys. Chem. C* **121**, 22049–22053 (2017). <https://doi.org/10.1021/acs.jpcc.7b05940>
  126. Wang, L.F., Ou, C.C., Striebel, K.A., et al.: Study of Mn dissolution from LiMn<sub>2</sub>O<sub>4</sub> spinel electrodes using rotating ring-disk collection experiments. *J. Electrochem. Soc.* **150**, A905 (2003). <https://doi.org/10.1149/1.1577543>
  127. Xia, Y., Zhou, Y., Yoshio, M.: Capacity fading on cycling of 4 V Li/LiMn<sub>2</sub>O<sub>4</sub> cells. *J. Electrochem. Soc.* **144**, 2593 (1997)
  128. Ohzuku, T., Kitagawa, M., Hirai, T.: Electrochemistry of manganese dioxide in lithium nonaqueous cell: III. X-ray diffractational study on the reduction of spinel-related manganese dioxide. *J. Electrochem. Soc.* **137**, 769–775 (1990). <https://doi.org/10.1149/1.2086552>
  129. Amatucci, G.G., Schmutz, C.N., Blyr, A., et al.: Materials' effects on the elevated and room temperature performance of CLiMn<sub>2</sub>O<sub>4</sub> Li-ion batteries. *J. Power Sources* **69**, 11–25 (1997). [https://doi.org/10.1016/s0378-7753\(97\)02542-1](https://doi.org/10.1016/s0378-7753(97)02542-1)
  130. Eriksson, T., Andersson, A.M., Bishop, A.G., et al.: Surface analysis of LiMn<sub>2</sub>O<sub>4</sub> electrodes in carbonate-based electrolytes. *J. Electrochem. Soc.* **149**, A69 (2002). <https://doi.org/10.1149/1.1426398>
  131. Koetschau, I., Richard, M.N., Dahn, J.R., et al.: Orthorhombic LiMnO<sub>2</sub> as a high capacity cathode for Li-ion cells. *J. Electrochem. Soc.* **142**, 2906–2910 (1995). <https://doi.org/10.1149/1.2048663>
  132. Myung, S.T., Komaba, S., Kumagai, N.: Orthorhombic LiMnO<sub>2</sub> as a high capacity cathode for lithium-ion battery synthesized by hydrothermal route at 170 °C. *Chem. Lett.* **30**, 80–81 (2001). <https://doi.org/10.1246/cl.2001.80>
  133. Wang, G., Yao, P., Zhong, S., et al.: Electrochemical study on orthorhombic LiMnO<sub>2</sub> as cathode in rechargeable lithium batteries. *J. Appl. Electrochem.* **29**, 1423–1426 (1999)
  134. Kim, J.M., Chung, H.T.: Electrochemical characteristics of orthorhombic LiMnO<sub>2</sub> with different degrees of stacking faults. *J. Power Sources* **115**, 125–130 (2003). [https://doi.org/10.1016/s0378-7753\(02\)00709-7](https://doi.org/10.1016/s0378-7753(02)00709-7)
  135. Davidson, I.J., McMillan, R.S., Murray, J.J., et al.: Lithium-ion cell based on orthorhombic LiMnO<sub>2</sub>. *J. Power Sources* **54**, 232–235 (1995). [https://doi.org/10.1016/0378-7753\(94\)02074-d](https://doi.org/10.1016/0378-7753(94)02074-d)
  136. Ohzuku, T., Ueda, A., Hirai, T.: LiMnO<sub>2</sub> as cathode for secondary lithium cell. *Chem. Express* **7**, 193–196 (1992)
  137. Reed, J., Ceder, G., van der Ven, A.: Layered-to-spinel phase transition in Li<sub>x</sub>MnO<sub>2</sub>. *Electrochem. Solid-State Lett.* **4**, A78 (2001). <https://doi.org/10.1149/1.1368896>
  138. Robertson, A.D., Bruce, P.G.: Mechanism of electrochemical activity in Li<sub>2</sub>MnO<sub>3</sub>. *Chem. Mat.* **15**, 1984–1992 (2003). <https://doi.org/10.1002/chin.200334010>
  139. Guerrini, N., Jin, L.Y., Lozano, J.G., et al.: Charging mechanism of Li<sub>2</sub>MnO<sub>3</sub>. *Chem. Mater.* **32**, 3733–3740 (2020). <https://doi.org/10.1021/acs.chemmater.9b04459>

140. Luo, K., Roberts, M.R., Hao, R., et al.: Charge-compensation in 3d-transition-metal-oxide intercalation cathodes through the generation of localized electron holes on oxygen. *Nat. Chem.* **8**, 684–691 (2016). <https://doi.org/10.1038/nchem.2471>
141. House, R.A., Rees, G.J., Pérez-Osorio, M.A., et al.: First-cycle voltage hysteresis in Li-rich 3d cathodes associated with molecular O<sub>2</sub> trapped in the bulk. *Nat. Energy* **5**, 777–785 (2020). <https://doi.org/10.1038/s41560-020-00697-2>
142. Li, X., Qiao, Y., Guo, S.H., et al.: Direct visualization of the reversible O<sup>2−</sup>/O<sup>−</sup> redox process in Li-rich cathode materials. *Adv. Mater.* **30**, 1705197 (2018). <https://doi.org/10.1002/adma.201705197>
143. House, R.A., Maitra, U., Jin, L.Y., et al.: What triggers oxygen loss in oxygen redox cathode materials? *Chem. Mater.* **31**, 3293–3300 (2019). <https://doi.org/10.1021/acs.chemmater.9b00227>
144. Zhuo, Z.Q., Dai, K.H., Qiao, R.M., et al.: Cycling mechanism of Li<sub>2</sub>MnO<sub>3</sub>: Li-CO<sub>2</sub> batteries and commonality on oxygen redox in cathode materials. *Joule* **5**, 975–997 (2021). <https://doi.org/10.1016/j.joule.2021.02.004>
145. Zhuo, Z.Q., Dai, K.H., Wu, J.P., et al.: Distinct oxygen redox activities in Li<sub>2</sub>MO<sub>3</sub> (M = Mn, Ru, Ir). *ACS Energy Lett.* **6**, 3417–3424 (2021). <https://doi.org/10.1021/acsenenergylett.1c01101>
146. Rana, J., Papp, J.K., Lebens-Higgins, Z., et al.: Quantifying the capacity contributions during activation of Li<sub>2</sub>MnO<sub>3</sub>. *ACS Energy Lett.* **5**, 634–641 (2020). <https://doi.org/10.1021/acsenenergylett.9b02799>
147. Li, X., Li, X.H., Monluc, L., et al.: Stacking-fault enhanced oxygen redox in Li<sub>2</sub>MnO<sub>3</sub>. *Adv. Energy Mater.* **12**, 2200427 (2022). <https://doi.org/10.1002/aenm.202200427>
148. Tan, X., Liu, R., Xie, C.X., et al.: Modified structural characteristics and enhanced electrochemical properties of oxygen-deficient Li<sub>2</sub>MnO<sub>3-δ</sub> obtained from pristine Li<sub>2</sub>MnO<sub>3</sub>. *J. Power Sources* **374**, 134–141 (2018). <https://doi.org/10.1016/j.jpowsour.2017.11.004>
149. Ning, F.H., Li, B., Song, J., et al.: Inhibition of oxygen dimerization by local symmetry tuning in Li-rich layered oxides for improved stability. *Nat. Commun.* **11**, 4973 (2020). <https://doi.org/10.1038/s41467-020-18423-7>
150. Zuba, M.J., Grenier, A., Lebens-Higgins, Z., et al.: Whither Mn oxidation in Mn-rich alkali-excess cathodes? *ACS Energy Lett.* **6**, 1055–1064 (2021). <https://doi.org/10.1021/acsenenergylett.0c02418>
151. Francis Amalraj, S., Markovsky, B., Sharon, D., et al.: Study of the electrochemical behavior of the “inactive” Li<sub>2</sub>MnO<sub>3</sub>. *Electrochim. Acta* **78**, 32–39 (2012). <https://doi.org/10.1016/j.electacta.2012.05.144>
152. Hu, E.Y., Yu, X.Q., Lin, R.Q., et al.: Evolution of redox couples in Li- and Mn-rich cathode materials and mitigation of voltage fade by reducing oxygen release. *Nat. Energy* **3**, 690–698 (2018). <https://doi.org/10.1038/s41560-018-0207-z>
153. Sathiy, M., Ramesha, K., Rouse, G., et al.: High performance Li<sub>2</sub>Ru<sub>1-y</sub>Mn<sub>y</sub>O<sub>3</sub> (0.2 ≤ y ≤ 0.8) cathode materials for rechargeable lithium-ion batteries: their understanding. *Chem. Mater.* **25**, 1121–1131 (2013). <https://doi.org/10.1021/cm400193m>
154. Okamoto, Y.: Ambivalent effect of oxygen vacancies on Li<sub>2</sub>MnO<sub>3</sub>: a first-principles study. *J. Electrochem. Soc.* **159**, A152–A157 (2011). <https://doi.org/10.1149/2.079202jes>
155. Xiao, R.J., Li, H., Chen, L.Q.: Density functional investigation on Li<sub>2</sub>MnO<sub>3</sub>. *Chem. Mater.* **24**, 4242–4251 (2012). <https://doi.org/10.1021/cm3027219>
156. Yu, X.Q., Lyu, Y.C., Gu, L., et al.: Understanding the rate capability of high-energy-density Li-rich layered Li<sub>1.2</sub>Ni<sub>0.15</sub>Co<sub>0.1</sub>Mn<sub>0.55</sub>O<sub>2</sub> cathode materials. *Adv. Energy Mater.* **4**, 1300950 (2014). <https://doi.org/10.1002/aenm.201300950>
157. Thackeray, M.M., Kang, S.H., Johnson, C.S., et al.: Li<sub>2</sub>MnO<sub>3</sub>-stabilized LiMO<sub>2</sub> (M = Mn, Ni, Co) electrodes for lithium-ion batteries. *J. Mater. Chem.* **17**, 3112 (2007). <https://doi.org/10.1039/b702425h>
158. Zheng, J.M., Myeong, S., Cho, W., et al.: Li- and Mn-rich cathode materials: challenges to commercialization. *Adv. Energy Mater.* **7**, 1601284 (2017). <https://doi.org/10.1002/aenm.201601284>
159. Gallagher, K.G., Croy, J.R., Balasubramanian, M., et al.: Correlating hysteresis and voltage fade in lithium- and manganese-rich layered transition-metal oxide electrodes. *Electrochem. Commun.* **33**, 96–98 (2013). <https://doi.org/10.1016/j.elecom.2013.04.022>
160. Croy, J.R., Gallagher, K.G., Balasubramanian, M., et al.: Quantifying hysteresis and voltage fade in xLi<sub>2</sub>MnO<sub>3</sub>·(1-x)LiMn<sub>0.5</sub>Ni<sub>0.5</sub>O<sub>2</sub> electrodes as a function of Li<sub>2</sub>MnO<sub>3</sub> content. *J. Electrochem. Soc.* **161**, 318–325 (2013). <https://doi.org/10.1149/2.049403jes>
161. Croy, J.R., Kim, D., Balasubramanian, M., et al.: Countering the voltage decay in high capacity xLi<sub>2</sub>MnO<sub>3</sub>·(1-x)LiMO<sub>2</sub> electrodes (M=Mn, Ni, Co) for Li<sup>+</sup>-ion batteries. *J. Electrochem. Soc.* **159**, A781–A790 (2012). <https://doi.org/10.1149/2.080206jes>
162. Zhang, K., Li, B., Zuo, Y.X., et al.: Voltage decay in layered Li-rich Mn-based cathode materials. *Electrochem. Energy Rev.* **2**, 606–623 (2019). <https://doi.org/10.1007/s41918-019-00049-z>
163. Sathiy, M., Abakumov, A.M., Foix, D., et al.: Origin of voltage decay in high-capacity layered oxide electrodes. *Nat. Mater.* **14**, 230–238 (2015). <https://doi.org/10.1038/nmat4137>
164. Assat, G., Glazier, S.L., Delacourt, C., et al.: Probing the thermal effects of voltage hysteresis in anionic redox-based lithium-rich cathodes using isothermal calorimetry. *Nat. Energy* **4**, 647–656 (2019). <https://doi.org/10.1038/s41560-019-0410-6>
165. Croy, J.R., Gallagher, K.G., Balasubramanian, M., et al.: Examining hysteresis in composite xLi<sub>2</sub>MnO<sub>3</sub>·(1-x)LiMO<sub>2</sub> cathode structures. *J. Phys. Chem. C* **117**, 6525–6536 (2013). <https://doi.org/10.1021/jp312658q>
166. Croy, J.R., Balasubramanian, M., Gallagher, K.G., et al.: Review of the US department of energy’s “deep dive” effort to understand voltage fade in Li- and Mn-rich cathodes. *Acc. Chem. Res.* **48**, 2813–2821 (2015). <https://doi.org/10.1021/acs.accounts.5b00277>
167. Konishi, H., Hirano, T., Takamatsu, D., et al.: Electrochemical reaction mechanisms under various charge-discharge operating conditions for Li<sub>1.2</sub>Ni<sub>0.13</sub>Mn<sub>0.54</sub>Co<sub>0.13</sub>O<sub>2</sub> in a lithium-ion battery. *J. Solid State Chem.* **262**, 294–300 (2018). <https://doi.org/10.1016/j.jssc.2018.03.028>
168. Wu, Y.Q., Xie, L.Q., He, X.M., et al.: Electrochemical activation, voltage decay and hysteresis of Li-rich layered cathode probed by various cobalt content. *Electrochim. Acta* **265**, 115–120 (2018). <https://doi.org/10.1016/j.electacta.2018.01.181>
169. Dreyer, W., Jamnik, J., Gohlke, C., et al.: The thermodynamic origin of hysteresis in insertion batteries. *Nat. Mater.* **9**, 448–453 (2010). <https://doi.org/10.1038/nmat2730>
170. Kasai, M., Nishimura, S., Gunji, A., et al.: Electrochemical study on xLi<sub>2</sub>MnO<sub>3</sub>·(1-x)LiNi<sub>1/3</sub>Co<sub>1/3</sub>Mn<sub>1/3</sub>O<sub>2</sub> (x = 0.5) layered complex cathode showing voltage hysteresis. *Electrochim. Acta* **146**, 79–88 (2014). <https://doi.org/10.1016/j.electacta.2014.08.073>
171. Li, L.S., Jacobs, R., Gao, P., et al.: Origins of large voltage hysteresis in high-energy-density metal fluoride lithium-ion battery conversion electrodes. *J. Am. Chem. Soc.* **138**, 2838–2848 (2016). <https://doi.org/10.1021/jacs.6b00061>
172. Cabana, J., Monconduit, L., Larcher, D., et al.: Beyond intercalation-based Li-ion batteries: the state of the art and challenges of electrode materials reacting through conversion reactions. *Adv.*

- Mater. **22**, E170–E192 (2010). <https://doi.org/10.1002/adma.201000717>
173. Hong, Y.S., Park, Y.J., Ryu, K.S., et al.: Synthesis and electrochemical properties of nanocrystalline  $\text{Li}[\text{Ni}_x\text{Li}_{(1-2x)/3}\text{Mn}_{(2-x)/3}] \text{O}_2$  prepared by a simple combustion method. *J. Mater. Chem.* **14**, 1424–1429 (2004). <https://doi.org/10.1039/b311888f>
  174. Ito, A., Sato, Y., Sanada, T., et al.: In situ X-ray absorption spectroscopy study of Li-rich layered cathode material  $\text{Li}[\text{Ni}_{0.17}\text{Li}_{0.2}\text{Co}_{0.07}\text{Mn}_{0.56}]\text{O}_2$ . *J. Power Sources* **196**, 6828–6834 (2011). <https://doi.org/10.1016/j.jpowsour.2010.09.105>
  175. Balasubramanian, M., McBreen, J., Davidson, I.J., et al.: In situ X-ray absorption study of a layered manganese-chromium oxide-based cathode material. *J. Electrochem. Soc.* **149**, A176 (2002). <https://doi.org/10.1149/1.1431962>
  176. Ohzuku, T., Nagayama, M., Tsuji, K., et al.: High-capacity lithium insertion materials of lithium nickel manganese oxides for advanced lithium-ion batteries: toward rechargeable capacity more than  $300 \text{ mAh g}^{-1}$ . *J. Mater. Chem.* **21**, 10179 (2011). <https://doi.org/10.1039/c0jm04325g>
  177. Lee, J.H., Hong, J.K., Jang, D.H., et al.: Degradation mechanisms in doped spinels of  $\text{LiM}_{0.05}\text{Mn}_{1.95}\text{O}_4$  ( $M=\text{Li, B, Al, Co, and Ni}$ ) for Li secondary batteries. *J. Power Sources* **89**, 7–14 (2000). [https://doi.org/10.1016/s0378-7753\(00\)00375-x](https://doi.org/10.1016/s0378-7753(00)00375-x)
  178. Xiang, M.W., Su, C.W., Feng, L.L., et al.: Rapid synthesis of high-cycling performance  $\text{LiMg}_x\text{Mn}_{2-x}\text{O}_4$  ( $x \leq 0.20$ ) cathode materials by a low-temperature solid-state combustion method. *Electrochim. Acta* **125**, 524–529 (2014). <https://doi.org/10.1016/j.electacta.2014.01.147>
  179. Arumugam, D., Kalaignan, G.P., VEDIAPPAN, K., et al.: Synthesis and electrochemical characterizations of nano-scaled Zn doped  $\text{LiMn}_2\text{O}_4$  cathode materials for rechargeable lithium batteries. *Electrochim. Acta* **55**, 8439–8444 (2010). <https://doi.org/10.1016/j.electacta.2010.07.033>
  180. Amarilla, J.M., Petrov, K., Picó, F., et al.: Sucrose-aided combustion synthesis of nanosized  $\text{LiMn}_{1.99-y}\text{Li}_y\text{M}_{0.01}\text{O}_4$  ( $M=\text{Al}^{3+}, \text{Ni}^{2+}, \text{Cr}^{3+}, \text{Co}^{3+}, y=0.01 \text{ and } 0.06$ ) spinels. *J. Power Sources* **191**, 591–600 (2009). <https://doi.org/10.1016/j.jpowsour.2009.02.026>
  181. Ryu, W.H., Eom, J.Y., Yin, R.Z., et al.: Synergistic effects of various morphologies and Al doping of spinel  $\text{LiMn}_2\text{O}_4$  nanostructures on the electrochemical performance of lithium-rechargeable batteries. *J. Mater. Chem.* **21**, 15337 (2011). <https://doi.org/10.1039/c1jm10146c>
  182. Xiao, L.F., Zhao, Y.Q., Yang, Y.Y., et al.: Enhanced electrochemical stability of Al-doped  $\text{LiMn}_2\text{O}_4$  synthesized by a polymer-pyrolysis method. *Electrochim. Acta* **54**, 545–550 (2008). <https://doi.org/10.1016/j.electacta.2008.07.037>
  183. Amaral, F.A., Bocchi, N., Brocenschi, R.F., et al.: Structural and electrochemical properties of the doped spinels  $\text{Li}_{1.05}\text{M}_{0.02}\text{Mn}_{1.98}\text{O}_{3.98}\text{N}_{0.02}$  ( $M = \text{Ga}^{3+}, \text{Al}^{3+}, \text{ or } \text{Co}^{3+}; \text{N} = \text{S}^{2-} \text{ or } \text{F}^-$ ) for use as cathode material in lithium batteries. *J. Power Sources* **195**, 3293–3299 (2010). <https://doi.org/10.1016/j.jpowsour.2009.12.002>
  184. Iqbal, M.J., Ahmad, Z.: Electrical and dielectric properties of lithium manganate nanomaterials doped with rare-earth elements. *J. Power Sources* **179**, 763–769 (2008). <https://doi.org/10.1016/j.jpowsour.2007.12.115>
  185. Amarilla, J.M., Rojas, R.M., Pico, F., et al.: Nanosized  $\text{LiMYMn}_2\text{-YO}_4$  ( $M=\text{Cr, Co and Ni}$ ) spinels synthesized by a sucrose-aided combustion method. *J. Power Sources* **174**, 1212–1217 (2007). <https://doi.org/10.1016/j.jpowsour.2007.06.056>
  186. Zhang, D., Popov, B.N., White, R.E.: Electrochemical investigation of  $\text{CrO}_{2.65}$  doped  $\text{LiMn}_2\text{O}_4$  as a cathode material for lithium-ion batteries. *J. Power Sources* **76**, 81–90 (1998). [https://doi.org/10.1016/s0378-7753\(98\)00143-8](https://doi.org/10.1016/s0378-7753(98)00143-8)
  187. Mandal, S., Rojas, R.M., Amarilla, J.M., et al.: High temperature Co-doped  $\text{LiMn}_2\text{O}_4$ -based spinels. Structural, electrical, and electrochemical characterization. *Chem. Mater.* **14**, 1598–1605 (2002). <https://doi.org/10.1021/cm011219v>
  188. Shaju, K.: Spinel phases,  $\text{LiM}_{1/6}\text{Mn}_{11/6}\text{O}_4$  ( $M=\text{Co, CoAl, CoCr, CrAl}$ ), as cathodes for lithium-ion batteries. *Solid State Ion.* **148**, 343–350 (2002). [https://doi.org/10.1016/s0167-2738\(02\)00072-3](https://doi.org/10.1016/s0167-2738(02)00072-3)
  189. Sun, Y.K., Jin, S.H.: Synthesis and electrochemical characteristics of spinel phase  $\text{LiMn}_2\text{O}_4$ -based cathode materials for lithium polymer batteries. *J. Mater. Chem.* **8**, 2399–2404 (1998). <https://doi.org/10.1039/a804483j>
  190. Cao, X., He, X., Wang, J., et al.: High voltage  $\text{LiNi}_{0.5}\text{Mn}_{1.5}\text{O}_4/\text{Li}_4\text{Ti}_5\text{O}_{12}$  lithium ion cells at elevated temperatures: carbonate-versus ionic liquid-based electrolytes. *ACS Appl. Mater. Interfaces* **8**, 25971–25978 (2016). <https://doi.org/10.1021/acsami.6b07687>
  191. Talyosef, Y., Markovsky, B., Salitra, G., et al.: The study of  $\text{LiNi}_{0.5}\text{Mn}_{1.5}\text{O}_4$  5-V cathodes for Li-ion batteries. *J. Power Sources* **146**, 664–669 (2005). <https://doi.org/10.1016/j.jpowsour.2005.03.064>
  192. Bhaskar, A., Mikhailova, D., Kiziltas-Yavuz, N., et al.: 3d-Transition metal doped spinels as high-voltage cathode materials for rechargeable lithium-ion batteries. *Prog. Solid State Chem.* **42**, 128–148 (2014). <https://doi.org/10.1016/j.progsolidstchem.2014.04.007>
  193. Hu, M., Pang, X.L., Zhou, Z.: Recent progress in high-voltage lithium ion batteries. *J. Power Sources* **237**, 229–242 (2013). <https://doi.org/10.1016/j.jpowsour.2013.03.024>
  194. Santhanam, R., Rambabu, B.: Research progress in high voltage spinel  $\text{LiNi}_{0.5}\text{Mn}_{1.5}\text{O}_4$  material. *J. Power Sources* **195**, 5442–5451 (2010). <https://doi.org/10.1016/j.jpowsour.2010.03.067>
  195. Xiao, J., Chen, X.L., Sushko, P.V., et al.: High-performance  $\text{LiNi}_{0.5}\text{Mn}_{1.5}\text{O}_4$  spinel controlled by  $\text{Mn}^{3+}$  concentration and site disorder. *Adv. Mater.* **24**, 2109–2116 (2012). <https://doi.org/10.1002/adma.201104767>
  196. Eglitis, R.I.: Theoretical prediction of the 5 V rechargeable Li ion battery using  $\text{Li}_2\text{CoMn}_3\text{O}_8$  as a cathode. *Phys. Scr.* **90**, 094012 (2015). <https://doi.org/10.1088/0031-8949/90/9/094012>
  197. Kraysberg, A., Ein-Eli, Y.: Higher, stronger, better... A review of 5 volt cathode materials for advanced lithium-ion batteries. *Adv. Energy Mater.* **2**, 922–939 (2012). <https://doi.org/10.1002/aenm.201200068>
  198. Chen, L., Fan, X.L., Hu, E.Y., et al.: Achieving high energy density through increasing the output voltage: a highly reversible 5.3 V battery. *Chem* **5**, 896–912 (2019). <https://doi.org/10.1016/j.chempr.2019.02.003>
  199. Guo, S.H., Zhang, S.C., He, X.M., et al.: Synthesis and characterization of Sn-doped  $\text{LiMn}_2\text{O}_4$  cathode materials for rechargeable Li-ion batteries. *J. Electrochem. Soc.* **155**, A760 (2008). <https://doi.org/10.1149/1.2965635>
  200. Tong, Q.S., Yang, Y., Shi, J.C., et al.: Synthesis and storage performance of the doped  $\text{LiMn}_2\text{O}_4$  spinel. *J. Electrochem. Soc.* **154**, A656 (2007). <https://doi.org/10.1149/1.2731036>
  201. Wang, C.Y., Lu, S.G., Kan, S.R., et al.: Enhanced capacity retention of Co and Li doubly doped  $\text{LiMn}_2\text{O}_4$ . *J. Power Sources* **189**, 607–610 (2009). <https://doi.org/10.1016/j.jpowsour.2008.09.104>
  202. Sun, X.J., Hu, X.H., Shi, Y., et al.: The study of novel multi-doped spinel  $\text{Li}_{1.15}\text{Mn}_{1.96}\text{Co}_{0.03}\text{Gd}_{0.01}\text{O}_{4+\delta}$  as cathode material for Li-ion rechargeable batteries. *Solid State Ion.* **180**, 377–380 (2009). <https://doi.org/10.1016/j.ssi.2009.01.011>
  203. Prabu, M., Reddy, M.V., Selvasekarapandian, S., et al.: (Li, Al)-co-doped spinel,  $\text{Li}(\text{Li}_{0.1}\text{Al}_{0.1}\text{Mn}_{1.8})\text{O}_4$  as high performance cathode for lithium ion batteries. *Electrochim. Acta* **88**, 745–755 (2013). <https://doi.org/10.1016/j.electacta.2012.10.011>
  204. Xiong, L.L., Xu, Y.L., Tao, T., et al.: Synthesis and electrochemical characterization of multi-cations doped spinel  $\text{LiMn}_2\text{O}_4$  used



- for lithium ion batteries. *J. Power Sources* **199**, 214–219 (2012). <https://doi.org/10.1016/j.jpowsour.2011.09.062>
205. Tran, H.Y., Täubert, C., Fleischhammer, M., et al.: LiMn<sub>2</sub>O<sub>4</sub> spinel/LiNi<sub>0.8</sub>Co<sub>0.15</sub>Al<sub>0.05</sub>O<sub>2</sub> blends as cathode materials for lithium-ion batteries. *J. Electrochem. Soc.* **158**, A556 (2011). <https://doi.org/10.1149/1.3560582>
  206. Numata, T., Amemiya, C., Kumeuchi, T., et al.: Advantages of blending LiNi<sub>0.8</sub>Co<sub>0.2</sub>O<sub>2</sub> into Li<sub>1+x</sub>Mn<sub>2-x</sub>O<sub>4</sub> cathodes. *J. Power Sources* **97/98**, 358–360 (2001). [https://doi.org/10.1016/s0378-7753\(01\)00753-4](https://doi.org/10.1016/s0378-7753(01)00753-4)
  207. Qiu, C.G., Liu, L.N., Du, F., et al.: Electrochemical performance of LiMn<sub>2</sub>O<sub>4</sub>/LiFePO<sub>4</sub> blend cathodes for lithium ion batteries. *Chem. Res. Chin. Univ.* **31**, 270–275 (2015). <https://doi.org/10.1007/s40242-015-4367-0>
  208. Du, Y.C., Huang, X.P., Zhang, K.Y., et al.: Thermal stability of LiFePO<sub>4</sub>/C-LiMn<sub>2</sub>O<sub>4</sub> blended cathode materials. *Sci. China Technol. Sci.* **60**, 58–64 (2017). <https://doi.org/10.1007/s11431-016-0329-7>
  209. Ren, H., Guo, Y.Q., Chen, Z.L., et al.: Synergetic effects of blended materials for Lithium-ion batteries. *Sci. China Technol. Sci.* **59**, 1370–1376 (2016). <https://doi.org/10.1007/s11431-016-0255-6>
  210. Wei, Q.L., Wang, X.Y., Yang, X.K., et al.: Spherical concentration-gradient LiMn<sub>1.87</sub>Ni<sub>0.13</sub>O<sub>4</sub> spinel as a high performance cathode for lithium ion batteries. *J. Mater. Chem.* **1**, 4010 (2013). <https://doi.org/10.1039/c3ta01698f>
  211. Jeong, M., Lee, M.J., Cho, J., et al.: Surface Mn oxidation state controlled spinel LiMn<sub>2</sub>O<sub>4</sub> as a cathode material for high-energy Li-ion batteries. *Adv. Energy Mater.* **5**, 1500440 (2015). <https://doi.org/10.1002/aenm.201500440>
  212. Lu, J., Zhan, C., Wu, T.P., et al.: Effectively suppressing dissolution of manganese from spinel lithium manganate via a nanoscale surface-doping approach. *Nat. Commun.* **5**, 5693 (2014). <https://doi.org/10.1038/ncomms6693>
  213. Walz, K.A., Johnson, C.S., Genthe, J., et al.: Elevated temperature cycling stability and electrochemical impedance of LiMn<sub>2</sub>O<sub>4</sub> cathodes with nanoporous ZrO<sub>2</sub> and TiO<sub>2</sub> coatings. *J. Power Sources* **195**, 4943–4951 (2010). <https://doi.org/10.1016/j.jpowsour.2010.03.007>
  214. Eftekhari, A.: Aluminum oxide as a multi-function agent for improving battery performance of LiMn<sub>2</sub>O<sub>4</sub> cathode. *Solid State Ion.* **167**, 237–242 (2004). <https://doi.org/10.1016/j.ssi.2004.01.016>
  215. Lim, S., Cho, J.: PVP-functionalized nanometre scale metal oxide coatings for cathode materials: successful application to LiMn<sub>2</sub>O<sub>4</sub> spinel nanoparticles. *Chem. Commun.* **37**, 4472 (2008). <https://doi.org/10.1039/b807973k>
  216. Kim, W.K., Han, D.W., Ryu, W.H., et al.: Al<sub>2</sub>O<sub>3</sub> coating on LiMn<sub>2</sub>O<sub>4</sub> by electrostatic attraction forces and its effects on the high temperature cyclic performance. *Electrochim. Acta* **71**, 17–21 (2012). <https://doi.org/10.1016/j.electacta.2012.03.090>
  217. Sun, Y.K., Hong, K.J., Prakash, J.: The effect of ZnO coating on electrochemical cycling behavior of spinel LiMn<sub>2</sub>O<sub>4</sub> cathode materials at elevated temperature. *J. Electrochem. Soc.* **150**, A970 (2003). <https://doi.org/10.1149/1.1580819>
  218. Kim, J.S., Johnson, C.S., Vaughey, J.T., et al.: The electrochemical stability of spinel electrodes coated with ZrO<sub>2</sub>, Al<sub>2</sub>O<sub>3</sub>, and SiO<sub>2</sub> from colloidal suspensions. *J. Electrochem. Soc.* **151**, A1755 (2004). <https://doi.org/10.1149/1.1793713>
  219. Chen, Q.Q., Wang, Y.B., Zhang, T.T., et al.: Electrochemical performance of LaF<sub>3</sub>-coated LiMn<sub>2</sub>O<sub>4</sub> cathode materials for lithium ion batteries. *Electrochim. Acta* **83**, 65–72 (2012). <https://doi.org/10.1016/j.electacta.2012.08.025>
  220. Lee, S.H., Jeong, M., Cho, J.: Optimized 4-V spinel cathode material with high energy density for Li-ion cells operating at 60 °C. *Adv. Energy Mater.* **3**, 1623–1629 (2013). <https://doi.org/10.1002/aenm.201300510>
  221. Shang, Y.S., Liu, J.L., Huang, T., et al.: Effect of heat treatment on the structure and electrochemical performance of FePO<sub>4</sub> coated spinel LiMn<sub>2</sub>O<sub>4</sub>. *Electrochim. Acta* **113**, 248–255 (2013). <https://doi.org/10.1016/j.electacta.2013.09.073>
  222. Lee, S.H., Yoon, G., Jeong, M., et al.: Hierarchical surface atomic structure of a manganese-based spinel cathode for lithium-ion batteries. *Angew. Chem. Int. Ed.* **54**, 1153–1158 (2015). <https://doi.org/10.1002/anie.201408853>
  223. Shang, H.F., Xia, D.G.: Spinel LiMn<sub>2</sub>O<sub>4</sub> integrated with coating and doping by Sn self-segregation. *Int. J. Miner. Metall. Mater.* **29**, 909–916 (2022). <https://doi.org/10.1007/s12613-022-2482-8>
  224. Liu, Y.B., Tan, L., Li, L.: Tris(trimethylsilyl) borate as an electrolyte additive to improve the cyclability of LiMn<sub>2</sub>O<sub>4</sub> cathode for lithium-ion battery. *J. Power Sources* **221**, 90–96 (2013). <https://doi.org/10.1016/j.jpowsour.2012.08.028>
  225. Koo, B., Lee, J., Lee, Y., et al.: Vinylene carbonate and tris(trimethylsilyl) phosphite hybrid additives to improve the electrochemical performance of spinel lithium manganese oxide/graphite cells at 60 °C. *Electrochim. Acta* **173**, 750–756 (2015). <https://doi.org/10.1016/j.electacta.2015.05.129>
  226. Han, G.B., Lee, J.N., Lee, D.J., et al.: Enhanced cycling performance of lithium metal secondary batteries with succinic anhydride as an electrolyte additive. *Electrochim. Acta* **115**, 525–530 (2014). <https://doi.org/10.1016/j.electacta.2013.11.015>
  227. Cho, J., Kim, Y.J., Kim, T.J., et al.: Enhanced structural stability of o-LiMnO<sub>2</sub> by sol-gel coating of Al<sub>2</sub>O<sub>3</sub>. *Chem. Mater.* **13**, 18–20 (2001). <https://doi.org/10.1021/cm000759+>
  228. Cho, J., Kim, T.J., Park, B.: The effect of a metal-oxide coating on the cycling behavior at 55 °C in orthorhombic LiMnO<sub>2</sub> cathode materials. *J. Electrochem. Soc.* **149**, A288 (2002). <https://doi.org/10.1149/1.1446870>
  229. Cho, J.: Stabilization of spinel-like phase transformation of o-LiMnO<sub>2</sub> during 55 °C cycling by sol-gel coating of CoO. *Chem. Mater.* **13**, 4537–4541 (2001). <https://doi.org/10.1021/cm0101935>
  230. Kim, T.J., Son, D., Cho, J., et al.: Enhancement of the electrochemical properties of o-LiMnO<sub>2</sub> cathodes at elevated temperature by lithium and fluorine additions. *J. Power Sources* **154**, 268–272 (2006). <https://doi.org/10.1016/j.jpowsour.2005.03.193>
  231. Cook, J.B., Kim, C., Xu, L.P., et al.: The effect of Al substitution on the chemical and electrochemical phase stability of orthorhombic LiMnO<sub>2</sub>. *J. Electrochem. Soc.* **160**, A46–A52 (2012). <https://doi.org/10.1149/2.048301jes>
  232. Guo, J.L., Cai, Y.J., Zhang, S.J., et al.: Core-shell structured o-LiMnO<sub>2</sub>@Li<sub>2</sub>CO<sub>3</sub> nanosheet array cathode for high-performance, wide-temperature-tolerance lithium-ion batteries. *ACS Appl. Mater. Interfaces* **8**, 16116–16124 (2016). <https://doi.org/10.1021/acsami.6b04616>
  233. Armstrong, A.R., Robertson, A.D., Gitzendanner, R., et al.: The layered intercalation compounds Li(Mn<sub>1-y</sub>Co<sub>y</sub>)O<sub>2</sub>: positive electrode materials for lithium-ion batteries. *J. Solid State Chem.* **145**, 549–556 (1999). <https://doi.org/10.1006/jssc.1999.8216>
  234. Quine, T.E., Duncan, M.J., Armstrong, A.R., et al.: Layered Li<sub>x</sub>Mn<sub>1-y</sub>Ni<sub>y</sub>O<sub>2</sub> intercalation electrodes. *J. Mater. Chem.* **10**, 2838–2841 (2000). <https://doi.org/10.1039/b007429m>
  235. Robertson, A.D., Armstrong, A.R., Bruce, P.G.: Influence of ion exchange conditions on the defect chemistry and performance of cobalt doped layered lithium manganese oxide based intercalation compounds. *Chem. Commun.* **20**, 1997–1998 (2000). <https://doi.org/10.1039/b002525f>
  236. Wu, X.M., Li, R.X., Chen, S., et al.: Comparative study of Co, Cr and Al-doped LiMnO<sub>2</sub> prepared by ion exchange.

- Bull. Mater. Sci. **31**, 109–113 (2008). <https://doi.org/10.1007/s12034-008-0019-z>
237. Chebiam, R.V., Prado, F., Manthiram, A.: Soft chemistry synthesis and characterization of layered  $\text{Li}_{1-x}\text{Ni}_{1-y}\text{Co}_y\text{O}_{2-\delta}$  ( $0 \leq x \leq 1$  and  $0 \leq y \leq 1$ ). Chem. Mater. **13**, 2951–2957 (2001). <https://doi.org/10.1021/cm0102537>
238. Robert Armstrong, A., Gitzendanner, R.: The intercalation compound  $\text{Li}(\text{Mn}_{0.9}\text{Co}_{0.1})\text{O}_2$  as a positive electrode for rechargeable lithium batteries. Chem. Commun. **17**, 1833–1834 (1998). <https://doi.org/10.1039/a803741h>
239. Robertson, A.D., Armstrong, A.R., Fowkes, A.J., et al.:  $\text{Li}_x(\text{Mn}_{1-y}\text{Co}_y)\text{O}_2$  intercalation compounds as electrodes for lithium batteries: influence of ion exchange on structure and performance. J. Mater. Chem. **11**, 113–118 (2001). <https://doi.org/10.1039/b002948n>
240. Jang, Y.I.: Stabilization of  $\text{LiMnO}_2$  in the  $\alpha$ - $\text{NaFeO}_2$  structure type by  $\text{LiAlO}_2$  addition. Electrochem. Solid-State Lett. **1**, 13 (1999). <https://doi.org/10.1149/1.1390619>
241. Davidson, I.J., McMillan, R.S., Slegel, H., et al.: Electrochemistry and structure of  $\text{Li}_{2-x}\text{Cr}_y\text{Mn}_{2-y}\text{O}_4$  phases. J. Power Sources **81**(82), 406–411 (1999). [https://doi.org/10.1016/s0378-7753\(98\)00221-3](https://doi.org/10.1016/s0378-7753(98)00221-3)
242. Ceder, G.: The stability of orthorhombic and monoclinic-layered  $\text{LiMnO}_2$ . Electrochem. Solid-State Lett. **2**, 550 (1999). <https://doi.org/10.1149/1.1390900>
243. Ammundsen, B., Desilvestro, J., Groutso, T., et al.: Formation and structural properties of layered  $\text{LiMnO}_2$  cathode materials. J. Electrochem. Soc. **147**, 4078 (2000). <https://doi.org/10.1149/1.1394022>
244. Ammundsen, B., Desilvestro, J., Groutso, T., et al.: Solid state synthesis and properties of doped  $\text{LiMnO}_2$  cathode materials. MRS Proc. **575**, 49 (1999). <https://doi.org/10.1557/proc-575-49>
245. Pang, W.K., Lee, J.Y., Wei, Y.S., et al.: Preparation and characterization of Cr-doped  $\text{LiMnO}_2$  cathode materials by Pechini's method for lithium ion batteries. Mater. Chem. Phys. **139**, 241–246 (2013). <https://doi.org/10.1016/j.matchemphys.2013.01.030>
246. Wang, H.F.: Origin of cycling stability in monoclinic- and orthorhombic-phase lithium manganese oxide cathodes. Electrochem. Solid-State Lett. **2**, 490 (1999). <https://doi.org/10.1149/1.1390880>
247. Radin, M.D., Hy, S., Sina, M., et al.: Narrowing the gap between theoretical and practical capacities in Li-ion layered oxide cathode materials. Adv. Energy Mater. **7**, 1602888 (2017). <https://doi.org/10.1002/aenm.201602888>
248. Liu, W., Oh, P., Liu, X.E., et al.: Nickel-rich layered lithium transition-metal oxide for high-energy lithium-ion batteries. Angew. Chem. Int. Ed. **54**, 4440–4457 (2015). <https://doi.org/10.1002/anie.201409262>
249. Yoon, C.S., Choi, M.H., Lim, B.B., et al.: Review: high-capacity  $\text{Li}[\text{Ni}_{1-x}\text{Co}_{x/2}\text{Mn}_{x/2}]\text{O}_2$  ( $x = 0.1, 0.05, 0$ ) cathodes for next-generation Li-ion battery. J. Electrochem. Soc. **162**, A2483–A2489 (2015). <https://doi.org/10.1149/2.0101514jes>
250. Kim, D., Gim, J., Lim, J., et al.: Synthesis of  $x\text{Li}_2\text{MnO}_3 \cdot (1-x)\text{LiMO}_2$  ( $M = \text{Cr, Mn, Co, Ni}$ ) nanocomposites and their electrochemical properties. Mater. Res. Bull. **45**, 252–255 (2010). <https://doi.org/10.1016/j.materresbull.2009.12.027>
251. Thackeray, M.M., Johnson, C.S., Vaughey, J.T., et al.: Advances in manganese-oxide “composite” electrodes for lithium-ion batteries. J. Mater. Chem. **15**, 2257 (2005). <https://doi.org/10.1039/b417616m>
252. Thackeray, M., Kang, S.H., Johnson, C., et al.: Comments on the structural complexity of lithium-rich  $\text{Li}_{1+x}\text{M}_{1-x}\text{O}_2$  electrodes ( $M = \text{Mn, Ni, Co}$ ) for lithium batteries. Electrochem. Commun. **8**, 1531–1538 (2006)
253. Lu, Z., Chen, Z., Dahn, J.: Lack of cation clustering in  $\text{Li}[\text{Ni}_x\text{Li}_{1/3-2x/3}\text{Mn}_{2/3-x/3}]\text{O}_2$  ( $0 < x \leq 1/2$ ) and  $\text{Li}[\text{Cr}_x\text{Li}_{(1-x)/3}\text{Mn}_{(2-2x)/3}]\text{O}_2$  ( $0 < x < 1$ ). Chem. Mat. **15**, 3214–3220 (2003)
254. Bréger, J., Jiang, M., Dupré, N., et al.: High-resolution X-ray diffraction, DIFFaX, NMR and first principles study of disorder in the  $\text{Li}_2\text{MnO}_3$ – $\text{Li}[\text{Ni}_{1/2}\text{Mn}_{1/2}]\text{O}_2$  solid solution. J. Solid State Chem. **178**, 2575–2585 (2005). <https://doi.org/10.1016/j.jssc.2005.05.027>
255. Jarvis, K.A., Deng, Z.Q., Allard, L.F., et al.: Atomic structure of a lithium-rich layered oxide material for lithium-ion batteries: evidence of a solid solution. Chem. Mater. **23**, 3614–3621 (2011). <https://doi.org/10.1021/cm200831c>
256. Zheng, J.M., Zhang, Z.R., Wu, X.B., et al.: The effects of  $\text{AlF}_3$  coating on the performance of  $\text{Li}[\text{Li}_{0.2}\text{Mn}_{0.54}\text{Ni}_{0.13}\text{Co}_{0.13}]\text{O}_2$  positive electrode material for lithium-ion battery. J. Electrochem. Soc. **155**, A775 (2008). <https://doi.org/10.1149/1.2966694>
257. Wu, Y., Manthiram, A.: Effect of surface modifications on the layered solid solution cathodes  $(1-z)\text{Li}[\text{Li}_{1/3}\text{Mn}_{2/3}]\text{O}_{2-z}\text{Li}[\text{Mn}_{0.5-y}\text{Ni}_{0.5-y}\text{Co}_y]\text{O}_2$ . Solid State Ion. **180**, 50–56 (2009). <https://doi.org/10.1016/j.ssi.2008.11.002>
258. Liu, S., Liu, Z.P., Shen, X., et al.: Surface doping to enhance structural integrity and performance of Li-rich layered oxide. Adv. Energy Mater. **8**, 1802105 (2018). <https://doi.org/10.1002/aenm.201802105>
259. Qing, R.P., Shi, J.L., Xiao, D.D., et al.: Cathode materials: enhancing the kinetics of Li-rich cathode materials through the pinning effects of gradient surface  $\text{Na}^+$  doping. Adv. Energy Mater. **6**, 1501914 (2016). <https://doi.org/10.1002/aenm.201670035>
260. Ning, F., Shang, H., Li, B., et al.: Surface thermodynamic stability of Li-rich  $\text{Li}_2\text{MnO}_3$ : effect of defective graphene. Energy Storage Mater. **22**, 113–119 (2019)
261. Li, B., Yan, H.J., Ma, J., et al.: Manipulating the electronic structure of Li-rich manganese-based oxide using polyanions: towards better electrochemical performance. Adv. Funct. Mater. **24**, 5112–5118 (2014). <https://doi.org/10.1002/adfm.201400436>
262. Gao, Y.R., Ma, J., Wang, Z.X., et al.: Vacancy-induced  $\text{MnO}_6$  distortion and its impacts on structural transition of  $\text{Li}_2\text{MnO}_3$ . Phys. Chem. Chem. Phys. **19**, 7025–7031 (2017). <https://doi.org/10.1039/c6cp08441a>
263. Gu, M., Belharouak, I., Zheng, J.M., et al.: Formation of the spinel phase in the layered composite cathode used in Li-ion batteries. ACS Nano **7**, 760–767 (2013). <https://doi.org/10.1021/nl305065u>
264. Xu, B., Fell, C.R., Chi, M.F., et al.: Identifying surface structural changes in layered Li-excess nickel manganese oxides in high voltage lithium ion batteries: a joint experimental and theoretical study. Energy Environ. Sci. **4**, 2223 (2011). <https://doi.org/10.1039/c1ee01131f>
265. Mohanty, D., Sefat, A.S., Kalnaus, S., et al.: Investigating phase transformation in the  $\text{Li}_{1.2}\text{Co}_{0.1}\text{Mn}_{0.55}\text{Ni}_{0.15}\text{O}_2$  lithium-ion battery cathode during high-voltage hold (4.5 V) via magnetic, X-ray diffraction and electron microscopy studies. J. Mater. Chem. A **1**, 6249 (2013). <https://doi.org/10.1039/c3ta10304h>
266. Wu, Y., Ma, C., Yang, J.H., et al.: Probing the initiation of voltage decay in Li-rich layered cathode materials at the atomic scale. J. Mater. Chem. A **3**, 5385–5391 (2015). <https://doi.org/10.1039/c4ta06856d>
267. Zheng, J.M., Xu, P.H., Gu, M., et al.: Structural and chemical evolution of Li- and Mn-rich layered cathode material. Chem. Mater. **27**, 1381–1390 (2015). <https://doi.org/10.1021/cm5045978>
268. Hua, W.B., Wang, S.N., Knapp, M., et al.: Structural insights into the formation and voltage degradation of lithium- and

- manganese-rich layered oxides. *Nat. Commun.* **10**, 5365 (2019). <https://doi.org/10.1038/s41467-019-13240-z>
269. Mohanty, D., Li, J.L., Abraham, D.P., et al.: Unraveling the voltage-fade mechanism in high-energy-density lithium-ion batteries: origin of the tetrahedral cations for spinel conversion. *Chem. Mater.* **26**, 6272–6280 (2014). <https://doi.org/10.1021/cm5031415>
270. Oh, P., Ko, M., Myeong, S., et al.: A novel surface treatment method and new insight into discharge voltage deterioration for high-performance  $0.4\text{Li}_2\text{MnO}_3\text{-}0.6\text{LiNi}_{1/3}\text{Co}_{1/3}\text{Mn}_{1/3}\text{O}_2$  cathode materials. *Adv. Energy Mater.* **4**, 1400631 (2014). <https://doi.org/10.1002/aenm.201400631>
271. Hu, E.Y., Lyu, Y.C., Xin, H.L., et al.: Explore the effects of microstructural defects on voltage fade of Li- and Mn-rich cathodes. *Nano Lett.* **16**, 5999–6007 (2016). <https://doi.org/10.1021/acs.nanolett.6b01609>
272. West, W.C., Soler, J., Smart, M.C., et al.: Electrochemical behavior of layered solid solution  $\text{Li}_2\text{MnO}_3\text{-LiMO}_2$  (M = Ni, Mn, Co) Li-ion cathodes with and without alumina coatings. *J. Electrochem. Soc.* **158**, A883 (2011). <https://doi.org/10.1149/1.3597319>
273. Sun, Y.K., Lee, M.J., Yoon, C.S., et al.: The role of  $\text{AlF}_3$  coatings in improving electrochemical cycling of Li-enriched nickel-manganese oxide electrodes for Li-ion batteries. *Adv. Mater.* **24**, 1192–1196 (2012). <https://doi.org/10.1002/adma.201104106>
274. Qiu, B., Wang, J., Xia, Y., et al.: Enhanced electrochemical performance with surface coating by reactive magnetron sputtering on lithium-rich layered oxide electrodes. *ACS Appl. Mater. Interfaces.* **6**, 9185–9193 (2014)
275. Wu, F., Zhang, X., Zhao, T., et al.: Multifunctional  $\text{AlPO}_4$  coating for improving electrochemical properties of low-cost  $\text{Li}[\text{Li}_{0.2}\text{Fe}_{0.1}\text{Ni}_{0.15}\text{Mn}_{0.55}]\text{O}_2$  cathode materials for lithium-ion batteries. *ACS Appl. Mater. Interfaces.* **7**, 3773–3781 (2015)
276. Park, K., Kim, J., Park, J.H., et al.: Synchronous phase transition and carbon coating on the surface of Li-rich layered oxide cathode materials for rechargeable Li-ion batteries. *J. Power Sources* **408**, 105–110 (2018). <https://doi.org/10.1016/j.jpowsour.2018.10.001>
277. Qiu, B., Zhang, M.H., Wu, L.J., et al.: Gas–solid interfacial modification of oxygen activity in layered oxide cathodes for lithium-ion batteries. *Nat. Commun.* **7**, 12108 (2016). <https://doi.org/10.1038/ncomms12108>
278. Shang, H.F., Ning, F.H., Li, B., et al.: Suppressing voltage decay of a lithium-rich cathode material by surface enrichment with atomic ruthenium. *ACS Appl. Mater. Interfaces* **10**, 21349–21355 (2018). <https://doi.org/10.1021/acsami.8b06271>
279. Zhang, X.D., Shi, J.L., Liang, J.Y., et al.: Suppressing surface lattice oxygen release of Li-rich cathode materials via heterostructured spinel  $\text{Li}_4\text{Mn}_5\text{O}_{12}$  coating. *Adv. Mater.* **30**, 1801751 (2018). <https://doi.org/10.1002/adma.201801751>
280. Peng, H., Zhao, S.X., Huang, C., et al.: In situ construction of spinel coating on the surface of a lithium-rich manganese-based single crystal for inhibiting voltage fade. *ACS Appl. Mater. Interfaces* **12**, 11579–11588 (2020). <https://doi.org/10.1021/acsami.9b21271>
281. Wu, F., Li, N., Su, Y.F., et al.: Spinel/layered heterostructured cathode material for high-capacity and high-rate Li-ion batteries. *Adv. Mater.* **25**, 3722–3726 (2013). <https://doi.org/10.1002/adma.201300598>
282. Zhu, Z., Yu, D.W., Yang, Y., et al.: Gradient Li-rich oxide cathode particles immunized against oxygen release by a molten salt treatment. *Nat. Energy* **4**, 1049–1058 (2019). <https://doi.org/10.1038/s41560-019-0508-x>
283. Shi, J.L., Zhang, J.N., He, M., et al.: Mitigating voltage decay of Li-rich cathode material via increasing Ni content for lithium-ion batteries. *ACS Appl. Mater. Interfaces* **8**, 20138–20146 (2016). <https://doi.org/10.1021/acsami.6b06733>
284. Sun, G., Yu, F.D., Que, L.F., et al.: Local electronic structure modulation enhances operating voltage in Li-rich cathodes. *Nano Energy* **66**, 104102 (2019). <https://doi.org/10.1016/j.nanoen.2019.104102>
285. Ku, K., Hong, J., Kim, H., et al.: Suppression of voltage decay through manganese deactivation and nickel redox buffering in high-energy layered lithium-rich electrodes. *Adv. Energy Mater.* **8**, 1800606 (2018). <https://doi.org/10.1002/aenm.201800606>
286. Zhu, Z., Gao, R., Waluyo, I., et al.: Stabilized Co-free Li-rich oxide cathode particles with an artificial surface preconstruction. *Adv. Energy Mater.* **10**, 2001120 (2020). <https://doi.org/10.1002/aenm.202001120>
287. Wang, Y.Q., Yang, Z.Z., Qian, Y.M., et al.: New insights into improving rate performance of lithium-rich cathode material. *Adv. Mater.* **27**, 3915–3920 (2015). <https://doi.org/10.1002/adma.201500956>
288. Dahiya, P.P., Ghanty, C., Sahoo, K., et al.: Suppression of voltage decay and improvement in electrochemical performance by zirconium doping in Li-rich cathode materials for Li-ion batteries. *J. Electrochem. Soc.* **165**, A3114–A3124 (2018). <https://doi.org/10.1149/2.0751813jes>
289. Yu, R.Z., Wang, G., Liu, M.H., et al.: Mitigating voltage and capacity fading of lithium-rich layered cathodes by lanthanum doping. *J. Power Sources* **335**, 65–75 (2016). <https://doi.org/10.1016/j.jpowsour.2016.10.042>
290. Eum, D., Kim, B., Kim, S.J., et al.: Voltage decay and redox asymmetry mitigation by reversible cation migration in lithium-rich layered oxide electrodes. *Nat. Mater.* **19**, 419–427 (2020). <https://doi.org/10.1038/s41563-019-0572-4>
291. Zuo, Y.X., Li, B., Jiang, N., et al.: A high-capacity O2-type Li-rich cathode material with a single-layer  $\text{Li}_2\text{MnO}_3$  superstructure. *Adv. Mater.* **30**, 1707255 (2018). <https://doi.org/10.1002/adma.201707255>
292. Cui, Z.H., Guo, X.X., Li, H.: Equilibrium voltage and overpotential variation of nonaqueous Li-O<sub>2</sub> batteries using the galvanostatic intermittent titration technique. *Energy Environ. Sci.* **8**, 182–187 (2015). <https://doi.org/10.1039/c4ee01777c>
293. Li, Q., Qiao, Y., Guo, S.H., et al.: Both cationic and anionic co-(de)intercalation into a metal-oxide material. *Joule* **2**, 1134–1145 (2018). <https://doi.org/10.1016/j.joule.2018.03.010>
294. Song, B.H., Tang, M.X., Hu, E.Y., et al.: Understanding the low-voltage hysteresis of anionic redox in  $\text{Na}_2\text{Mn}_3\text{O}_7$ . *Chem. Mater.* **31**, 3756–3765 (2019). <https://doi.org/10.1021/acs.chemmater.9b00772>
295. Assat, G., Delacourt, C., Corte, D.A.D., et al.: Editors' choice—practical assessment of anionic redox in Li-rich layered oxide cathodes: a mixed blessing for high energy Li-ion batteries. *J. Electrochem. Soc.* **163**, A2965–A2976 (2016). <https://doi.org/10.1149/2.0531614jes>
296. Wang, Q.S., Sarkar, A., Wang, D., et al.: Multi-anionic and-cationic compounds: new high entropy materials for advanced Li-ion batteries. *Energy Environ. Sci.* **12**, 2433–2442 (2019). <https://doi.org/10.1039/c9ee00368a>
297. Lim, H.D., Lee, B., Zheng, Y.P., et al.: Rational design of redox mediators for advanced Li-O<sub>2</sub> batteries. *Nat. Energy* **1**, 16066 (2016). <https://doi.org/10.1038/nenergy.2016.66>
298. Dai, K.H., Mao, J., Zhuo, Z.Q., et al.: Negligible voltage hysteresis with strong anionic redox in conventional battery electrode. *Nano Energy* **74**, 104831 (2020). <https://doi.org/10.1016/j.nanoen.2020.104831>
299. Du, K., Zhu, J.Y., Hu, G.R., et al.: Exploring reversible oxidation of oxygen in a manganese oxide. *Energy Environ. Sci.* **9**, 2575–2577 (2016). <https://doi.org/10.1039/c6ee01367h>

300. Gent, W.E., Lim, K., Liang, Y.F., et al.: Coupling between oxygen redox and cation migration explains unusual electrochemistry in lithium-rich layered oxides. *Nat. Commun.* **8**, 2091 (2017). <https://doi.org/10.1038/s41467-017-02041-x>
301. Ben Yahia, M., Vergnet, J., Saubanère, M., et al.: Unified picture of anionic redox in Li/Na-ion batteries. *Nat. Mater.* **18**, 496–502 (2019). <https://doi.org/10.1038/s41563-019-0318-3>
302. Konishi, H., Hirano, T., Takamatsu, D., et al.: Origin of hysteresis between charge and discharge processes in lithium-rich layer-structured cathode material for lithium-ion battery. *J. Power Sources* **298**, 144–149 (2015). <https://doi.org/10.1016/j.jpowsour.2015.08.056>
303. Li, B., Sougrati, M.T., Rouse, G., et al.: Correlating ligand-to-metal charge transfer with voltage hysteresis in a Li-rich rock-salt compound exhibiting anionic redox. *Nat. Chem.* **13**, 1070–1080 (2021). <https://doi.org/10.1038/s41557-021-00775-2>
304. Li, B., Kumar, K., Roy, I., et al.: Capturing dynamic ligand-to-metal charge transfer with a long-lived cationic intermediate for anionic redox. *Nat. Mater.* **21**, 1165–1174 (2022). <https://doi.org/10.1038/s41563-022-01278-2>
305. House, R.A., Maitra, U., Pérez-Osorio, M.A., et al.: Superstructure control of first-cycle voltage hysteresis in oxygen-redox cathodes. *Nature* **577**, 502–508 (2020). <https://doi.org/10.1038/s41586-019-1854-3>
306. House, R.A., Marie, J.J., Pérez-Osorio, M.A., et al.: The role of O<sub>2</sub> in O-redox cathodes for Li-ion batteries. *Nat. Energy* **6**, 781–789 (2021). <https://doi.org/10.1038/s41560-021-00780-2>
307. Urban, A., Abdellahi, A., Dacek, S., et al.: Electronic-structure origin of cation disorder in transition-metal oxides. *Phys. Rev. Lett.* **119**, 176402 (2017). <https://doi.org/10.1103/physrevlett.119.176402>
308. Lun, Z.Y., Ouyang, B., Cai, Z.J., et al.: Design principles for high-capacity Mn-based cation-disordered rocksalt cathodes. *Chem* **6**, 153–168 (2020). <https://doi.org/10.1016/j.chempr.2019.10.001>
309. Yao, Z.P., Kim, S., He, J.G., et al.: Interplay of cation and anion redox in Li<sub>4</sub>Mn<sub>2</sub>O<sub>5</sub> cathode material and prediction of improved Li<sub>4</sub>(Mn, M)<sub>2</sub>O<sub>5</sub> electrodes for Li-ion batteries. *Sci. Adv.* **4**, eaao6754 (2018). <https://doi.org/10.1126/sciadv.aao6754>
310. Hwang, J., Myeong, S., Jin, W., et al.: Excess-Li localization triggers chemical irreversibility in Li- and Mn-rich layered oxides. *Adv. Mater.* **32**, 2001944 (2020). <https://doi.org/10.1002/adma.202001944>
311. Zuo, C.J., Hu, Z.X., Qi, R., et al.: Double the capacity of manganese spinel for lithium-ion storage by suppression of cooperative Jahn-Teller distortion. *Adv. Energy Mater.* **10**, 2000363 (2020). <https://doi.org/10.1002/aenm.202000363>
312. Zheng, C., Radhakrishnan, B., Chu, I.H., et al.: Effects of transition-metal mixing on Na ordering and kinetics in layered P2 oxides. *Phys. Rev. Appl.* **7**, 064003 (2017). <https://doi.org/10.1103/physrevapplied.7.064003>
313. de Boisse, B.M., Liu, G., Ma, J., et al.: Intermediate honeycomb ordering to trigger oxygen redox chemistry in layered battery electrode. *Nat. Commun.* **7**, 1–9 (2016)
314. Li, Q., Xu, S., Guo, S.H., et al.: A superlattice-stabilized layered oxide cathode for sodium-ion batteries. *Adv. Mater.* **32**, 1907936 (2020). <https://doi.org/10.1002/adma.201907936>
315. Lu, Z.H., Donabarger, R.A., Dahn, J.R.: Superlattice ordering of Mn, Ni, and Co in layered alkali transition metal oxides with P2, P3, and O3 structures. *Chem. Mater.* **12**, 3583–3590 (2000). <https://doi.org/10.1021/cm000359m>
316. Cabana, J., Chernova, N.A., Xiao, J., et al.: Study of the transition metal ordering in layered Na<sub>x</sub>Ni<sub>1-x/2</sub>Mn<sub>1-x/2</sub>O<sub>2</sub> (2/3 ≤ x ≤ 1) and consequences of Na/Li exchange. *Inorg. Chem.* **52**, 8540–8550 (2013). <https://doi.org/10.1021/ic400579w>
317. Yuan, D.D., Liang, X.M., Wu, L., et al.: A honeycomb-layered Na<sub>3</sub>Ni<sub>2</sub>SbO<sub>6</sub>: a high-rate and cycle-stable cathode for sodium-ion batteries. *Adv. Mater.* **26**, 6301–6306 (2014). <https://doi.org/10.1002/adma.201401946>
318. Wang, P.F., Guo, Y.J., Duan, H., et al.: Honeycomb-ordered Na<sub>3</sub>Ni<sub>1.5</sub>M<sub>0.5</sub>BiO<sub>6</sub> (M = Ni, Cu, Mg, Zn) as high-voltage layered cathodes for sodium-ion batteries. *ACS Energy Lett.* **2**, 2715–2722 (2017). <https://doi.org/10.1021/acsenenergylett.7b00930>
319. Zhao, C.L., Wang, Q.D., Lu, Y.X., et al.: Decreasing transition metal triggered oxygen redox activity in Na-deficient oxides. *Energy Storage Mater.* **20**, 395–400 (2019). <https://doi.org/10.1016/j.ensm.2018.10.025>
320. Li, Y.J., Wang, X.F., Gao, Y.R., et al.: Native vacancy enhanced oxygen redox reversibility and structural robustness. *Adv. Energy Mater.* **9**, 1803087 (2019). <https://doi.org/10.1002/aenm.201803087>
321. Yang, L., Liu, Z.P., Liu, S., et al.: Superiority of native vacancies in activating anionic redox in P2-type Na<sub>2/3</sub>[Mn<sub>7/9</sub>Mg<sub>1/9</sub>□<sub>1/9</sub>]O<sub>2</sub>. *Nano Energy* **78**, 105172 (2020). <https://doi.org/10.1016/j.nanoen.2020.105172>
322. Huang, W.Y., Lin, C., Qiu, J.M., et al.: Delocalized Li@Mn<sub>6</sub> superstructure units enable layer stability of high-performance Mn-rich cathode materials. *Chem* **8**, 2163–2178 (2022). <https://doi.org/10.1016/j.chempr.2022.04.012>
323. Kim, S.W., Nam, K.W., Seo, D.H., et al.: Energy storage in composites of a redox couple host and a lithium ion host. *Nano Today* **7**, 168–173 (2012). <https://doi.org/10.1016/j.nantod.2012.04.004>
324. George, E.P., Raabe, D., Ritchie, R.O.: High-entropy alloys. *Nat. Rev. Mater.* **4**, 515–534 (2019). <https://doi.org/10.1038/s41578-019-0121-4>
325. Miracle, D.B., Senkov, O.N.: A critical review of high entropy alloys and related concepts. *Acta Mater.* **122**, 448–511 (2017). <https://doi.org/10.1016/j.actamat.2016.08.081>
326. Feng, G., Ning, F., Song, J., et al.: Sub-2 nm ultrasmall high-entropy alloy nanoparticles for extremely superior electrocatalytic hydrogen evolution. *J. Am. Chem. Soc.* **143**, 17117–17127 (2021)
327. Jiang, Y.S., Yu, F.D., Que, L.F., et al.: Revealing the thermodynamics and kinetics of in-plane disordered Li<sub>2</sub>MnO<sub>3</sub> structure in Li-rich cathodes. *ACS Energy Lett.* **6**, 3836–3843 (2021). <https://doi.org/10.1021/acsenenergylett.1c01904>
328. Zhao, C.L., Ding, F.X., Lu, Y.X., et al.: High-entropy layered oxide cathodes for sodium-ion batteries. *Angew. Chem. Int. Ed.* **59**, 264–269 (2020). <https://doi.org/10.1002/anie.201912171>
329. Sarkar, A., Velasco, L., Wang, D., et al.: High entropy oxides for reversible energy storage. *Nat. Commun.* **9**, 3400 (2018). <https://doi.org/10.1038/s41467-018-05774-5>
330. Rost, C.M., Sachet, E., Borman, T., et al.: Entropy-stabilized oxides. *Nat. Commun.* **6**, 1–8 (2015)
331. Xiao, B., Wu, G., Wang, T.D., et al.: High-entropy oxides as advanced anode materials for long-life lithium-ion batteries. *Nano Energy* **95**, 106962 (2022). <https://doi.org/10.1016/j.nanoen.2022.106962>
332. Gu, Z.Y., Guo, J.Z., Cao, J.M., et al.: An advanced high-entropy fluorophosphate cathode for sodium-ion batteries with increased working voltage and energy density. *Adv. Mater.* **34**, 2270110 (2022). <https://doi.org/10.1002/adma.202270110>
333. Ma, Y.J., Ma, Y., Dreyer, S.L., et al.: High-entropy metal-organic frameworks for highly reversible sodium storage. *Adv. Mater.* **33**, 2170269 (2021). <https://doi.org/10.1002/adma.202170269>
334. Ding, F.X., Zhao, C.L., Xiao, D.D., et al.: Using high-entropy configuration strategy to design Na-ion layered oxide cathodes with superior electrochemical performance and thermal stability. *J. Am. Chem. Soc.* **144**, 8286–8295 (2022). <https://doi.org/10.1021/jacs.2c02353>

335. Lun, Z.Y., Ouyang, B., Kwon, D.H., et al.: Cation-disordered rocksalt-type high-entropy cathodes for Li-ion batteries. *Nat. Mater.* **20**, 214–221 (2021). <https://doi.org/10.1038/s41563-020-00816-0>
336. Wang, J.H., Yamada, Y., Sodeyama, K., et al.: Fire-extinguishing organic electrolytes for safe batteries. *Nat. Energy* **3**, 22–29 (2017). <https://doi.org/10.1038/s41560-017-0033-8>
337. Zhao, Q., Stalin, S., Zhao, C.Z., et al.: Designing solid-state electrolytes for safe, energy-dense batteries. *Nat. Rev. Mater.* **5**, 229–252 (2020). <https://doi.org/10.1038/s41578-019-0165-5>
338. Famprakis, T., Canepa, P., Dawson, J.A., et al.: Fundamentals of inorganic solid-state electrolytes for batteries. *Nat. Mater.* **18**, 1278–1291 (2019). <https://doi.org/10.1038/s41563-019-0431-3>
339. Gao, Z.H., Sun, H.B., Fu, L., et al.: All-solid-state batteries: promises, challenges, and recent progress of inorganic solid-state electrolytes for all-solid-state lithium batteries. *Adv. Mater.* **30**, 1870122 (2018). <https://doi.org/10.1002/adma.201870122>
340. Cheng, Z.W., Liu, T., Zhao, B., et al.: Recent advances in organic-inorganic composite solid electrolytes for all-solid-state lithium batteries. *Energy Storage Mater.* **34**, 388–416 (2021). <https://doi.org/10.1016/j.ensm.2020.09.016>
341. Fan, L.Z., He, H.C., Nan, C.W.: Tailoring inorganic–polymer composites for the mass production of solid-state batteries. *Nat. Rev. Mater.* **6**, 1003–1019 (2021). <https://doi.org/10.1038/s41578-021-00320-0>



**Jin Song** received his B.Sc. degree in materials science and engineering from Peking University in 2017 and is currently a Ph.D. candidate at the School of Materials Science and Engineering, Peking University. Mr. Song's research focuses on novel cathode materials for Li-ion batteries and Na-ion batteries.



**Hangchao Wang** obtained his Master degree at Beijing University of Chemical Technology, Beijing, China. He is now pursuing his Ph.D. degree at the School of Materials Science and Engineering, Peking University, Beijing, China. During the post-graduate period, he was focused on designing and synthesizing novel solid polymer electrolytes.



**Yuxuan Zuo** obtained his B.Sc. degree at Zhejiang University in 2013 and his Ph.D. degree at Peking University in 2018 with his Ph.D. research being mainly focused on voltage fading and voltage hysteresis mechanisms of anion redox in Li-rich cathodes under the guidance of Prof. Xia. Currently, Dr. Zuo is a post-doctoral candidate with Prof. Xia and his research focuses on Li-ion batteries and other energy storage systems such as Na-ion batteries and OER catalysts.



**Kun Zhang** is currently a Ph.D. student at the School of Materials Science and Engineering, Peking University under the supervision of Prof. Dingguo Xia. Ms. Zhang's research primarily focuses on the basic issues of Li-ion batteries and the design of novel battery structures.



**Tonghuan Yang** obtained his M.Sc. degree in materials science and engineering from Tianjin University of Technology in 2019 and is currently an Eng.D. candidate at the Beijing Key Laboratory of Theory and Technology for Advanced Battery Materials at Peking University. Mr. Yang's research mainly focuses on novel cathode/anode materials with high energy density for Li-ion batteries as well as other related energy storage materials.



**Yali Yang** received her B.Sc. degree in materials science and engineering from Nankai University in 2019 and is currently a Ph.D. candidate at the Beijing Key Laboratory of Theory and Technology for Advanced Battery Materials at the College of Material Science and Engineering, Peking University. Ms. Yang's research focuses on Li-rich cathode materials.



**Chuan Gao** received his B.Sc. degree in materials science and engineering from Peking University in 2020 and is currently a Ph.D. candidate at the School of Materials Science and Engineering, Peking University. Mr. Gao's research focuses on novel cathode materials for Li-ion batteries.



**Wukun Xiao** received her B.Sc. degree at Hebei University of Technology in 2020 and is currently a Ph.D. candidate under the supervision of Prof. Dingguo Xia at Peking University and the Beijing Key Laboratory of Theory and Technology for Advanced Battery Materials. Ms. Xiao's research mainly focuses on design of novel cathode materials' structures for Li-ion batteries.



**Tao Chen** received his bachelor degree and master degree from Central South University, China. He is pursuing his Ph.D. degree in Materials Science at Peking University. His current research interest includes high-efficiency catalysts.



**Tie Luo** is currently an undergraduate at the College of Engineering, Peking University, and will become a Ph.D. candidate under the guidance of Prof. Dingguo Xia in 2023 at the Beijing Key Laboratory of Theory and Technology for Advanced Battery Materials. Mr. Luo's research mainly focuses on synthesis of novel cathode materials of Li-ion batteries.



**Guang Feng** obtained his Ph.D. degree in the department of energy and resources engineering at Peking University in 2020 under the guidance of Prof. Xia. Currently, Dr. Feng is a postdoctoral candidate with Prof. Xia and his current research mainly focuses on developing novel nanomaterials for electrocatalysis and other related energy storage applications.



**Dingguo Xia** obtained his Master degree in physical chemistry from the Harbin Institute of Technology and his Ph.D. degree in metallurgical physical chemistry from the University of Beijing Science and Technology. He worked as a professor in the College of Environmental and Energy Engineering at Beijing University of Technology from 1995 to 2010. He has worked at Peking University since May, 2010 and supervises researchers working on lithium-ion battery materials, low-temperature fuel-cell catalysis, and DFT investigation of energy materials.



**Zewen Jiang** received his bachelor's degree from the College of Chemistry and Molecular Sciences at Wuhan University, China in 2018. He is currently a Ph.D. student at Hubei Key Laboratory of Electrochemical Power Sources in Wuhan University and he has been exchanged to Peking University under the supervision of Prof. Dingguo Xia as a visiting student since 2020. His research focuses on developing high energy density cathode materials for lithium-ion batteries and mechanisms of anionic redox in cathodes.

mechanisms of anionic redox in cathodes.